FUNCTIONAL CHARACTERIZATION OF A NOVEL HEXOSAMINIDASE, CG7985, IN *DROSOPHILA* EYE DEVELOPMENT

by

Ferdi Rıdvan Kıral

B.S., Molecular Biology and Genetics, Middle East Technical University, 2012

Submitted to the Institute for Graduate Studies in
Science and Engineering in partial fulfilment of
the requirements for the degrees of
Master of Science

Graduate Program in Molecular Biology and Genetics
Boğaziçi University

2015

For those who died alone…

ACKNOWLEDGEMENTS

First and foremost, I would like to express my deepest gratitude to Charles Darwin, Ramón y Cajal, Thomas Hunt Morgan, Eric Kandel, Vilayanur Ramachandran and numerous other scientists for their efforts to shed light on the path that I and junior scientists like me are trying to follow and illuminate it more.

I would like to express my sincere gratitude to my supervisor Assoc. Prof. Arzu Çelik. She was always supportive but yet challenging that made this thesis process very didactic and fruitful.

I am also grateful to Assoc. Prof. Tolga Emre and Assoc. Prof. Ferruh Özcan for devoting their valuable time to evaluate this thesis and make helpful comments.

I also owe a thank to Radoslaw Ejsmont and Prof. Bassem Hassan for their valuable contributions to CRISPR experiments.

A huge hug goes to my lovely labmates Ece Terzioğlu Kara, Çağrı Çevrim, Bahar Şahin, Stefan Köstler, Kaan Mika, Duygu Koldere, Xalid Bayramlı, Yiğit Kocagöz, Mehmet Can Demirler, Metin Özdemir, Ece Sönmez, Çağatay Aydın, and Deniz Yüzak for their valuable support and friendship.

Çağrı Çevrim and Gizem Sancer deserve more than a simple thank you. Çağrı was like a second supervisor for me. If I learned one thing from this study, Çağrı was the reason without a doubt. Gizem Sancer, the woman I love, taught me to see the bright side of life whenever I felt bad. This work would not have been possible without them.

Lastly, I would like to thank the members of the rock bands Pink Floyd, Metallica, Radiohead, Bathory, Pentagram, and others that I cannot recall for keeping me awake with their spectacular songs in the long nights I spent in the lab.

ABSTRACT

FUNCTIONAL CHARACTERIZATION OF A NOVEL HEXOSAMINIDASE, CG7985, IN *DROSOPHILA* EYE DEVELOPMENT

CG7985 is one of the four hexosaminidases encoded by the *Drosophila* genome. Although the other three hexosaminidases have been well-characterized in terms of their enzymatic activities and metabolic pathways in which they function, CG7985 is the only uncharacterized hexosaminidase in *Drosophila*. Phylogenetic analysis of CG7985 showed that it differs from the other hexosaminidases grouping together with vertebrate HexDC and *C.elegans* HEX-2. This sub-branching in the hexosaminidase family comes along with a functional difference. Although the other three hexosaminidases have been shown to cleave N-acetyl-β-D-glucosamine residues, the homologs of CG7985 have been shown to cleave N-acetyl-β-D-galactosamine residues. This slight difference in substrate specificity might result in an important functional difference. Although other hexosaminidases have roles in chitin metabolism and N-Glycan biosynthesis, CG7985 has a presumed role in the ganglioside degradation pathway. We chose the *Drosophila* eye as a model to functionally characterize CG7985. The expression pattern and protein localization of CG7985 by means of different transgenic lines and a peptide antibody against CG7985 have revealed that it is localized to photoreceptor R7, in the morphogenetic furrow, and the anterior part of the eye imaginal disc. The accumulation of gangliosides due to defective degradation causes a particular type of well-known diseases called lysosomal storage disorders. In these disorders, the storage of waste products in lysosomes often results in enlargement and eventual rupture of lysosomes. This phenomenon, called lysosomal cell death (LCD), triggers apoptosis by a Cathepsin-mediated process. We have shown that the loss-of-function of *CG7985* by means of both analysis of mutant and RNAi knockdown resulted in the enlargement of lysosomes. Also, the cells with enlarged lysosomes have been shown to be apoptotic. An unexpected effect of the loss-of-function of *CG7985* was the overgrowth of the eye imaginal discs. In an attempt to understand this effect, we have analysed several signalling pathways and have shown that apoptotic cells induce compensatory proliferation in neighboring cells emitting a diffusible growth factor, Wingless.

ÖZET

ÖZGÜN BİR HEXOSAMİNİDAZ OLAN CG7985'İN *DROSOPHİLA* GÖZ GELİŞİMİNDE İŞLEVSEL KARAKTERİZASYONU

CG7985 *Drosophila* genomu tarafından ifade edilen dört hexosaminidazdan bir tanesidir. Diğer üç hexosaminidaz enzim aktivitesi ve rol aldıkları metabolik yolaklar yönünden iyi bir şekilde karakterize edilmiş olmalarına ragmen, CG7985 *Drosophila*'da karakterize edilmemiş tek hexosaminidazdır. CG7985'in filogenetik analizi göstermiştir ki omurgalılarda bulunan HexDC ve *C.elegans* HEX-2 ile aynı grup içinde bulunmaktadır ve böylece diğer *Drosophila* hexosaminidazlarından ayrılır. Hexosaminidaz ailesi içindeki evrimsel yan dallanma fonksiyonel bir farklılığın da göstergesidir. *Drosophila*'daki diğer üç hexosaminidaz özel olarak N-asetil-β-D-glukozamin kısımlarını keserken, CG7985 homologları HexDC ve HEX-2'nun özel olarak N-asetil-β-D-galaktozamin kısımlarını kesmektedir. Substrat özgünlüğündeki bu küçük farklılık önemli bir işlevsel farklılığa yol açabilmektedir. Diğer hexosaminidazlar kitin metabolizması ve N-Glikan biyosentezinde rol oynerken, CG7985'in gangliyozid yıkımında görev aldığı tahmin edilmektedir. CG7985'i işlevsel olarak karakterize etmek için biz *Drosophila* gözünü model olarak seçtik. Farklı transgenik suşlarla ve bir peptit antikoru yardımıyla CG7985'in ifade şeklinin ve protein lokalizasyonunun R7 fotoreseptöründe, farklılaşma dalgası içinde ve göz imaginal diskinin anteriyor tarafında konumlandığını gösterdik. Yıkımındaki sorunlar nedeniyle ganliyozid birikintilerinin iyi bilinen lizozomal depolama hastalıklarının bir türüne neden olduğu bilinmektedir. Atık maddelerin lizozomlarda birikmesi lizozomların genişlemesine ve ileri aşamalarda patlamasına neden olmaktadır. Bu durum lizozomal hücre ölümü (LHÖ) olarak bilinir ve Kathepsinlerin yer aldığı bir mekanizmayla hücreler apoptoza sürüklenir. Biz CG7985'in mutant veya anlatım azaltılması yoluyla işlevsel kaybının lizozomal genişlemelere sebebiyet verdiğini gösterdik. Ayrıca lizozomları genişleyen hücrelerin apoptotik oldukları da gösterildi. CG7985'in işlevsel kaybının beklenmeyen sonucu göz imaginal disklerinde aşırı büyümeye yol açmasıydı. Bu durumun da apoptotik hücrelerin Wingless adı verilen bir yayılabilir büyüme faktörünü salgılayarak komşu hücrelerde bölünmeyi tetiklediğini göstererek açıkladık.

TABLE OF CONTENTS

LIST OF FIGURES

LIST OF TABLES

LIST OF SYMBOLS

g	Gram
kb	Kilobase
L	Liter
ml	Mililiter
mm	Milimeter
M	Molar
ng	Nanogram
nm	Nanometer
rpm	Revolutions per minute
v	Volume
w	Weight
µg	Microgram
µm	Micrometer
µl	Microliter

LIST OF ACRONYMS/ABBREVIATIONS

DNA	Deoxyribonucleic Acid
dsRED	Discosoma Species Red Fluorescent Protein
EGFR	Epidermal Growth Factor Receptor
FRT	FLP Recombination Target
GFP	Green Fluorescent Protein
MF	Morphogenetic Furrow
NGS	Normal Goat Serum
PBS	Phosphate Buffered Saline
PFA	Paraformaldehyde
pH	Power of Hydrogen
PR	Photoreceptor
RNA	Ribonucleic Acid
RNAi	RNA Interference
RT-PCR	Reverse transcription polymerase chain reaction
UAS	Upstream Activating Sequence

1. INTRODUCTION

Almost everything that we know today is the result of curiosity. Curiosity, the irrepressible desire to know, is not the characteristic of dead matter. Instead, it is the result of thousands of thousands of years of evolution to structure unconscious matter as a substance which produces consciousness. Needless to say, it is the brain, which is complex, high-throughput living machinery with a tremendous capacity to receive, store, and interpret messages from the outside world. Perhaps, one of the hardest questions scientists ever face to answer is "how do millions of neurons form delicate structures by which different functions emerge?". One key to understand and find an answer to this question is to comprehend the developmental processes, which produce millions of neurons of specific types, locations, and a spectrum of interactions. Since the human brain has an extraordinary complexity that is beyond our understanding with present biotechnological tools, scientists generally take advantage of a reductionist approach, that is, they use simpler models like murine or insect brains. Although this approach contains a problem in itself like the applicability of findings in simpler models to more complex systems, it has been proven many times that organisms share biological processes throughout the evolutionary hierarchy. Taken this fact into account, the compound eye of the fruit fly *Drosophila melanogaster* with its neuronal networks formed by a small number of neurons is one of the most powerful models, and yet complex enough to attribute functional and organizational schemes of neurons to more complex systems. Besides, cheap breeding, short reproduction time and more importantly a great number of genetic manipulation tools make it an invaluable model in neurosciences (Moses *et al.*, 2001).

1.1. *Drosophila* Eye Development

The adult *Drosophila* eye consists of about 800 small, hexagonal facets called ommatidia. Each ommatidium contains 8 photoreceptor cells, R1 to R8, and 11 accessory cells, including lens secreting cone cells, pigment cells, and bristle cells (Maas *et al.*, 2010). Photoreceptors can be categorized into three groups according to the type of

rhodopsin they express and hence the ability to catch different wavelengths of light. Those from R1 to R6 are called outer photoreceptors. They express Rhodopsin 1 (Rh1), which detects a broader spectrum of light than other rhodopsins. Outer photoreceptors in *Drosophila* are the functional equivalent of rod photoreceptors in vertebrates. Like rod cells, they are specialized for motion detection in dim-lit environments. The other photoreceptors, R7 and R8, are called inner photoreceptors. They are the functional equivalent of cone photoreceptors in vertebrates and like them are specialized in color detection in well-lit environments. Unlike outer photoreceptors, they do not express the same kind of rhodopsins. R7 expresses either Rhodopsin 3 (Rh3) or Rhodopsin 4 (Rh4), which are sensitive to ultraviolet light. On the other hand, R8 expresses Rhodopsin 5 (Rh5) or Rhodopsin 6 (Rh6), which are sensitive to wavelengths in the blue and green spectrum, respectively (Silver and Rebay, 2005). The inner photoreceptors have also an important role in determining different subsets of ommatidia. The expression of different combinations of Rhodopsins in photoreceptors R7 and R8 give rise to different subsets of ommatidia. Rh3-expressing R7 photoreceptors are always coupled with Rh5 expressing R8 photoreceptors, which form pale ommatidia and Rh4-expressing R7 photoreceptors are always coupled with Rh6-expressing R8 photoreceptors, which form yellow ommatidia. In addition, at the dorsal outer edge of the eye, both R7 and R8 photoreceptors express Rh3, which form the third kind of ommatidia called dorsal rim area (DRA). DRA region is specialized to detect polarized light. (Morante *et al.*, 2007). Recently, another subset of ommatidia has been determined, called dorsal yellow ommatidia, in which one photoreceptor one Rhodopsin rule is broken. In dorsal yellow ommatidia, Rh3 and Rh4 coexpress in photoreceptor R7 but the underlying photoreceptor R8 still expresses Rh6. It has been shown that Iroquois-Complex (IroC) induces co-expression of Rhodopsins but the exact mechanism is yet to be elucidated (Mazzoni *et al*., 2008).

Formation of the exquisite structure of the *Drosophila* eye with a defined number of ommatidia is the result of a fine-tuned developmental program that is executed from embryogenesis to the end of morphogenesis. It is reasonable to divide this developmental program into three categories: (i) early eye development, in which retinal determination genes commit cells to the eye fate, (ii) formation of the growth center, in which the complex interaction of signaling pathways results in the formation of a growth center to increase the number of cells and volume of the larval eye disc, (iii) photoreceptor

specification, in which a certain number of cells are differentiated into photoreceptors in a sequential order.

1.1.1. Early Eye Development

Adult *Drosophila* compound eyes are derived from a monolayer epithelium called eye imaginal disc. During embryogenesis, a defined number of cells migrate towards a developmentally determined position in the embryo and start to grow there asynchronously from the rest of the organism to form the eye primordium (Held *et al.,* 2002). In the eye primordium, cells gain the so-called "eye fate" through the activation of a set of genes, which are collectively called retinal determination network (Figure 1.1a). Some of the experimentally determined members of the network are the Eyeless (Ey) which is the homolog of Pax6 genes in vertebrates, Twin of Eyeless (Toy), Pax6-like factor Eye gone (eyg), Twin of eyegone (Toe), Six family member Sine oculis (So), the zinc finger transcription factor Teashirt (Tsh), the protein phosphatase Eyes absent (Eya), and a homolog of the Ski/Sno oncogenes Dachshund (Dac) (Kumar *et al.,* 2011). In general, mutations in one or more of the genes in the retinal determination network cause complete failure of the formation of the eye. Conversely, ectopic activation of them at another position of the embryo causes formation of patches of eye tissue but not a fully-grown eye. Thus, the initial activity of the genes from the retinal determination network commits cells to a defined fate and affects the rest of the developmental program to form a fully developed adult eye tissue (Bonini *et al.,* 1993; Cheyette *et al.,* 1994; Weasner *et al.,* 2007; Yao *et al.,* 2008).

The retinal determination network is not organized in a strict hierarchy. In general, downstream elements in the network control the expression level of genes at the top of the network. Inside the retinal determination network is a core network, which constitutes a couple of genes that promotes eye specification and growth (Figure 1.1b). In this core network, Ey is a key transcription factor. It has been shown that loss-of-function of Ey causes a severe reduction in eye size (Quiring *et al.,* 1994). On the other hand, ectopic expression of *ey* rescues the growth defects in the eye (Jang *et al.,* 2003). Together, these observations suggest that Ey is one of the master regulators in the specification and growth

of the eye tissue. Ey exerts its effect on specification and growth by directly activating Sine oculis (So)-Eyes absent (Eya) complex. The loss of either member of So-Eya complex is characterized by a dramatic loss of adult eye tissue (Figure 1.1c). Although important in specification of eye tissue, So-Eya complex also regulates cell proliferation by binding to an enhancer element within the *stinger* (*stg*) locus, an important cell cycle gene in *Drosophila* (Jemc and Rebay, 2007).

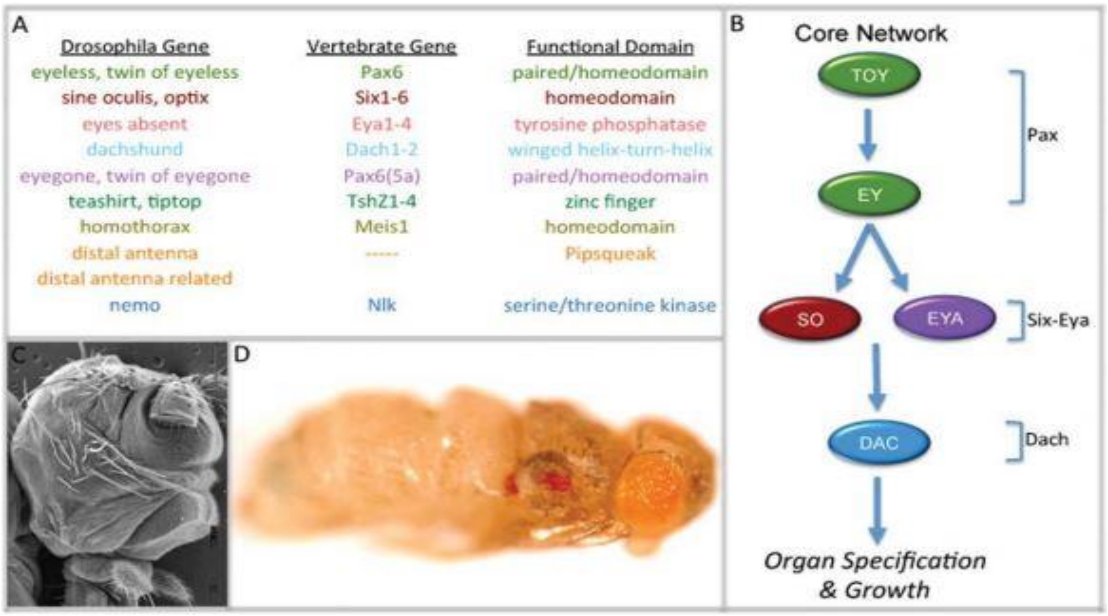

Figure 1.1. The retinal determination network: genes, pathways, loss and gain-of-function phenotypes. A: List of the retinal determination genes in flies, vertebrate homologs and functional domains. B: Core network pathway in the retinal determination network. C: Scanning electron microscope image of an eye absent mutant fly head. D: An adult fly in which eyeless is mis-expressed. Note red ectopic eye tissues on halters and wings (adapted from Kumar et al., 2011).

1.1.2. Formation of the Growth Center

In the *Drosophila* larval life cycle and also during eye development, there are three stages called instars. Initially, in the beginning of the first instar, the eye imaginal disc shows only ventral identity by the expression of a ventral selector gene called *lobe* (Singh *et al.*, 2003). At the end of the first instar stage, this homogeneity is broken when the expression of dorsal selector genes starts in a subset of the eye field. Through the second

instar, localized expression of ventral and dorsal selector genes generates two distinct areas in the eye field: ventral and dorsal (Singh *et al.,* 2005). Expression patterns of dorsal and ventral selector genes meet at the midline of the eye imaginal disc but never cross it. One of the most important dorsal selector genes in the eye is the *Iroquious-Complex* (*Iro-C*), which is actually not a single gene, but a complex of three genes called *araucan* (*ara*), *caupolican* (*caup*), and *mirror* (*mirr*). Analysis of *mirr* mutant clones in the dorsal side of the eye has been shown to cause dorso-ventral polarity reversals suggesting its necessity for cells to gain dorsal fate (McNeill *et al.,* 1997).

Splitting the eye imaginal disc into two compartments with distinct molecular identities has an important consequence on the growth of the disc. Iro-C, at the dorsal side, inhibits the expression of *fringe* (*fng*), which encodes for a *N*-acetylglucosaminyltransferase. The most important function of Fringe is to modify the Notch receptor by catalyzing the reaction of the attachment of *N*-acetylglucosamine residues to its EGF-like repeats (Moloney *et al,* 2000). By doing so, it modifies the Notch receptor in a way that it becomes responsive to one of its ligands, Delta (Dl), but cannot interact with its other ligand, Serrate (Ser) (Okajima and Irvine, 2002). The expression of *ser* is dependent on the ventral selector gene *lobe* and *fng* and the expression of *dl* is dependent on the expression of dorsal selector genes (Chern and Choi, 2002). Therefore, like the expression of the selector genes, the expression of Notch ligands is also restricted to distinct compartments. Since Fringe modifies the Notch receptor only at the ventral side and the modified Notch receptor can only interact with Delta, the only possible interaction between them takes place at the midline of the eye imaginal disc. In the same manner, since the unmodified Notch receptor at the dorsal side (due to lack of *fng* expression) can only interact with Serrate whose expression is restricted to the ventral side, again the only possible interaction between them takes place at the midline, although this time signal is transmitted in the reverse direction. This reciprocal transmission of Notch signal restricts the active Notch signalling in a stripe on the midline of the eye imaginal disc. Since the Notch signalling is an important factor for growth, the activated Notch signalling on the equator of the eye imaginal disc forms a growth center on this line (Figure 1.2a). The ubiquitous expression of *fng* or the loss-of-function of the Notch signalling completely block growth and the resulting adult eye resembles the mutants of effects of the retinal determination network genes (Dominguez and de Celis, 1998). Moreover, the activation of

Notch signalling causes overgrowth of the eye tissue (Reynolds-Kenneally and Mlodzik, 2005).

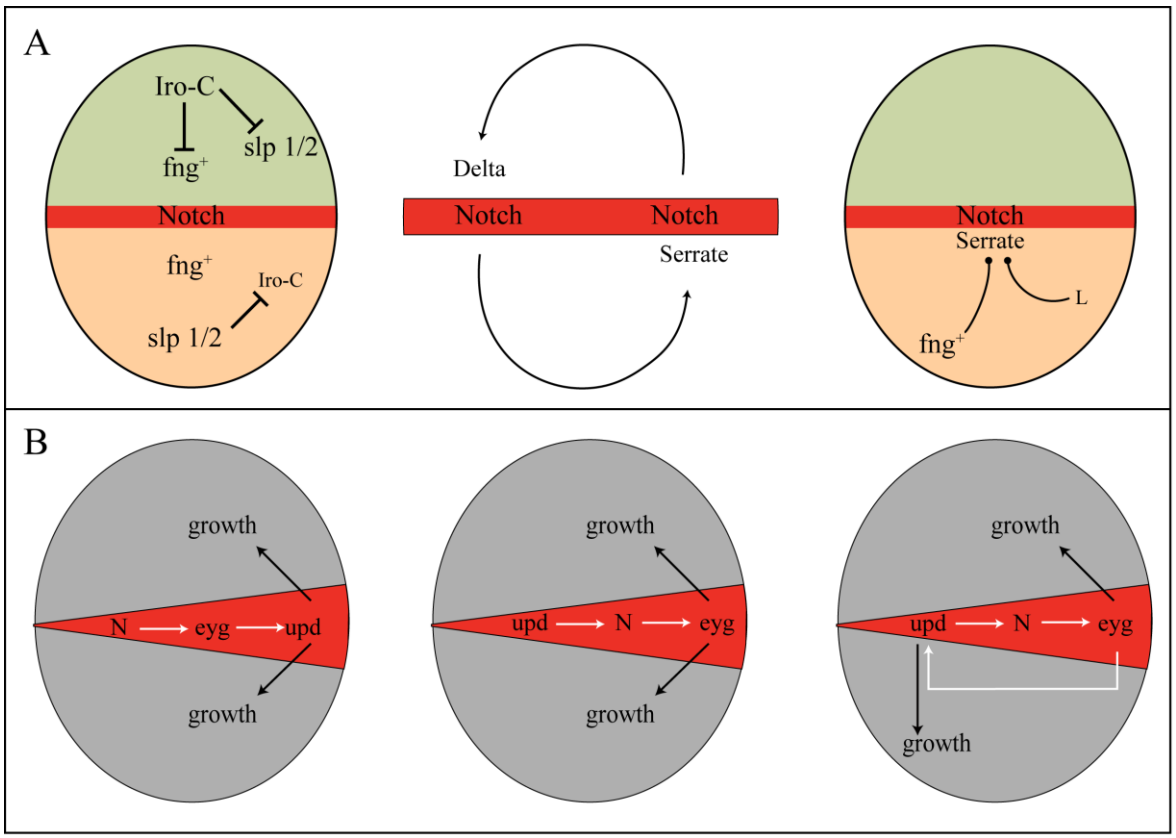

Figure 1.2. Formation of the growth center at the midline and Notch mediated growth signalling. A: Schematic diagram of the restricted Notch signalling to the midline by the activation of selector genes. B: Different models depicting the genetic hierarchy of Notch mediated growth in the eye (adapted from Kumar *et al*., 2011).

Restricted Notch signalling at the midline of the eye imaginal disc activates Notch effector genes, transcription factors, and other signalling cascades, downstream of it to mediate the growth of the eye. The first link between Notch signalling and the downstream effectors was identified by the comparisons of expression patterns. The expression of *eyegone* (*eyg*), a Pax-6 like transcription factor in flies, has been shown to overlap that of Notch signal activation at the midline (Yao *et al.,* 2008). A functional interaction between Notch signalling and Eyg has come from a series of studies, in which the forced expression of *eyg* has been shown to rescue the growth defects associated with the loss-of-function of *N*. In the same manner, the effects of over-activated Notch signalling have been shown to be reversed by the loss-of-function of *eyg* (Chao *et al.,* 2004; Dominguez *et al.,* 2004).

Therefore, the available findings so far point out that Eyg is a downstream effector of Notch signalling that promotes growth of the eye.

The JAK/STAT (Janus Kinase/Signal Transducers and Activators of Transcription) signalling cascade is proven to be one of the global regulators of the tissue growth. In *Drosophila*, the deficiency of the ligand of the JAK/STAT pathway, *unpaired* (*upd*), results in flies with small eyes. In contrast, the ubiquitous expression of *upd* in the eye causes excessive proliferation in the eye imaginal disc ending in overgrowth in the eye (Tsai and Sun, 2004). Like overlapped expression of *N* and *eyg*, the expression pattern of *upd* also matches with the region where Notch signalling is active (Tsai and Sun, 2004). There are two opposite thoughts about the place of the JAK/STAT pathway in the growth of the eye. One school of thought places the JAK/STAT pathway on the top of the growth control circuit claiming that it promotes Notch signalling activity and eventually Notch signalling activates *eyg* expression by which the growth signal is transmitted (Gutierriz-Avino *et al.*, 2009). On the other hand, the findings in the opponent's studies put forward that the JAK/STAT signalling is the downstream effector of Notch/Eyg coupling, in which Notch signalling sits at the top, activating *eyg* expression and eventually Eyg promotes the expression of *upd*. Since Upd is a diffusible factor, it diffuses from the posterior tip of the eye imaginal disc and mediates the omnidirectional growth of the disc (Figure 1.2b leftmost and middle figures). A great number of evidence supports the latter model. First of all, the loss-of-function of either *N* or *eyg* results in a reduction of *upd* expression while the forced expression of them causes an increase. Moreover, the loss-of-function of *upd* results in block of *N*/*eyg*-dependent growth (Chao *et al.*, 2004; Reynold-Kenneally and Mlodzik, 2005). Although these two models contradict each other, it is possible that both modes of growth control can co-exist together if the Notch and JAK/STAT pathways are incorporated by a positive feedback loop. In such a scenario, Eyg, promoted by Notch signalling, could contribute to the growth of the eye disc, while it promotes the expression of *upd* by a positive feedback loop (Figure 1.2b rightmost figure).

1.1.3. Photoreceptor Specification

The first and second instars of the larval eye development represent the stages for

commitment to the eye fate and enlargement of the eye imaginal disc by asynchronous cell divisions. Specification of photoreceptors and formation of ommatidial lattice begin in the third instar stage by the appearance of an indentation called the morphogenetic furrow (MF) (Ready *et al.,* 1976). The MF sweeps progressively from posterior to anterior of the eye imaginal disc. Undifferentiated and asynchronously proliferating cells reside in the anterior side of the MF, whereas cells posterior to it are organized in columns of regularly spaced ommatidia with differentiated photoreceptors. At the end of the third instar, an average of 30 ommatidial columns form through the entire retinal field (Tomlinson and Ready, 1987).

At the onset of the third instar, the expression of a secreted protein called Hedgehog (Hh) boosts at the posterior tip of the eye imaginal disc, which initiates the movement of the MF. Differentiated photoreceptors through the movement of the MF also start to express *hh*, which maintains the movement of the MF across the retinal field (Heberlein *et al.,* 1995). Other than Hedgehog signalling, Notch, Bone Morphogenetic Protein (BMP), JAK/STAT and EGFR pathways contribute to the initiation and progression of MF movement and differentiation of photoreceptors (Ekas *et al.,* 2006; Kumar and Moses, 2001; Wiersdorff *et al.,* 1996). However, the activity of these signalling cascades must be kept under a tight control to prevent formation of ectopic furrows. Findings so far suggest that this task is falls largely on Wingless (Wg) signalling. It is especially expressed at the anterio-lateral sides of the eye imaginal disc to regulate Dpp signalling. It has been shown that downregulation of Wg signalling results in ectopic eye formation and ubiquitous expression of *wg* causes complete failure of eye formation (Ma and Moses, 1995).

Differentiation of 8 photoreceptors in each ommatidium posterior to the MF is a sequential process. Inside the furrow, the preclusters of five cells are formed and through Notch-mediated lateral inhibition only one cell differentiates as photoreceptor. This very first differentiated cell is photoreceptor R8, which is also known as founder cell since it recruits other photoreceptors sequentially to form the final ommatidial lattice. The recruitment process occurs in a specific order, which is largely mediated by Spitz, the ligand of the EGFR pathway secreted by photoreceptor R8. The two cells adjacent to photoreceptor R8 receive this signal first and become R2 and R5 photoreceptors. Later, additional two cells are recruited into the emergent ommatidium and become

photoreceptors R3 and R4. Before the recruitment of other photoreceptors, a final round of cell division takes place in a stripe along the eye imaginal disc, which is called the second mitotic wave. Then, from the newly populated cells, first the R1 and R6 photoreceptor pair and finally photoreceptor R7 are recruited to the ommatidium (Moses *et al.*, 2001) (Figure 1.3).

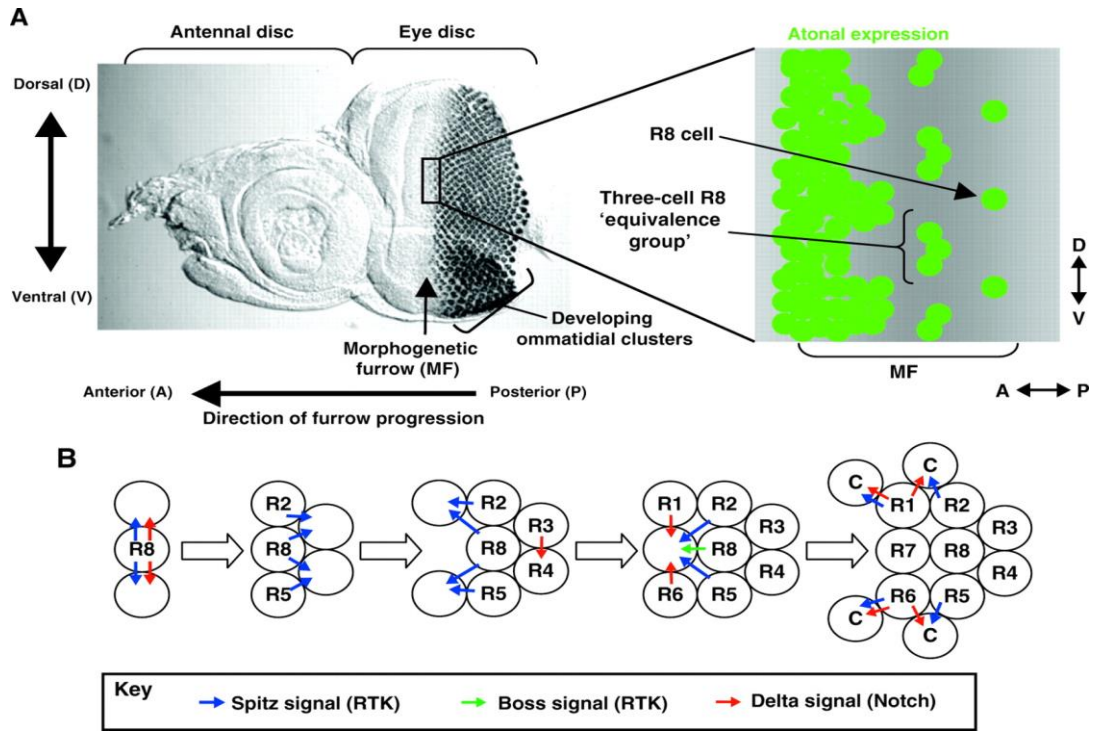

Figure 1.3. The sequential differentiation of photoreceptors in the third instar eye imaginal disc. A: Differentiation of R8 photoreceptors from equivalence groups through Notch-mediated lateral inhibition. B: Sequential recruitment of other photoreceptors and cone cells by the action of different signalling pathways (adapted from Graham *et al.*, 2010).

The differentiation of photoreceptor R7 has a special place among others. It requires signalling through two receptor tyrosine kinases, Sevenless (Sev) and EGFR. Unlike EGFR, which is activated by a diffusible growth factor Spitz, the ligand of Sev is a transmembrane protein called Bride of Sevenless (Boss). Sev is located on the membrane of photoreceptor R7 and Boss is located on the membrane of photoreceptor R8. Therefore, there must be a direct contact between photoreceptors R7 and R8 for the differentiation of photoreceptor R7. Boss is only expressed on the R8 cells, but Sev is expressed on several cells, including R1, R6, R3, and R4. After differentiation of R1, R6, R3 and R4, these cells start to express a transcription factor called Seven up (Svp). Svp prevents these cells to

receive the Boss-Sev signal so that only presumptive R7 cell receives this signal and differentiates. In Svp mutants, all four cells become extra R7 photoreceptors (Miller *et al.*, 2008).

1.2. Hexosaminidases and Their Roles in Ganglioside Metabolism

1.2.1. Metabolism, Function, and Traffic of Gangliosides

Eukaryotes and a few genus of bacteria contain a class of lipids called glycosphingolipids. Glycosphingolipids have two different parts in their structure, a ceramide backbone and a sugar head group. The ceramide backbone, being highly hydrophobic, is inserted in the cellular membrane, whereas its sugar head group floats mainly in the extracellular side of the cell. Gangliosides are one of the classes of glycosphingolipids containing sialic acid residues. They are the main surface glycans on neuronal cells comprising 10-20% of all lipids on their cellular membranes (Fahy *et al.*, 2005). Gangliosides are also classified according to the number of sialic acid residues attached to a galactose residue. There are four classes of gangliosides namely asialo-, a-, b-, and c-series that contains 0, 1, 2, 3 sialic acid residues, respectively (Yu *et al.*, 2007). The synthesis of gangliosides and other glycosphingolipids begins in the endoplasmic reticulum and they are further modified in the Golgi apparatus by the sequential addition of carbohydrate moieties. The addition of carbohydrates is catalyzed by specific glycosyltransferases.

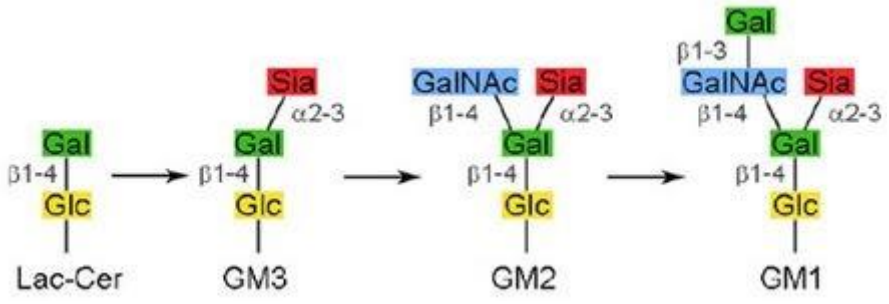

Figure 1.4. The synthesis of gangliosides sequentially from lactosylceramide backbone (adapted from Tsai *et al.*, 2003).

The synthesis starts on a lactosylceramide backbone. First, the simplest ganglioside GM3 is synthesized by the attachment of sialic acid to the lactosylceramide backbone. GM3 serves as a precursor for the synthesis of complex gangliosides. The addition of N-acetylgalactosamine (GalNAc) residue by β1-4-N-acetylgalactosaminyltransferase to GM3 forms GM2 gangliosides. GM2 ganglioside is further converted into GM1 by the addition of galactose (Gal) residue by β1-3 galactosyltransferase (Yu *et al.,* 2008) (Figure 1.4).

Gangliosides are found in every tissue, but they are especially enriched in the nervous system. Localizing to the plasma membrane, they are involved in cell-cell recognition, adhesion and signal transduction. Gangliosides are not randomly distributed on the plasma membrane. Instead, they are localized in specific cell surface microdomains called lipid rafts together with other membrane components such as sphingomyelins and cholesterol. Moreover, it has been shown that gangliosides are colocalized with signalling and adhesion molecules in lipid rafts (van Meer and Lisman, 2002). The importance of gangliosides has been revealed by the observation that lactosylceramide-deficient mouse embryos die at 7.5 days of development (Yamashita *et al.,* 1999). Other mouse models in which different kinds of ganglioside synthase enzymes are mutated also show the importance of the different kinds of gangliosides. Mutant mice lacking GM3 synthase exhibits enhanced insulin sensitivity due to increased phosphorylation of the insulin receptor (Yamashita *et al.,* 2003). Knock-out mice deficient for β1-4-GalNAc transferase exhibits decreased myelination, axonal degeneration as well as neural degeneration and glial enlargement (Sigiura *et al.*, 2005).

As stated before, gangliosides are synthesized in the lumen of ER and further modified in Golgi apparatus by the action of different glycosltransferases. Later, the fully modified gangliosides are transported in secretory vesicles and fused to the plasma membrane at specific positions in a way that their sugar backbones face the outer membrane leaflet. On the cellular membrane, they can be further modified by specific neuraminidases and eventually they will enter the endosomal-lysosomal pathway. Through recycling endosomes, a fraction of internalized gangliosides turn back to the plasma membrane to keep a balanced distribution of gangliosides in lipid rafts. On the other hand, the majority of them will be further transferred from early endosomes to late endosomes and finally to lysosomes to undergo sequential degradation by hydrolytic enzymes. The

monomers formed by the degradation of gangliosides are further transferred to the ER/Golgi network to synthesize new gangliosides. About 90% of the newly synthesized gangliosides are formed by the monomers of degraded gangliosides in the late endosome/lysosome system. Therefore, a healthy, sequential degradation of gangliosides in the late endosome/lysosome has prime importance to keep the amount of gangliosides on the plasma membrane balanced (Walkley *et al.*, 2004) (Figure 1.5).

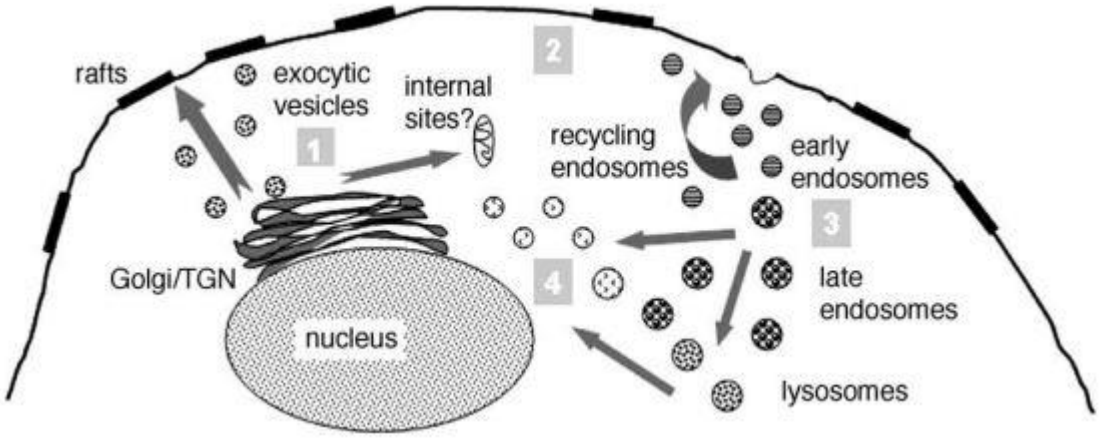

Figure 1.5. Schematic overview of the ganglioside trafficking. (1) Gangliosides are synthesized and modified in the ER/Golgi network and send to lipid rafts on the plasma membrane. (2) Some of the internalized gangliosides turn back to the plasma membrane by recycling endosomes. (3) The rest go through endosomal/lysosomal degradation pathway. (4) Monomers recycle back to the ER/Golgi network to built up new gangliosides (adapted from Walkley *et al.*, 2004).

1.2.2. Hexosaminidases

Hexosaminidases, a class in glycosyl hydrolase 20 family, are enzymes which catalyze the removal of terminal N-acetyl-β-D-glucosamine and N-acetyl-β-D-galactosamine residues. They are degradative enzymes located in late endosomes and lysosomes to mediate the degradation of gangliosides and other macromolecules with terminal N-acetyl-β-D-hexosamine residues. In *Homo sapiens* and all other vertebrates, there are three well-known isozymes namely Hexosaminidase A (HexA), Hexosaminidase B (HexB), and Hexosaminidase S (HexS), but recently another hexosaminidase called Hexosaminidase D (HexDC) was identified. *HexA* and *HexB* genes encode for α and β subunits, respectively. An α/β heterodimer forms HexA which is the primary enzyme

responsible for GM2 hydrolysis to convert it into the simpler GM3 ganglioside. β/β homodimer forms HexB and α/α homodimer forms HexS. HexA itself is unable to hydrolyze GM2 gangliosides. An activator protein called GM2 activator protein presents the ganglioside to be degraded by HexA (Hou *et al.,* 1996).

Unlike the well-studied lysosomal hexosaminidases, HexDC has been shown to be a nucleocytoplasmic enzyme. It has a preferential bias towards N-acetyl-β-D-galactosamine residues. Although it is a nucleocytoplasmic enzyme, its homologs in invertebrates have been shown to have a transmembrane domain. Therefore, unlike HexDC, they are not expected to be cytosolic enzymes (Gutternigg *et al.,* 2009). Recently, the expression level of HexDC has been shown to be elevated in synovial fluid samples and synovial membranes of rheumatoid arthritis patients. This is the only publication that shows that the activity of HexDC might have disease relevance (Pasztoi *et al.,* 2012).

1.2.3. Lysosomal Storage Disorders

Lysosomes are acidic organelles that are characterized by the presence of numerous lysosomal hydrolases. Macromolecules are delivered to lysosomes through the endosomal pathway to be degraded to their basic components by these hydrolases. Degradation of macromolecules and cellular waste products in lysosomes is important for the normal functioning of several cellular metabolic events such as signal transduction, cell division, and neurotransmission. Therefore, any disruption of the function of hydrolases leads to the accumulation of waste products, which is enough to drive cells to a diseased state (Parkinson-Lawrence *et al.,* 2010).

Lysosomal storage disorders (LSD) are a large group of about 50 diseases. Although the primary reason for the emergence of LSDs is the dysfunction of lysosomal hydrolases, proteins involved in vesicular trafficking and transport of molecules inside and outside of lysosomes have also been shown to cause similar phenotypes of LSDs (Hopwood and Brooks, 1997). Defects in ganglioside catabolism can be divided into two groups in which different kinds of hydrolases are defective. GM1 gangliosidosis, which is the result of dysfunction of β-galactosidase, can mainly be characterized by progressive psychomotor

deterioration. The onset and severity of the resulting disease can be different depending on the nature of the mutation (Caciotti *et al.,* 2011). GM2 gangliosidosis, which shows a broad spectrum of symptoms, including progressive neurological deterioration, neuronal apoptosis, visceromegaly etc. is the result of dysfunction in the β-hexosaminidase enzyme. There are two types of GM2 gangliosidosis. Tay-Sachs disease is the result of mutation in the *HexA* gene whereas mutation in *HexB* causes Sandhoff disease. Both are rare autosomal recessive genetic disorders. Symptoms like deterioration of nerve cells, mental and physical disabilities begin around the age of six months and result in death by the age of four (Gravel *et al.,* 2001).

After years of research, it is possible to list some conspicuous symptoms of both types of gangliosidosis in the nervous system. One change that appears to be unique to gangliosidosis is the formation of excess dendritic neurites sprouting from axon hillocks and the enlargement of axon hillocks which is called meganeurites. In normal neuronal cells, it has been discovered that there is a link between elevated number of GM2 bearing vesicles and the formation of new dendritic neurites. Therefore, the accumulation of GM2 gangliosides seems to trigger ectopic neurite formation by an unknown mechanism (Cox and Cachon-Gonzalez, 1998; Walkley *et al.,* 2000). One of the other symptoms prominent in gangliosidosis is the secondary storage of other substrates. Gangliosides and cholesterols are located together in lipid rafts on the plasma membrane. Sequestration of gangliosides in lysosomes is accompanied by the accumulation of cholesterols, which completely disrupts cholesterol turnover. Likewise, cholesterol accumulation due to the defective gene *npc1* also causes secondary accumulation of gangliosides (Pagano *et al.,* 2000). The discovery of the co-accumulation of lipid raft components in the endolysosomal system, which is referred to as log-jams, have revealed a fact that most of the signalling events are affected in LSDs since lipid rafts are the relay stations for signalling cascades (Ceresa and Schmid, 2000). Other than the aforementioned symptoms, most of the LSDs are linked to progressive neurodegeneration. In a mouse model of Tay-Sachs disease, GM2 ganglioside accumulation in lysosomes has been shown to cause neuronal death by apoptosis. Although the effect is prominent, the exact reason that triggers the apoptotic signal remains to be elucidated. It might be speculated that the accumulation of gangliosides causes swelling of lysosomes, which eventually leaks degradative enzymes to the cytosol leading to autolysis of the cells. Alternatively, disruption of the turnover of lipid raft components

might result in complete blockage or ectopic activation of signalling pathways with roles in the survival of the cells (Huang *et al.*, 1997).

1.2.4. *Drosophila* Models of Lysosomal Storage Disorders

Drosophila melanogaster is a versatile model that has been used in medical research over a century. It has been shown to be a good model for neurodegenerative disorders like Alzheimer's disease and Parkinson's disease and proven to give similar symptoms as in vertebrate conjugates for many other diseases. There are three well-known examples of LSD models in *Drosophila*. One of them is the result of a mutation in *dnpc1* gene. Like its vertebrate counterpart *npc1* gene, null mutant of *dnpc1* causes Niemann-Pick C disease which is characterized by the excessive accumulation of cholesterols in late endosomes and lysosomes. In *Drosophila*, the null mutant of *dnpc1* results in early lethality, which is attributed to decrease in the level of ecdysone hormone due to its cholesterol-dependent biosynthesis. *Dnpc1* null brains show an excessive increase in cholesterol level and progressive accumulation of multilamellar and multivesicular organelles in neurons, which leads neurodegeneration (Philips *et al.*, 2008). Another example of LSD in *Drosophila* is the result of a mutation in *benchwarmer* (*bnch*) gene. Bnch is predicted to be a lysosomal sugar carrier and its dysfunction has been shown to cause increased carbohydrate storage, which results in enlarged lysosomal and late endosomal inclusions. In adult null *bnch* flies, age-dependent synaptic dysfunction and neuronal degeneration, which causes decrease in neuronal viability have been observed (Dermaut *et al.*, 2005). The last example of LSD in *Drosophila* is the result of a mutation in the gene named *spinster* (*spin*). *Spin* has been characterized by the accumulation of autofluorescent lipofuscin-like pigments in mutant neurons. Lupofuscin accumulation in neurons is the characteristic of neurodegenerative disorders. Careful localization studies established that Spinster is a component of the late endosomes and Spinster-labelled organelles are mainly present in presynaptic nerve endings and throughout postsynaptic muscles in neuromuscular junctions. Spin mutants have been shown to lead to increased synaptic growth and this phenotype has been linked to increased Dpp signalling, which is the homolog of TGF-β signalling in vertebrates (Sweeney and Davis, 2002). Recently, Spin has been shown to control Dpp signalling during glial migration in the *Drosophila* eye. Normally, CNS-derived glial cells move from

the optic lobe to the eye imaginal disc following the axons of photoreceptor cells under the control of Dpp signalling. *Spin* mutants are characterized by glial overmigration, which is the result of excessive Dpp signalling. Therefore, it is obvious that Spin has an inhibitory role on Dpp signalling (Yuva-Aydemir *et al.*, 2011).

1.3. CG7985: A Novel Hexosaminidase in *Drosophila*

CG7985 is a novel *Drosophila* hexosaminidase that belongs to the GH20-GcnA-like family under the glycosyl hydrolase 20 hexosaminidase superfamily. The catalytic domain of GH20-GcnA-like family members catalyzes the reaction of the removal of terminal N-acetyl-β-D-galactosamine (NAG) residues. The enzymes in this family are known to be poisoned by first-row transition metals and especially the members in bacterial species are activated by forming homodimers (Langley *et al.*, 2007). The genomic locus of *CG7985* is about 14 kb long containing two exons and a large intron with possible enhancer elements preceding exons. It encodes for a hexosaminidase which is 708 amino acids long and about 82 kDa in mass.

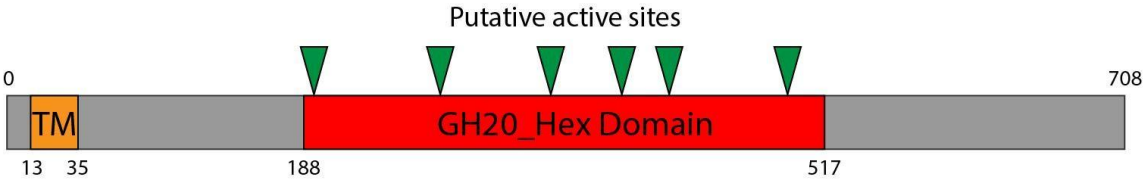

Figure 1.6. The protein structure of CG7985. There is a putative transmembrane domain (TM) between amino acids 13 and 35 and a hexosaminidase domain between amino acids 188 and 517 with its highly conserved, six putative active sites.

The primary amino acid structure of CG7985 contains a 20 amino acid long, highly hydrophobic region between amino acids 13 and 35, which presumably forms a transmembrane domain. Between amino acids 188 and 517, it contains a GH20-GcnA-like catalytic domain with a N-acetyl-β-D-galactosaminidase function. This region comprises six putative active sites which are highly conserved throughout the animal kingdom (Figure 1.6).

The *Drosophila melanogaster* genome encodes for four different hexosaminidases. Hexo1 and Hexo2 are hexosaminidases with roles in chitin catabolism. They cleave long, repetitive N-acetyl-β-D-glucosamine residues in the chitin structure. Moreover, Hexo1 has been shown to have role in N-glycan biosynthesis (Leonard *et al.*, 2005). The third kind of hexosaminidase, which is called Fused lobes (Fdl), is specific to the biosynthesis of N-glycans in invertebrates. It is the key enzyme to generate paucimannosidic N-glycans.

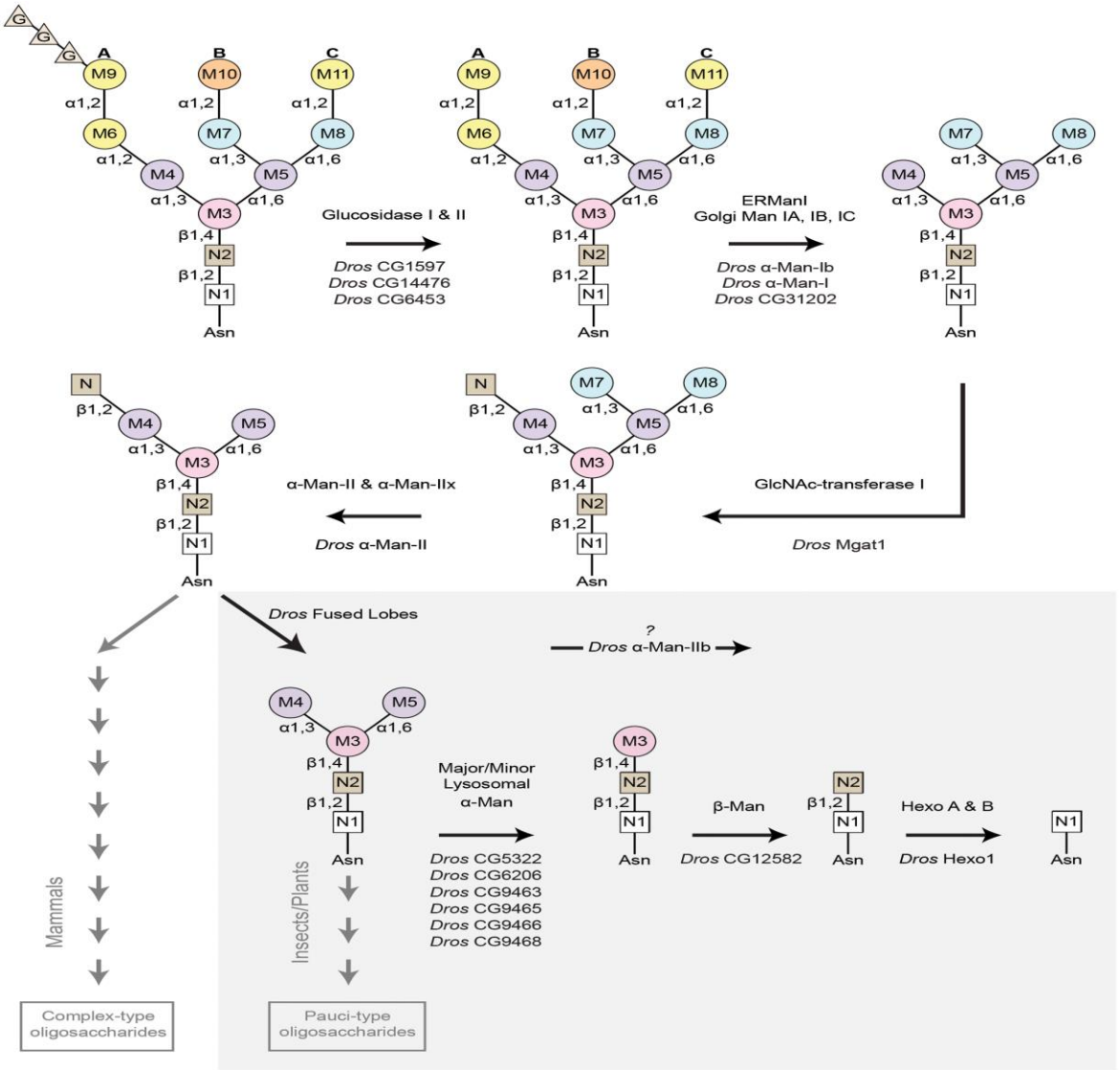

Figure 1.7. Different routes of the biosynthesis of N-glycans invertebrates and vertebrates. *Drosophila* Fused lobes is the key enzyme to generate paucimannosidic type of N-glycans in invertebrates by cleaving terminal N-acetyl-β-D-glucosamine residue. Hexo1 and different kinds of α- and β-mannosidases further trim N-glycans.

Normally, the majority of N-glycans in vertebrates are in a complex form, which is generated by the sequential action of different glycosyltransferases. On the contrary, in invertebrates, the biosynthesis of N-glycans follows almost the same pathway but in the end complex types of N-glycans are converted into simple, paucimannosidic types of N-glycans by the action of Fused lobe hexosaminidases and different kinds of mannosidases (Rosenbaum *et al.*, 2014) (Figure 1.7).

CG7985 differs from the other hexosaminidases having specificity to N-acetyl-β-D-galactosamine residues instead of N-acetyl-β-D-glucosamine. Fused lobes, Hexo1, and Hexo2 have all been shown to specifically cleave N-acetyl-β-D-glucosamine residues. Only Fused lobes has been shown to remove N-acetyl-β-D-galactosamine residues under extreme conditions (Dragosits *et al.*, 2015). The vertebrate homolog of CG7985, HexDC and the *C.elegans* homolog Hex2 have also been shown to be specific to N-acetyl-β-D-galactosamine residues (Dragotis *et al.*, 2015; Gutternigg *et al.*, 2009). Having this specificity, CG7985 is the only hexosaminidase in *Drosophila* to have a role in the ganglioside degradation pathway since an N-acetyl-β-D-galactosamine must be cleaved in the conversion of GM2 type of ganglioside into the basic GM3 type.

1.4. CRISPR/Cas9: A New Era in Genome Editing

For years, adaptive immunity, which is the result of cooperation of the complex cellular machinery and signalling pathways has been considered as a property of the eukaryotic immune system. However, recently, surprisingly sophisticated adaptive immunity that relies on small RNAs targeting specific sequences of foreign nucleic acids has been discovered in bacteria and archaea. Mechanism of this complex adaptive immunity can be called “molecular vaccination” since short sequence of foreign DNA is integrated into a repetitive locus in the host chromosome known as CRISPR and when bacteria or archaea is infected by the same invader, this sequence is used to recognize and degrade the invader’s genetic material (Sorek *et al.*, 2013).

CRISPRs were originally identified in the *E.coli* genome in 1987 as 29-nucleotide repeats separated by unique 32-nucleotide spacer sequences. Later, the same repeat-spacer-

repeat pattern was also identified in different bacteria and archaea genomes. However, the function of these repeats remained to be elucidated until it has been realized that many of these spacer sequences were identical to viral or plasmid sequences. Now it is clear that CRISPRs serve as a genetic memory of infection and it is a very efficient defence mechanism of bacteria and archaea against viral and plasmid infections (Wiedenheft *et al.*, 2012).

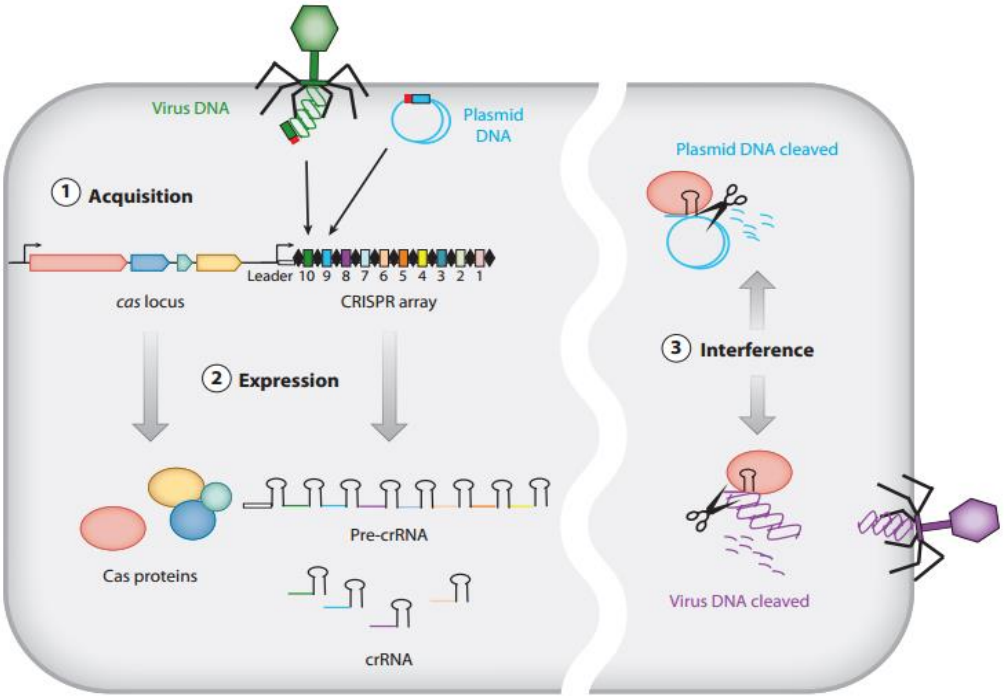

Figure 1.8. Three stages of CRISPR-mediated adaptive immunity. (1) In acquisition, a certain genomic region of the invader is recognized, cut and integrated into CRISPR locus. (2) In expression, CRISPR locus is expressed as a pre-crRNA and then further processed to generate crRNAs. (3) In interference, upon infection by an invader, a certain crRNA specific to infectious agent's genome recognizes region of interest and generates DSB by recruiting Cas9 endonuclease.

CRISPR-based adaptive immunity takes place in three stages: acquisition, expression, and interference. In the acquisition phase, upon infection by a virus or a plasmid, a certain machinery in the bacterial cell recognizes a specific region in the foreign DNA to cut it off and integrate into the CRISPR locus. Sequences in foreign DNA selected for integration are called protospacers, and these sequences are flanked by a short sequence motif called PAM sequence. In the expression phase, the CRISPR locus is initially expressed as a long precursor crRNA (pre-crRNA). Later, this long precursor is further

processed to generate a library of crRNAs in which each of them is specific for a certain region of the genome of one specific invader. In the type II system, which is modified as a genome editing tool, pre-crRNA is cleaved by host-encoded RNase III and another constituent of the system, transactivating cr-RNA (tra-crRNA). In the final phase, interference, when the same bacterium is infected with a virus or plasmid from which a certain DNA sequence has been previously taken and integrated into the CRISPR locus, the crRNA recognizes that DNA sequence and recruits Cas9 endonuclease to the target site with the help of tra-crRNA to generate DSB and hence degrade the genome of the invader (Sorek *et al.*, 2013) (Figure 1.8).

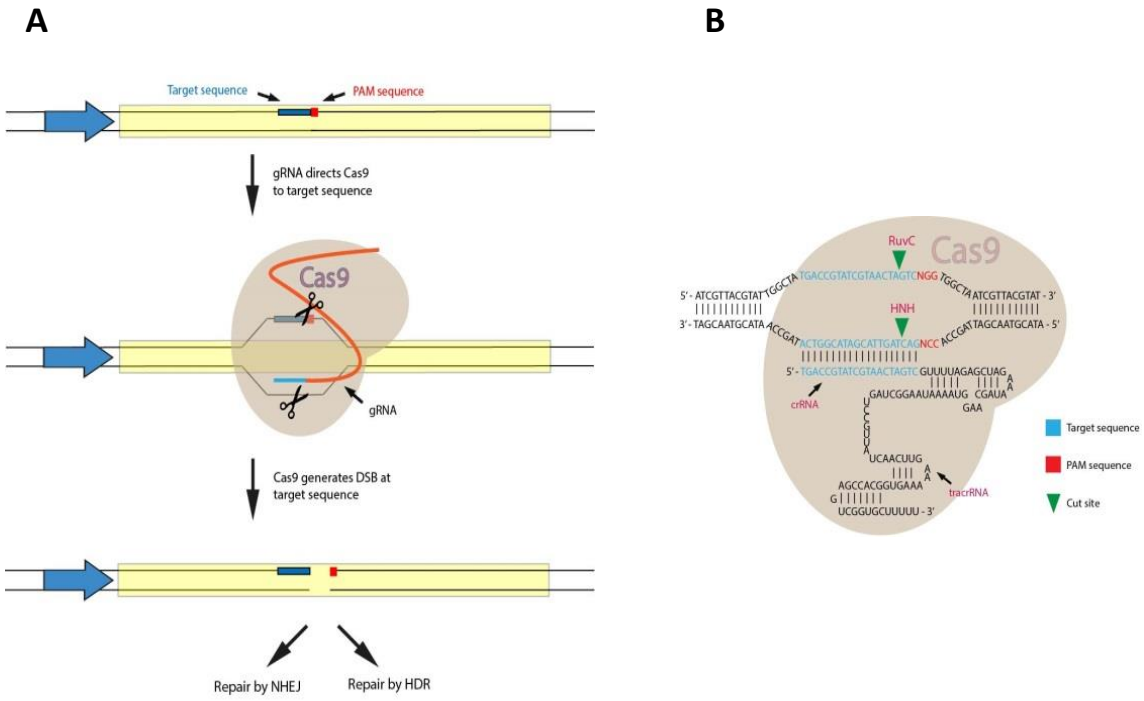

Figure 1.9. Generation of DSB by Cas9 endonuclease. A: crRNA (blue) complements with the target sequence and tra-crRNA (orange) to recruit Cas9 to generate DSB. B: The close view of crRNA-tracrRNA-Cas9 ternary complex loaded on target sequence to generate DSB.

As briefly stated before, there are three constituents of the CRISPR/Cas9 system that form a ternary complex to generate a DSB at the sequence of interest. crRNA complements with the target sequence to recruit Cas9 endonuclease to generate DSB. However, it has been shown that the presence of a noncoding RNA called tra-crRNA is necessary for Cas9 to function properly. There are two critical functions of tra-crRNA: triggering pre-crRNA

processing by the host enzyme RNAse III and subsequently activating crRNA-guided cleavage of DNA by Cas9. Furthermore, a single chimeric RNA, which constitutes both crRNA and tra-crRNA has also been shown to be active (Jinek *et al*., 2012). Cas9 endonuclease contains two single-strand specific nuclease domains namely HNH domain and RuvC-like domain. HNH domain generates a single-stranded break at the complementary strand whereas RuvC-like domain generates a single-stranded break at the noncomplementary strand. The simultaneous action of these two domains collectively generates a DSB (Ma *et al*., 2014) (Figure 1.9).

Generation of DSB activates DNA repair mechanisms inside the cell. As briefly stated before, there are two primary DNA repair pathways in the cell. One is dependent on homologous sequence (HDR) and the other one repairs DSB adding or deleting a couple of bases at the position of the DSB to seal the gap (NHEJ).

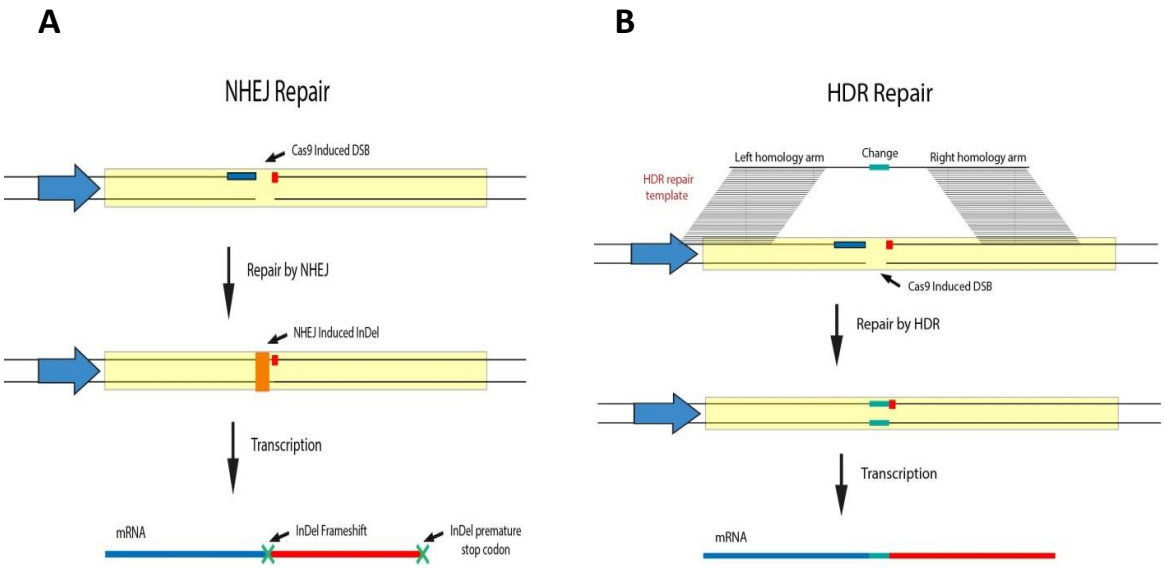

Figure 1.10. Schematic view of repair pathways upon DSB generation. A: NHEJ repair pathway. A couple of nucleotides are added or deleted to repair DSB generating frameshift mutation. B: HDR repair pathway. Homology arms are used by the cell to repair DSB. Meanwhile, a specific change between homology arms is integrated into the genome.

Unless a homology sequence is supplied to the cell, it will use NHEJ to repair DSB. Targeting one of the exons of a gene to generate DSB, NHEJ pathway will generate a frameshift mutation at the position of DSB by adding or deleting a couple of nucleotides. This induced frameshift mutation inside a coding exon will directly change the mRNA

sequence and subsequently the primary amino acid sequence of the protein that is translated by this mRNA. Therefore, using NHEJ is a very good strategy to generate a nonfunctional protein to reveal its function for the organism. On the other hand, when a homologous sequence is supplied to the cell, the cell will preferentially use the HDR pathway to repair the DSB. In this way, a specific DNA sequence flanked by two homology arms that are homologous to the target sequence can be inserted into the genome. The cell will use this homologous sequence to repair the DSB and a specific DNA sequence will be inserted into the genome at a specific position. Therefore, the HDR pathway is a great way to edit the genome at a desired position (Gratz *et al.*, 2014) (Figure 1.10).

1.5. Genetic Tools of *Drosophila*

1.5.1. Gal4/UAS System

The last two decades have seen an enormous increase in the number of genetic tools used in model organisms. This expansion is particularly apparent in *Drosophila melanogaster*. The Gal4/UAS system has a special place in a fly geneticist's swiss army knife, since it gives a chance to control expression of genes both in a spatiotemporal manner and in a specific tissue or cell population. As the name implies, the Gal4/UAS system relies on two components: Gal4, a transcriptional activator from the yeast *S.cerevisiae*, whose expression is bound to the activity of enhancer or promoter elements of specific genes and an upstream activation sequence (UAS) to which Gal4 binds to activate expression of a transgene that lies downstream of the UAS. Over the last decade, a vast number of Gal4 and UAS lines have been generated in *Drosophila* that cover almost all the annotated genes in the *Drosophila* genome. Since the Gal4/UAS system is a bipartite system, the transgene that lies downstream of UAS is not expressed in the absence of Gal4. Therefore, the only possible way to express a transgene under the control of UAS is to cross it with a specific Gal4 line. In this way, different combinations of Gal4 and UAS lines can be crossed together to observe the effect of the targeted gene in the offspring (Duffy *et al.*, 2002) (Figure 1.11).

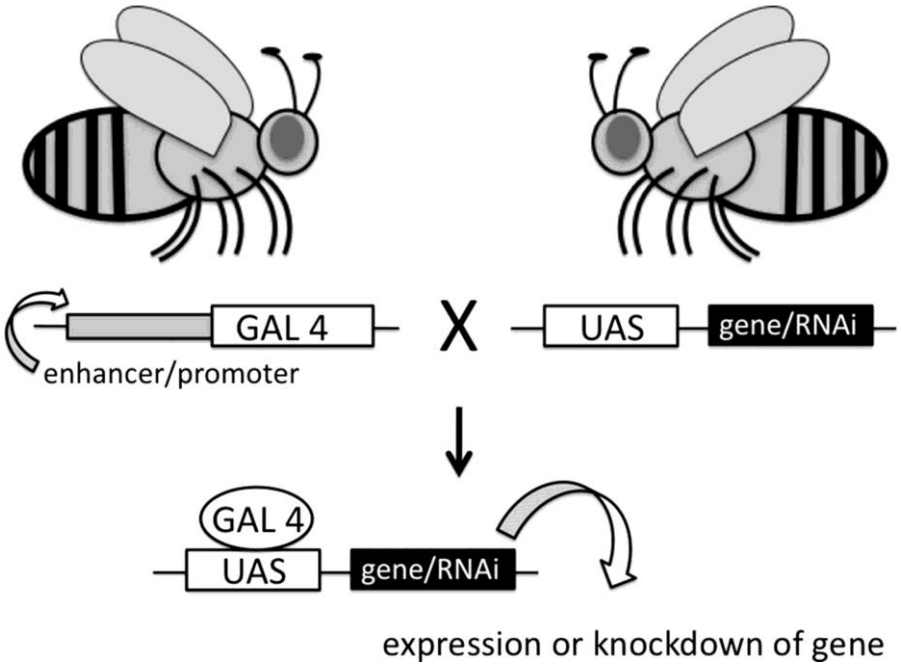

Figure 1.11. The Gal4/UAS binary system. A *Drosophila* line encoding Gal4 protein whose activity depends on upstream enhancer/promoter elements is crossed to a line containing UAS with a downstream gene or dsRNA sequence. The effect of expression or knockdown of a gene will be visible in the offspring (adapted from Neckameyer and Argue, 2012).

The powerful and yet simple nature of the Gal4/UAS system has also paved the way for its use in knockdown studies. Since it is possible to ectopically express any given sequence by this system, in a short time, a large repertoire of double-stranded RNAs (dsRNA) has been cloned to the downstream of UAS. The expression of dsRNA by the simple cross of a Gal4 and a UAS line has led to specific downregulation of the expression of a given gene in a given tissue by the destruction of mRNA molecules. This system is now used as a powerful alternative to mutant studies and since it is possible to downregulate the expression of a gene specifically in a given population of cells by using a Gal4 line with a restricted expression pattern, different functions of genes can be identified in different tissues or cell populations. Last but not least, this system made genome-wide screens to identify novel players in a given molecular process possible. In this way, several members of signalling cascades have been identified (Neckameyer and Argue, 2012).

1.5.2. Trapping the Fly: Enhancer Traps and Protein Traps

The trapping strategy in *Drosophila* and other model organisms makes use of transposable elements, which are DNA sequences that can change their position within the genome by jumping from one place to another. The basis of an enhancer trap strategy is to insert a P-transposable element (or P-elements in short) into the *Drosophila* genome. The difference between natural transposable elements and P-elements is that natural transposable elements contain the coding region for the enzyme, transposase, which makes the element constantly jump from one place to another. On the other hand, P-elements used in enhancer trap analyses have had the transposase gene completely removed. Once a P-element is inserted in a defined position in the genome, the *Drosophila* line carrying the P-element is crossed to another *Drosophila* line encoding a transposase to make the P-elements jumps to different positions in the genome. After generation of thousands of such lines in which P-elements are located in different positions, the lines are isogenized to get rid of transposase and prevent P-elements to jump further, making lines stable (O'Kane *et al.*, 1987).

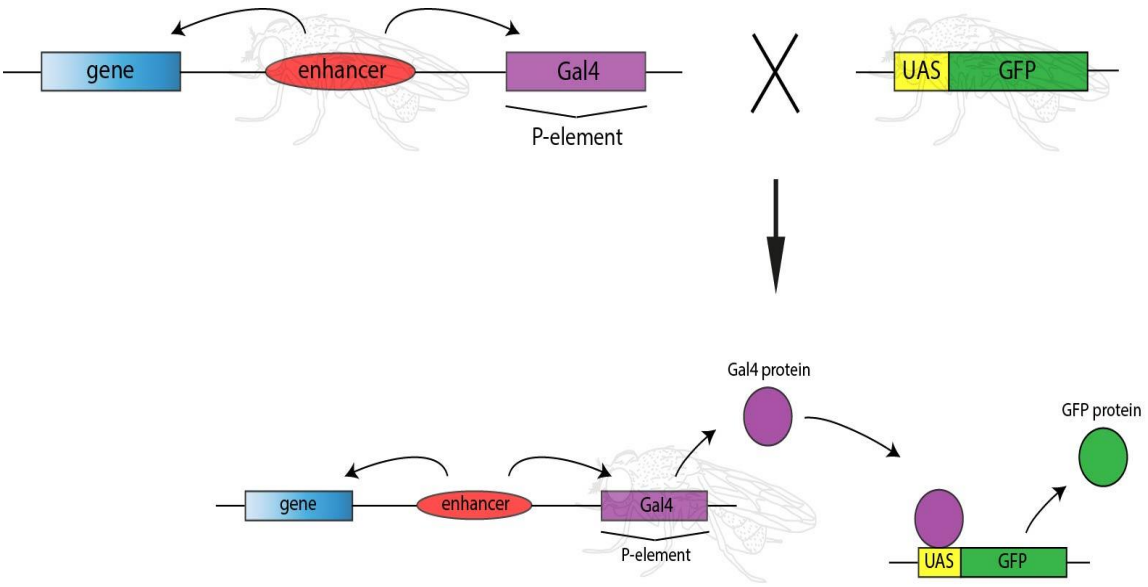

Figure 1.12 Schematic view of enhancer trap analysis. P-element containing minimal promoter and Gal4 coding sequence is inserted nearby an enhancer element. Enhancer elements activates the expression of both Gal4 and the nearby gene. When this line is crossed with a line containing GFP fused to UAS, Gal4 binds to UAS to activate GFP expression. GFP expression will mimic the expression of the nearby gene.

The P-elements that are inserted into the genome carry specific sequences other than transposable elements. Originally, they carried a reporter gene fused to a minimal promoter, which is activated by nearby enhancer elements. In later studies, the reporter sequence has been replaced with a Gal4 sequence to allow the use of the enhancer trap lines used in the Gal4/UAS system. Basically, when a P-element is inserted near an enhancer element, which normally activates the expression of a gene in close proximity, the same enhancer element also triggers the activation of the minimal promoter to express a reporter or the Gal4. In this way, the expression pattern of the reporter or Gal4 mimics the expression pattern of the nearby gene (Figure 1.12). Therefore, enhancer trap lines in *Drosophila* are useful to reveal the expression pattern of genes (Ward *et al.*, 2002).

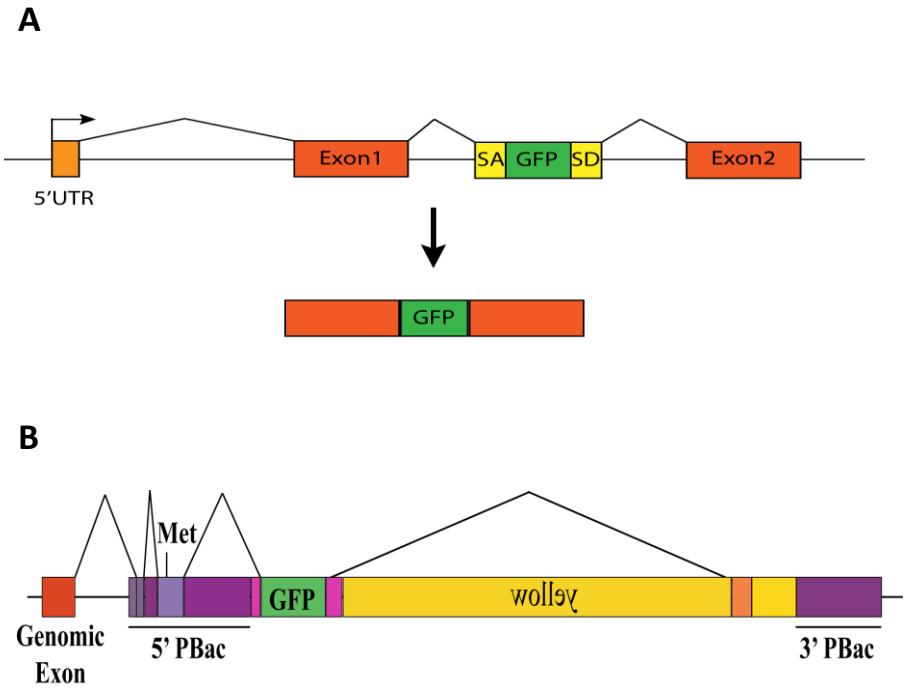

Figure 1.13. Different outcomes of GFP insertion in protein trap strategy. A: When GFP coding sequence with splicing acceptor and donor sequences inserted between two coding exons, a GFP tag protein is produced. B: When GFP coding sequence is inserted between 5'UTR and a coding exon, GFP might splice to cryptic exons that it finds inside the P-element. It generates a protein with GFP in it (adapted from Quinones-Coello *et al.*, 2006).

The generation of protein trap lines follows the same basic strategy with one difference. In protein trap lines, P-elements inserted into the genome do not contain minimal promoter fused to a reporter or Gal4 sequence. Instead, they contain a GFP

sequence which is flanked by splicing acceptor and donor sequences. Therefore, the GFP cannot be expressed on its own but it is spliced into the transcript if it is inserted into one of the introns of a gene. Thus, in protein trap lines, GFP-tagged proteins are produced in their endogenous loci (Figure 1.13a). The superiority of protein traps over enhancer traps is that they directly give information about the protein subcellular localization. Doing so, for most of the proteins, it makes the generation of antibodies for each protein unnecessary (Morin *et al.,* 2001).

Although the protein traps have originally been described as an integration of GFP protein inside the endogenous protein behaving like one of its exons, it is not the case for some integration events. If the GFP coding sequence with splicing sites is inserted between two coding exons, then it generates a tagged protein in which GFP is located between two protein regions encoded by endogenous exons. However, when the GFP sequence is inserted upstream of the coding exons, it can either generate a GFP-tagged protein from N-terminus or unexpectedly the GFP coding sequence is spliced with some cryptic exons from sequences inside the P-element and no tagged protein is produced. In such a case, a 25-30 kDa protein containing GFP is formed and the expression of GFP resembles the endogenous expression of the nearby gene. Normally, in such lines, it is expected that the endogenous expression level of the nearby gene is not affected but if the GFP coding sequence is inserted near the promoter elements of the nearby gene, then it might hinder the expression of the gene generating complete mutant lines or hypomorphs. It has been shown that the lethality rate in such lines is higher than the normal protein trap lines (Quinones-Coello *et al.,* 2006). Historically, both enhancer and protein traps have been used for mutant or hypomorph analysis if the insertion event has been shown to cause complete loss or decrease in the expression of the nearby gene.

1.5.3. Creating Mosaics by FRT/Flp-mediated Mitotic Recombination

Genome wide screens for mutations which affect different genes have revealed that many of the mutations cause embryonic or early lethality. Therefore, it is not possible to uncover the effects of those mutations in later stages of development when the whole organism is mutant. However, it is possible to limit the effects of loses or gains of genetic

functions to specific tissues or cell types or even to a defined developmental stage by using genetic mosaic techniques. Creating genetic mosaics can also be helpful even if the mutation is not lethal. In such a case, generating mutant clones in an otherwise wild-type tissue might show if the function of the gene of interest is needed cell autonomously or non-cell autonomously.

One of the last improvements in creating genetic mosaics in *Drosophila* is to make use of a specific DNA sequence and an enzyme which are derived from yeast. FLP recombinase is an enzyme which drives mitotic recombination between two FLPase recombination targets (FRTs). If a fly has two FRTs in identical positions on homologous chromosomes, the expression of FLPase can cause recombination between two FRT sites.

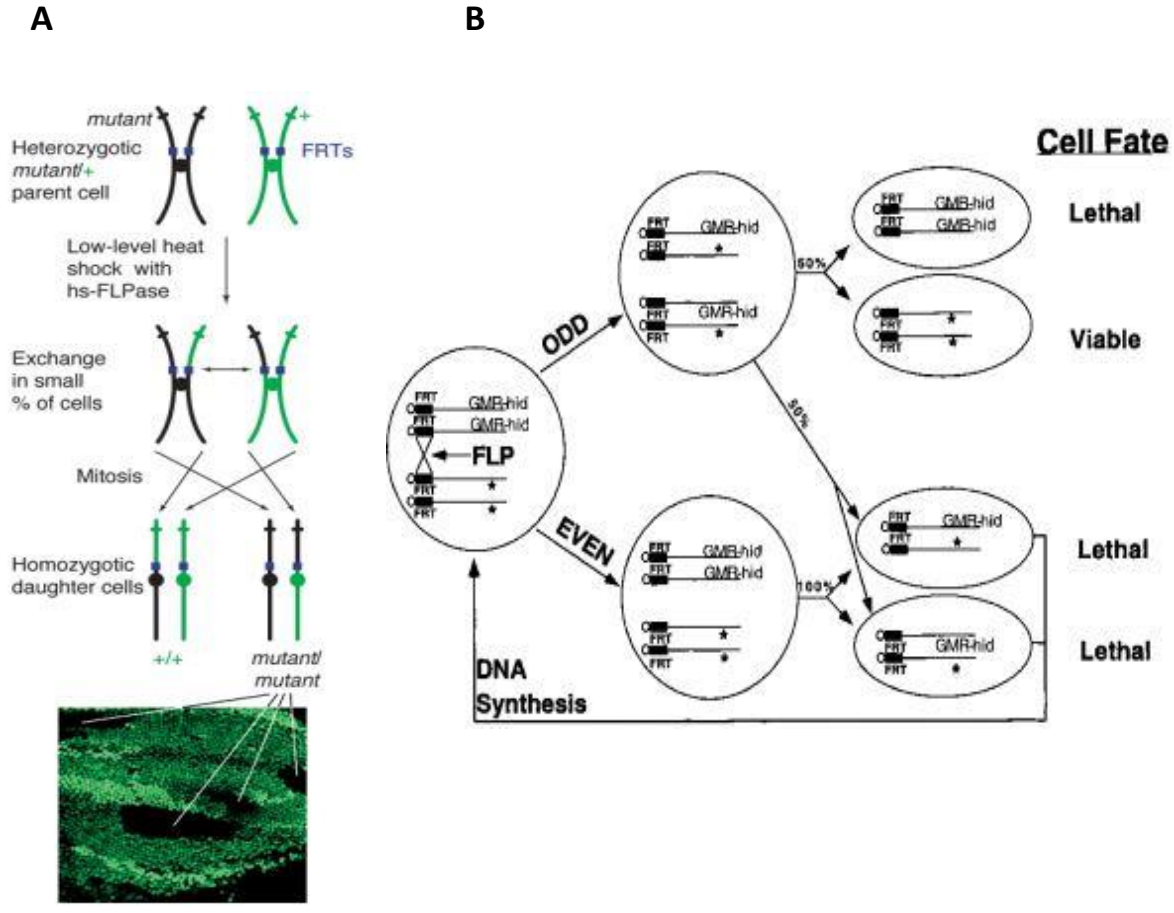

Figure 1.14. Genetic mosaic techniques by FRT/Flp system in *Drosophila*. A: Generation of mutant clones in an otherwise wild-type organism. The lack of reporter expression indicates the homozygous mutant tissue patches (adapted from Blair *et al.*, 2003). B: A method to generate whole eye mutants. Cells containing one or two copies of GMR-hid transgene are lethal and the only viable cells are those bearing the mutant of interest in homozygous state (adapted from Stowers and Schwarz, 1999).

In *Drosophila*, there are ready-to-use FRT lines in which FRT sequences are inserted at defined positions. Also, several FLPase lines have been generated, in which some of them are bound to the activity of certain tissue specific genes to generate clones only in a given tissue and some others are bound to the activity of a heat-shock promoter hence one can induce mitotic recombination in a defined temporal stage of development. The general usage of this system is to recombine one FRT source with the mutation of interest and the other one with a reporter. When this two lines are crossed to each other and FLPase induces the mitotic recombination, the exchange of chromosome arms will take place in a small population of cells generating homozygote clones in terms of both mutation and reporter. Therefore, the areas that lack reporter expression define the homozygous mutant clones (Blair *et al.*, 2003) (Figure 1.14a).

In the end of the last millennium, a genetic method to generate *Drosophila* eyes composed of mitotic clones of single genotype has been put at the disposal of fly geneticists. In this system, researchers combine the Gal4/UAS system and the FRT/Flp system. Specifically, they used an eye-specific Gal4 driver *ey*-Gal4 in combination with UAS-FLP to express FLP in mitotically active eye precursor cells creating the possibility for homozygous mitotic clones to be produced at cell division. The key and the third component of the system is the cell death gene *head involution defective* (*hid*), which is fused to the promoter of the photoreceptor specific gene *gmr*. When the mutation of interest and the GMR-hid transgene are recombined to FRT containing chromosome arms and mitotic recombination is induced by the eye specific expression of FLP, all the photoreceptors, which contain one or two copies of the GMR-hid gene will die, but cells which contain the mutant of interest in homozygous manner will be viable if the mutations do not cause lethality (Figure 1.14b). The advent of this method paved the way for analysis of eye phenotypes, by making the entire eye homozygous for the mutation. This technique eliminates the necessity to analyse phenotypes in small clonal patches (Stowers and Schwarz, 1999).

2. AIM OF THE STUDY

Hexosaminidases are known to be functioning in ganglioside degradation pathway in vertebrates. In *Drosophila* three well-known hexosaminidases Fused lobes, Hexo-1 and Hexo-2 have been shown to function in chitin metabolism and N-Glycan biosynthesis. Being an uncharacterized hexosaminidase, CG7985 has been proposed by us as the only hexosaminidase in *Drosophila* to function in ganglioside degradation pathway. This hypothesis depends on its different substrate specificity than other *Drosophila* hexosaminidases. In our study, we chose *Drosophila* eye as a model to functionally characterize CG7985. Our aim was to first show expression pattern and protein localization of CG7985 in the larval eye imaginal disc and then to show the effects of loss-of-function of CG7985 in the eye development by means of mutant and knockdown analysis. We hypothesized that our findings about the function of CG7985 in the *Drosophila* eye development will shed light on the possible functions of vertebrate HexDC, which is the homolog of CG7985.

3. MATERIALS AND METHODS

3.1. Biological Material

Flies were kept in incubators under constant temperature (25°C) and humidity (80%) in a 12:12 day:night cycle unless otherwise stated. Commercially available fly food (Nutri-Fly™ Bloomington Formulation, Genesee Scientific, USA) was prepared as 175 g fly food in 1 L of water with an addition of 6 ml of propionic acid per liter.

Table 3.1. *Drosophila melanogaster* strains used in this study.

Name of line	Chr. No.	Description
Gal4 Drivers		
AC887-Gal4	3	Gal4 sequence is inserted in the first intron of *CG7985* gene. Gal4 activity depends on the enhancer elements of *CG7985* gene.
act5c-Gal4	2	Expresses Gal4 under the control of the promoter of *actin* gene. It supplies ubiquitous Gal4 activity
ey-Gal4	2	Expresses Gal4 under the control of 3.5 kb of *eyeless* enhancer. Gal4 expressed in all eye cells except glia
gmr-Gal4	2	Expresses Gal4 under the control of the promoter of *gmr* gene. Gal4 expressed posterior to morphogenetic furrow in third instar eye imaginal disc
lgmr-Gal4	2	Expresses Gal4 under the control of the promoter of *gmr* gene. Its activity is enhanced compared to *gmr*-Gal4 line
moody-Gal4	2	Expresses Gal4 under the control of the promoter of *moody* gene. Gal4 specifically expressed in subperineurial glial cells.
repo-Gal4	3	Expresses Gal4 under the control of the promoter of *repo* gene. Gal4 specifically expressed in all glial cells.
UAS Constructs		
UAS-Dicer2	1	Expresses Dicer2 under the control of UAS
UAS-GFP.nls	2	UAS fusion to cDNA of GFP with a nuclear localization signal

Table 3.1. *Drosophila melanogaster* strains used in this study (cont.).

UAS-GFP.nls	3	UAS fusion to cDNA of GFP with a nuclear localization signal
UAS-mCD8:GFP	2	mCD8 membrane protein fused to GFP and their expression is controlled by UAS
UAS-*CG7985*-RNAi	2	Expresses double stranded RNAi of *CG7985* under the control of UAS
UAS-*CG7985*	2	Expresses cDNA of *CG7985* under the control of UAS
UAS-*Rab4*:mRFP	2	*Rab4* is fused with RFP and their expression is controlled by UAS. It labels early endosomes
UAS-*Rab7*:mRFP	2	*Rab7* is fused with RFP and their expression is controlled by UAS. It labels late endosomes
UAS-*Rab7*:mRFP	3	*Rab7* is fused with RFP and their expression is controlled by UAS. It labels late endosomes
UAS-RFP.Golgi	2	RFP is tagged with Golgi localization signal and its expression is control by UAS. It labels Golgi
UAS-RFP.KDEL	3	RFP is tagged with ER localization signal and its expression is control by UAS. It labels ER
UAS-*dpp*:LacZ	3	*Decapentaplegic* is tagged with LacZ and its expression is controlled by UAS.
UAS-*dpp*:GFP	3	*Decapentaplegic* is tagged with GFP and its expression is controlled by UAS.
UAS-*N*-RNAi	2	Expresses double stranded RNAi of *Notch* under the control of UAS
UAS-N^{EC}	1	Expresses dominant negative form of *Notch* under the control of UAS
General Stocks		
y w	1	Yellow body color and white eye phenotype
w^{1118}	1	White eye phenotype
CG7985 (BAC)	2	Transgenic *CG7985* construct inserted in the genome by BAC recombineering
CG7985:eGFP (BAC)	2	Transgenic *CG7985* construct fused with GFP inserted in the genome by BAC recombineering
$CG7985^{CPTI100032}$	3	Protein trap line of *CG7985* in which GFP sequence with splice acceptor and donor sites is inserted in the first intron of *CG7985*
$CG7985^{CPTI100032}$, FRT82B	3	Protein trap line of *CG7985* is recombined with FRT site on 82B map position
FRT82B	3	FRT site on 82B map position
FRT82B, *GMR-hid*	3	Expresses eye-specific cell-death gene, *hid*, recombined to an FRT site on 82B map position
FRT82B, *GMR*-myrRFP	3	Expresses eye-specific membrane-targeting RFP recombined to an FRT site on 82B map position

Table 3.1. *Drosophila melanogaster* strains used in this study (cont.).

y, *vasa*-Cas9, U6-tracrRNA	1	Expresses germline specific Cas9 protein under the control of *vasa* promoter and expresses transactivating crRNA under the control of *Drosophila* U6 promoter
w, Lig4[169]	1	Expresses mutated form of Ligase 4
Balancers and Markers		
CyO	2	Balancer chromosome with curly wings
Sp	2	Supernumerary bristles marker
TM2	3	Balancer chromosome with large halteres and/or with bristles on halteres
TM6B	3	Balancer chromosome with humeral and tubby markers

3.2. Chemicals and Supplies

Chemicals used in this study were obtained from Fisher Scientific, Sigma Aldrich, Molecular Probes or Roche unless stated otherwise.

3.2.1. Chemical Supplies

The chemicals used in this study are listed in Table 3.2.

Table 3.2. List of chemicals used in this study.

Chemical	Manufacturer
1 kb Marker	NEB, USA (N3232L)
Bovine Serum Albumin	Sigma-Aldrich, USA (A9647)
EDTA	Sigma-Aldrich, USA (59417C)
Ethidium Bromide solution	Sigma Life Sciences, USA (E1510)
$MgCl_2$	Riedel-de Haen, Germany (13152)
NaCl	Sigma-Aldrich, USA (S7653)
Normal Donkey Serum (NDS)	Millipore (S26-100ML)
Paraformaldehyde	Sigma-Aldrich, USA (P6148)
Sodium Deoxycholate	Sigma-Aldrich, USA (30970)
Tris	Sigma-Aldrich, USA (T6066)
Triton X-100	AppliChem, USA (A4975)
Trizol	MRC, USA (TR118)

3.2.2. Buffers and Solutions

Buffers and solutions in this study are listed in Table 3.3 with their contents.

Table 3.3. Buffers and solutions used in this study.

Buffer/Solution	Content
Formaldehyde Solution (16%)	8 g paraformaldehyde in 50 ml dH_2O 1M NaOH until solution becomes transparent
Grinding Buffer	0.2 M Sucrose 0.1 M Tris, pH 9.2 50 mM EDTA 0.5% SDS
LB Agar	5 g/L NaCl 10 g/L Tryptone 5 g/L Yeast extract 14 g/L Agar
LB Broth	5 g/L NaCl 10 g/L Tryptone 5 g/L Yeast extract
Non-ionic Lysis Buffer	20 mM Tris-Cl pH 8.0 50 mM NaCl 1% NP-40 2 mM EDTA 1X Roche Protease Inhibitor Cocktail
PaxDD	10 g BSA 3 g Sodium Deoxycholate 3 ml Triton X-100 50 ml Normal Donkey Serum 100 ml 10X PBS dH_2O to 1 L
PBS (1X)	137 mM NaCl 2.7 mM KCl 10 mM Na_2HPO_4 1.8 mM KH_2PO_4
PBX3	0.3% Triton X-100 in 1X PBS
RIPA Buffer	150 mM NaCl 1.0% Triton X-100 0.5% Sodium deoxycholate 0.1% SDS 50 mM Tris, pH 8.0

Table 3.3. Buffers and solutions used in this study (cont.).

Running Buffer (1X)	25 mM Tris 192 mM glycine 0.1% SDS
Squishing Buffer	10 mM Tris, pH 8.0 1 mM EDTA 25 mM NaCl
TAE buffer (1X)	40 mM Tris-Cl 1 mM EDTA 0.1% Acetic acid
TBS (1X)	50 mM Tris-Cl, pH 7.5 150 mM NaCl
TBS-T	0.05% Tween 20 in TBS
Transfer Buffer (1X)	25 mM Tris 192 mM glycine 20 % methanol

3.2.3. Oligonucleotide Primers

Primers were diluted with dH_2O to obtain a final concentration of 100 pmol/µl. Diluted primers were stored at -20 °C. CRISPR_HA_F and CRISPR_HA_R primers stand for 20 bp short primers used to amplify 3 kb genomic region containing 5' and 3' gRNA targets in the middle. CRISPR_HA_overhang primers are 70 bp long primers that contain 50 bp of common region to both ends of homology arms and linearized vector backbone, which were later used in Gibson assembly reaction. 3 kb PCR products from previous reactions are used as templates to generate 1.5 kb homology arms with corresponding overhangs. The rest of the CRISPR primers are used to determine the presence of inserts in the *Drosophila* genome after homologous recombination has taken place. A detailed protocol of the CRISPR experiment is given in section 3.6.

Table 3.4. Primers used in the course of this study.

Primer Name	**Primer Sequence (5' to 3')**	**T_m °C**
CRISPR_5'HA_F	GCATTTTTCTGCCTCATAAC	54.3
CRISPR_5'HA_F_overhang	CGTTGTAAAACGACGGCCAGTGAATTGTAA TACGACTCACTATAGGACTGGCATTTTTCTG CCTCATAAC	84.8

Table 3.4. Primers used in the course of this study (cont.).

CRISPR_5'HA_R	GTTGTGGGCGGATTTATATA	54.3
CRISPR_5'HA_R_overhang	TTTTTTCACTGCCCCCAACTGAGAGAACTCAAAGGTTACCCCAGTTGGGGCTATATAAATCCGCCCACAAC	87
CRISPR_3'HA_F	GGTATACGACGAGTACACGG	60.5
CRISPR_3'HA_F_overhang	CCCTTTAGTGAGGGTTAATTCCGAGCTTGGCGTAATCATGGTCATAGCTGGTATACGACGAGTACACGG	87.1
CRISPR_3'HA_R	CAAGAAGAGAGCTCGCCCGG	64.6
CRISPR_3'HA_R_overhang	CCGGGGCGAGCTCTAGCTCTAATTGAATTAGTCTCTAATTGAATTAGATCCCCGGGCGAGCTCTCTTCTTG	87.1
CG7985_up_seq_F	ATTCCCGAAATAAGCGCAAC	56.4
CG7985_up_seq_R	GGCGCCAAATAAATATCCAA	54.3
CG7985_dn_seq_F	AGGGCTGCAACTACGAAATG	58.4
CG7985_dn_seq_R	TGAACTGTCCATACCCAGCA	58.4
Insert_up1-2_attP_R	CCCCCTGAACCTGAAACATA	58.4
Insert_up1-2_3xp3_F	ACTCTAGCGGTACCCCGATT	60.5
Insert_dn_3xp3_R	TGGAACTTCGCGTACTTGAG	58.4
RT-PCR_junc_fwd	ACGAACTGCGGGACTTCCTC	62.5
RT_PCR_exon2_rev	GTCTCTGTGGCCAAGTGCGT	62.5
RT-PCR_junc_rev	GAGGAAGTCCCGCAGTTCGT	62.5
RT-PCR_exon1_fwd	TGTCTGGCCTGGTGCTTCTC	62.5

3.2.4. Antibodies

Primary and secondary antibodies used in the immunohistochemistry experiments are listed with their dilution ratios in Table 3.4. All primary antibodies were kept at 4°C and the secondary antibodies were kept at -20°C. For the dilution of primary and secondary antibodies, the blocking solution PAXD was used. Dilution of Alexa secondary antibodies was 1:800 except when they are used after the incubation of tissues with anti-GFP antibody (Abcam). In that case, secondary antibodies were diluted to 1:200 with the blocking solution PAXD. High noise-to-signal ration of this anti-GFP antibody was also eliminated by increased washing time with PBX3.

Table 3.5. Antibodies used in the course of this study.

Name	Antigen	Species	Dilution	Source
Primary Antibodies				
Anti-β-gal	β-galactosidase	Rabbit	1:5000	Cappel
Anti-Elav	Elav	Mouse	1:20	DSHB (9F8A9)
Anti-Elav	Elav	Rat	1:20	DSHB (7E8A10)
Anti-GFP	GFP	Chicken	1:1000	Abcam (ab13970)
Anti-GFP	GFP	Rabbit	1:500	Torrey Pines (TP401)
Anti-Pros	Prospero	Mouse	1:20	DSHB (MR1A)
Anti-Repo	Repo	Mouse	1:20	DSHB (8D12)
Anti-Wg	Wingless	Mouse	1:20	DSHB (4D4-s)
Anti-pH-H3	Phospho-histone H3	Mouse	1:100	Temecula (3H10)
Anti-pH-H3	Phospho-histone H3	Rabbit	1:100	Cell Signaling (S10)
Anti-Cas3	Caspase 3	Rabbit	1:200	BD Pharmingen
Anti-Dl-ext	Extracellular domain of Delta	Mouse	1:50	DSHB (C594.9B-s)
Anti-N-ext	Intracellular domain of Notch	Mouse	1:50	DSHB (C17.9C6-s)
Anti-N-int	Extracellular domain of Delta	Mouse	1:50	DSHB (C458.2H-s)
Secondary Antibodies				
Alexa 488	Chicken	Goat	1:200	Invitrogen
Alexa 488	Rabbit	Goat	1:800	Invitrogen
Alexa 488	Rabbit	Donkey	1:800	Invitrogen
Alexa 555	Mouse	Donkey	1:800	Invitrogen
Alexa 555	Rabbit	Goat	1:800	Invitrogen
Alexa 633	Rat	Goat	1:800	Invitrogen
Alexa 647	Rat	Donkey	1:800	Invitrogen
Alexa 647	Rabbit	Goat	1:800	Invitrogen
Cy3	Mouse	Goat	1:800	Invitrogen

3.2.5. Embedding Media

Tissues which have been stained with fluorescent substrates and dyes were embedded in Vectashield Embedding Medium (Vector Laboratories, Inc). Embedded tissues were kept at 4 °C until visualized by confocal microscopy.

3.2.6. Disposable Labware

Disposable labware used during this study are given in Table 3.6.

Table 3.6. Disposable labware used in this study.

Material	**Manufacturer**
Culture tubes (14 ml)	Greiner Bio-One, Belgium
Filter Tips	Greiner Bio-One, Belgium
Microscope cover glass	Fisher Scientific, UK
Microscope slides	Fisher Scientific, UK
PCR tubes (200 µl)	Bio-Rad, USA
Petri Dishes, 60 x 15 mm	TPP Techno Plastic Products AG, Switzerland
Pipette Tips	VWR, USA
Plastic Pasteur pipettes	TPP Techno Plastic Products AG, Switzerland
PVDF membrane	Roche Life Science
Syringe (1cc)	Becton, Dickinson and Company, USA
Syringe (2cc)	Becton, Dickinson and Company, USA
Syringe (5cc)	Becton, Dickinson and Company, USA
Test Tubes, 0.5 ml	Citotest Labware Manufacturing, China
Test Tubes, 1.5 ml	Citotest Labware Manufacturing, China
Test Tubes, 2 ml	Citotest Labware Manufacturing, China
Test Tubes, 15 ml	Becton, Dickinson and Company, USA
Test Tubes, 50 ml	Becton, Dickinson and Company, USA

3.2.7. Equipment

Equipment used in this study is listed in Table 3.7.

Table 3.7. Equipment used in this study.

Equipment	Manufacturer
Autoclave	Astell Scientific Ltd., UK
Centrifuges	Eppendorf, Germany (Centrifuge 5424, 5417R)
Confocal Microscope	Leica Microsystems, USA (TCS SP5)
Electrophoresis Equipment	Bio-Rad Labs, USA
Fluorescence Stereomicroscope	Leica Microsystems, USA (MZ16FA)
Freezers	Arçelik, Turkey
Gel Documentation System	Bio-Rad Labs, USA (Gel Doc XR)
Heating Block	Fisher Scientific, France
Heating Magnetic Stirrer	IKA, China (RCT Basic)
Incubator	Weiss Gallenkamp, USA (Incubator Plus Series)
Laboratory Bottles	Isolab, Germany
Micropipettes	Eppendorf, Germany
Microwave oven	Vestel, Turkey
Mini-PROTEAN Tetra Cell	Bio-Rab Labs, USA
pH meter	WTW, Germany (Ph330i)
Refrigerators	Arçelik, Turkey
Stereo Microscope	Olympus, USA (SZ61)
Thermal Cycler	Bio-Rad Labs, USA (C1000 Thermal Cycler)

3.3. Histological Methods

3.3.1. Immunohistochemistry

Third instar wandering larvae were placed one by one in a drop of PBS on a dissecting silicon pad. Eye discs were dissected as attached to the mouth hook and brain, and collected in PBS in a glass staining dish sitting on ice. Tissues were fixed with 4% paraformaldehyde (PFA) in PBS for 15 min on a shaker at 200 rpm at room temperature. Then, tissues were washed for three times with PBX3 for 10 min. Blocking was done with PAXDD solution for 2 hours at room temperature. After blocking, primary antibodies were diluted in PAXDD and the tissues were incubated overnight at 4°C. On the second day, the primary antibody mix was either discarded or kept at 4°C for further use (up to three times). Tissues were washed for three times with PBX3 for 10 min. An appropriate secondary antibody mix was prepared in PAXDD and tissues were incubated for 2 hours at room temperature. The staining dish was covered with aluminum foil since secondary antibodies are light sensitive. After washing tissues for three times in PBX3 for 10 min, eye discs were separated from brains and mouth hooks. Finally, eye discs were mounted on a slide with Vectashield. The edges of the cover slip were sealed with nail polish to prevent the loss of Vectashield by evaporation. Mounted eye discs were visualized with a Leica TCS SP5 confocal microscope. The images were further processed either with Image J or Adobe Photoshop CS6.

3.3.2. Lysotracker Staining

Third instar wandering larvae were placed in drops of PBS on a dissecting silicon pad. Eye discs were dissected as attached to the mouth hook and brain, and collected in PBS in a glass staining dish sitting on ice. Tissues were incubated in 1:1000 dilution of Lysotracker Red DND-99 (Invitrogen) in PBS for 10 min. After several quick washes, tissues were fixed with 4% paraformaldehyde for 15 min. Tissues were washed three times in PBS for 10 min and then mounted on a slide with Vectashield. The edges of the cover slips were sealed with nail polish to prevent the loss of Vectashield by evaporation.

Mounted eye discs were visualized with a Leica TCS SP5 confocal microscope. The images were further processed either with Image J or Adobe Photoshop CS6.

3.3.3. LipidTOX Staining

Third instar wandering larvae were placed in drops of PBS on a dissecting silicon pad. Eye discs were dissected as attached to the mouth hook and brain, and collected in PBS in a glass staining dish sitting on ice. Tissues were fixed with 4% paraformaldehyde for 15 min and washed three times for 10 min with PBS. Tissues were incubated in a 1:1000 dilution of LipidTOX Phospholipidosis and Steatosis Detection Stain (Invitrogen) in PBS for 10 min. Tissues were washed three times in PBS for 10 min and then mounted on a slide with Vectashield. The edges of the cover slips were sealed with nail polish to prevent the loss of Vectashield by evaporation. Mounted eye discs were visualized with Leica TCS SP5 confocal microscope. The images were further processed either with Image J or Adobe Photoshop CS6.

3.4. Biochemical Methods

3.4.1. Protein Extraction

Young adult flies or third instar wandering larvae were used to extract total protein. 5-10 adults or larvae were placed in a 1.5 ml Eppendorf tube. 70 µl lysis buffer with 1X Protease inhibitor cocktail (diluted from 100X stock) was added on each specimen and they were homogenized thoroughly using a pestle. After the tissues were completely homogenized, they were incubated on ice for 30 min. The crude extract was centrifuged at 4°C for 10 min at 13200 rpm. The clear part of the supernatant between pellet and lipid rich upper layer was collected and put in a new 1.5 ml Eppendorf tube. 3X Laemmli's buffer was diluted to a final concentration of 1X. The proteins were boiled at 95°C for 5 min in order to denature them and break the disulphide bonds.

3.4.2. SDS-PAGE

The percentage of the resolving gel was chosen according to the size of the protein to be resolved. Generally, an 8% resolving gel was preferred since it provides enough separation between the proteins in the size range of 25-100 kDa. First, the resolving gel was poured and the top was covered with isopropanol to make sure that the upper edge of the gel became smooth and on the same level at every point. After polymerization, the isopropanol was discarded and the stacking gel was poured on top of the resolving gel. 4 µl prestained protein ladder and 15-20 µl of each protein sample were loaded. The gel was run in 1X running buffer at 120 V until all samples reached the resolving gel and then it was switched to 80 V.

3.4.3. Western Blotting

1X transfer buffer was prepared from a 10X stock by the addition of 20% methanol and distilled water and chilled in the freezer. PVDF membrane was activated in methanol for 3 min and then equilibrated in transfer buffer. The gel sandwich was prepared in the order of fiber pad, 3 Whatman papers, membrane, gel, 3 Whatman papers, and fiber pad from the white side to the black side of the cassette. The proteins on the gel were transferred to the membrane under 200 mA constant current for 2 hours in the cold room. The tank was placed on the stir plate and a magnetic stirrer inside the tank constantly homogenized the transfer buffer to prevent fluctuations in the current. After the transfer, the membrane was stained with Ponceau's Red, which unspecifically binds to every protein present on the membrane. After the validation of transfer of proteins by Ponceau's Red, the membrane was washed twice with TBS-T for 10 mins. The membrane was blocked with 5% non-fat milk in TBS-T for 1 hour at room temperature. The appropriate dilution of primary antibody was prepared in 5% non-fat milk in TBS-T. The membrane was incubated with primary antibody solution overnight at 4°C. The next day, the membrane was washed three times with TBS-T for 10 min. The HRP-linked secondary antibody was diluted in 5% non-fat milk in TBS-T and the membrane was incubated with secondary antibody solution for 2 hours at room temperature. The membrane was washed three times with TBS-T for 10 mins. Meanwhile, 20X HRP revealing kit (Cell Signaling)

was diluted to 1X in ddH_2O and the membrane was incubated in this solution for 3 mins. The membrane was placed on a glass surface and Stella documentation system was used to detect the chemiluminescent signal. Later images were processed with Adobe Photoshop CS6.

3.5. Molecular Biological Techniques

3.5.1. Genomic DNA Extraction

The contents of the squishing buffer which was used in single fly genomic DNA extraction and the grinding buffer used in phenol-chloroform extraction are shown in Table 3.3.

3.5.1.1. Single Fly Genomic DNA Extraction. A single fly was placed in a 200 µl PCR tube. 50 µl squishing buffer with 1X Proteinase K (diluted from 100X stock) was sucked up into the pipette tip. The fly was smashed with the pipette tip until all the body appendages were disintegrated. The PCR tube was placed into the thermocycler and incubated at 37°C for 30 mins to digest the plasma membrane and release the DNA content of the cells. Then, an incubation at 95°C was performed for 2 min to heat-kill the Proteinase K. The tube was centrifuged for 7 min at 13200 rpm and the supernatant was transferred into a new Eppendorf tube for further use. 1 µl of this DNA was used for each 50 µl of PCR reaction.

3.5.1.2. Phenol-Chloroform Extraction. 5 adult flies from each genotype were placed into a 1.5 ml Eppendorf tube. They were briefly soaked in liquid nitrogen to make the grinding step easier. 100 µl of grinding buffer was put in each tube and the flies were crushed with a pestle until all the body appendages were broken into small pieces. Then, all tubes were vortexed rigorously for 10 seconds and placed in a water bath at 65°C for 10 min. 75 µl of 8 M potassium acetate (KAc) was added and vortexed briefly. Tubes were put on ice and incubated for at least 15 min. 0.5 ml of phenol:chloroform (1:1) was added and the tubes were vortexed vigorously for 30 seconds. All tubes were centrifuged for 5 min at 13200 rpm. Supernatants were transferred into new tubes. 1 ml of absolute ethanol was added to

each tube and they were incubated at room temperature for 4 hours. The DNA was precipitated by centrifuging the tubes for 15 min at 13200 rpm. All ethanol was discarded and the pellets were washed with 70% ethanol for a couple of times by centrifuging tubes repeatedly. After the final washing step, tubes were air dried for 10 min, and 100 µl elution buffer was added to each tube. Pellets were dissolved overnight at 4°C. 2 µl of DNA was used for each 50 µl PCR reaction.

3.5.2. Plasmid DNA Isolation

3.5.2.1. Small Scale Plasmid DNA Isolation (MiniPrep). QIAprep Spin Miniprep Kit (QIAGEN) was used to obtain plasmid DNA using the manufacturer's suggestions. Briefly, 5 ml of an overnight bacterial culture was precipitated in a 2 ml test tube by centrifuging at 10000 rpm for 1 min 3 times in a row. The pellet was resuspended in 250 µl of Buffer P1. 250 µl of Buffer P2 was added and the solution was mixed by inverting the tube several times until the solution became clear. 350 µl Buffer N3 was added and mixed immediately through inverting the tube several times. The mixture was centrifuged for 10 mins at 13200 rpm. The supernatant was applied to the spin column and centrifuged for 30 seconds at 11000 rpm. The flow-through was discarded. 750 µl of Buffer PE was added to the column and centrifuged for 30 seconds at 11000 rpm. To increase the quality of DNA, the washing step was repeated one more time and the column was centrifuged for a last time without adding Buffer PE to remove all residual buffer. The spin column was placed in a new 1.5 ml Eppendorf tube and 50 µl of buffer EB was added and incubated for 5 min at room temperature. Finally, the spin column was centrifuged for 1 min at 13200 rpm.

3.5.2.2. Large Scale Plasmid DNA Isolation (MidiPrep). QIAGEN Plasmid *Plus* Midi Kit was used to obtain a larger amount of plasmid DNA by following the manufacturer's suggestions. Briefly, 25-50 ml of an overnight bacterial culture was harvested by centrifuging at 10000 rpm for 15 mins at 4°C. The pellet was resuspended in 2 ml Buffer P1. 2 ml of Buffer P2 was added and the tube was gently mixed by inverting until the solution appeared viscous. It was incubated at room temperature for 3 min. 2 ml of ice-cold Buffer P3 was added and mixed by inverting the tube several times. Then, it was incubated for 15 mins on ice and centrifuged for 30 mins at 6000 rpm at 4°C. Meanwhile, the

QIAGEN-100 column was equilibrated by adding 2 ml of Buffer QBT. The supernatant was applied to the column and filtered through the column by gravitational force. After flow through, the column was washed two times with Buffer QC for 10 mins. The column was placed in a new 15 ml falcon tube. 5 ml of Buffer QF was applied to the column to elute the DNA. 3.5 ml of ice-cold isopropanol was added to the eluted DNA, mixed well and centrifuged for 30 min at 6000 rpm at 4°C. The supernatant was removed and the pellet was washed twice with 70% ethanol by centrifuging for 15 min at 6000 rpm at 4°C. The pellet was air dried for 30 min. It is resuspended in 50 µl of Buffer EB.

3.5.3. Total RNA Isolation

5 third instar larvae were collected and put into a 2 ml test tube. 800 µl Trizol was added and the larvae were homogenized by the pestle. To dissolve nucleoprotein complexes, the mixture was incubated 5 min at room temperature. 160 µl RNase-free chloroform was added and mixed well by inverting the tube 4-6 times. The mixture was incubated at room temperature for 15 min and then centrifuged at 12000 rpm for 15 min at 4°C. The aqueous phase was transferred to a new 1.5 ml test tube and 400 µl isopropanol was added. The RNA was precipitated after a 10 min at room temperature and centrifuged at 10000 rpm for 10 min at 4°C. The supernatant was discarded and the pellet was washed twice with 1 ml 75% ethanol by centrifuging at 7500 rpm for 5 min. Finally, the residual ethanol was removed and the tube was left to air dry for 10 min. The pellet was dissolved in 20 µl of DEPC-treated distilled water.

3.5.4. Restriction Digestion of DNA

Restriction enzymes were used to digest DNA according to manufacturer's suggestions. Briefly, DNA was incubated with appropriate buffer of a given restriction enzyme in water bath at 37°C for 1 hour.

3.5.5. Ligation

Ligations were performed with T4 DNA ligase (New England Biolabs) overnight at

16°C according to manufacturer's suggestions. The enzyme was heat-inactivated at 65°C for 10 min to terminate ligation reaction.

3.5.6. Dephosphorylation

Dephosphorylation reaction was performed with Antarctic Phosphatase (New England Biolabs) according to the manufacturer's suggestions. The enzyme removes the 5' phosphate groups, which prevents the religation of vector DNA after the digestion reaction. The enzyme was heat-inactivated at 65°C for 10 min.

3.5.7. DpnI Digestion

DpnI restriction enzyme was used to eliminate the template DNA to decrease the number of false-positive colonies after transformation. After the PCR reaction, 1 µl of DpnI was added to the reaction and incubated for 1 hour at 37°C.

3.5.8. Transformation

Transformation reactions were performed after ligation or Gibson assembly reaction.

3.5.8.1. Chemical Transformation. 50 µl ready-to-use chemically-competent bacteria stored at -80°C were thawed on ice. The ligation (or Gibson assembly) product was added to the bacteria and incubated on ice for 30 min. The mixture was then heat-shocked at 42°C for 45 sec. The tube was put back on ice and incubated for 5 min. 1 ml of LB was added to the tube and recovery of bacteria was allowed at 37°C by vigorous shaking at 250 rpm. 100 µl of bacteria were plated on an agar plate with the appropriate antibiotics and incubated overnight at 37°C.

3.5.8.2. Preparation of Electrocompetent Cells. 5 ml of LB was inoculated with 500 µl of overnight culture. After the optical density (OD) of bacteria reached 0.8, the tube containing the bacteria was incubated on ice for 30 min. It was centrifuged at 6000 rpm for 15 min at 4°C. 1 ml of ice-cold dH_2O was put into the tube. It was centrifuged at 13200

rpm for 30 sec. The pellet was resuspended in 1 ml of 7% DMSO and centrifuged again at 13200 rpm for 1 min at 4°C. All the liquid was discarded and the pellet was resuspended in 100 µl of 7% DMSO.

3.5.8.3. Electroporation. 50 µl of DMSO-treated bacteria was added to the ligation (or Gibson assembly) reaction. The mix was put into an electroporation cuvette and electroporation was performed by applying 1.8 kV current to the cuvette. 1 ml of LB was immediately added and the mix was transferred to a new 1.5 ml test tube. The bacteria were incubated at 37°C for 30 min for the recovery of bacteria. 100 µl of bacteria were plated on an agar plate containing the appropriate antibiotics and incubated at 37°C overnight.

3.5.9. Reverse Transcription and cDNA Synthesis

cDNA from total RNA was generated by using a cDNA synthesis kit (Invitrogen, SuperScript First-Strand) according to the manufacturer's suggestions. Briefly, 1 µg of RNA was added to a 0.2 ml PCR tube and the volume was brought to 12 ml by adding dH_2O. 0.5 µl of a random hexamer primer and 0.5 µl of an oligo dT primer were added making the final volume 13 µl and mixed well. The mix was incubated for 10 min at 65°C in a thermo cycler. Meanwhile, a mastermix for cDNA synthesis reaction was prepared on ice. To do so, 4 µl reverse transcriptase buffer, 2 µl dNTPs, 0.5 µl RNase inhibitor, and 0.5 µl reverse transcriptase were mixed. 7 µl of this mix was added to 13 µl of the previous mix and the tube was incubated in a thermo cycler with the following cycling conditions: 22°C for 10 min, 55°C for 30 min, 85°C for 5 min. The reaction was kept at 4°C until further use. Before using the cDNA for further steps, 180 µl of dH_2O was added.

3.5.10. Polymerase Chain Reaction

3.5.10.1. Conventional PCR. Preparation of the mastermix and the cycling conditions were adjusted according to the type of DNA polymerase and suggested annealing temperatures of primers. For Q5 high-fidelity DNA polymerase, 1X Q5 reaction buffer, 200 µM dNTP, 0.5 µM of each primer, 1 µl of template DNA, and 1 unit (20 units/ml) of

Q5 DNA polymerase were mixed and the final volume was adjusted to 50 µl with dH_2O. 98°C was used as denaturing temperature instead of the regular 95°C and annealing temperature for each primer set was determined using NEB T_m calculator for Q5 DNA polymerase. Q5 DNA polymerase was used when mutation rate was needed to be kept very low because of its high proofreading activity. For Homemade Taq polymerase, 1X Taq polymerase buffer, 300 µM dNTP, 0.5 µM of each primer, 1 µl of template DNA, and 1 unit of Homemade Taq polymerase were mixed and the final volume was adjusted to 30 µl with dH_2O. Regular denaturation and extension temperatures were used (95°C and 72°C, respectively). Annealing temperature was determined as 4°C below the lowest T_m of the primer pair.

3.5.10.2. Two-step PCR. Two-step PCR was used to integrate extra DNA sequences at the end of PCR product, which is normally not present in the template. For this purpose, overhang primers were used, which contains normal 20 bp homologous to a specific region of the template DNA and additional 20-50 bp overhang DNA, which needs to be integrated into the PCR product. The cycling conditions in a two-step PCR are different from that of a conventional PCR. Here, in the first 5 cycles, the annealing temperature of the homologous 20 bp is used. Then, in the following 25 cycles, the annealing temperature is increased to 67°C to allow the integration of the overhangs into the PCR product.

3.5.10.3. Colony PCR. After transformation of the ligation product into bacteria and incubation of the plated bacteria on an agar plate overnight, the putative positive colonies that appeared on the agar plate were screened to find bacterial colonies, which contain the desired ligation product. To do so, several bacterial colonies were picked using a pipette tip one by one and first each colony was streaked on a replica plate and then resuspended in 21.6 µl dH_2O. Each tube containing a different bacterial colony was heated to 95°C for 15 min to break open the bacterial cells. Meanwhile, a mastermix was prepared by mixing 1 unit of Homemade Taq polymerase, 1X Taq polymerase buffer, 1.25 mM $MgCl_2$, 300 µM dNTP, and 0.5 µM of each primer for each colony and added into each PCR tube containing bacterial cells. The PCR reaction was run at appropriate reaction conditions in a thermal cycler and 5 µl of the PCR product was run on a 1% agarose gel.

3.5.11. Agarose Gel Electrophoresis

A 1 % agarose gel (w/v) was prepared in 1X TAE. After dissolving the agarose in TAE by boiling it in a microwave, it was allowed to cool down and then ethidium bromide was added in a final concentration of 30 ng/ml. Meanwhile, samples were prepared by addition of appropriate volume of 6X loading dye so that the final concentration of loading dye became 1X. In the first well, 5 µl of 1 kb Marker (Roche) was loaded and the other wells were loaded with appropriate amount of samples. The gel was run at 100V for 30 min to 1 hour and visualized using the Gel-Doc System (Bio-Rad, USA).

3.5.12. Gel Extraction of DNA

The piece of the DNA to be extracted was excised using a clean scalpel. The gel slice was weighed and transferred to a 1.5 ml test tube. For each 100 mg of agarose gel 200 µl Buffer NTI was added (Nucleospin Gel and PCR Clean-up Kit, Macherey-Nagel). The sample was incubated for 10 min at 50°C (incubation time was increased if solid agarose particle was observed). The nucleospin gel column was placed into a 2 ml collection tube and the whole sample was loaded onto the column. The sample was centrifuged for 30 sec at 11,000 rpm and the flow-through was discarded. The column was placed in the same collection tube and 700 µl Buffer NT3 was loaded. The sample was centrifuged for 30 sec at 11,000 rpm and the flow-through was discarded. This step was repeated one more time. The column was centrifuged again to remove all residual buffer and placed into a new 1.5 ml test tube. 20 µl of pre-warmed Buffer NE was added to the column and incubated at room temperature for 3 min. Finally, the sample was eluted by centrifuging for 1 min at 11,000 rpm.

3.5.13. PCR Purification

2 volumes of Buffer NTI was added for each 1 volume of PCR reaction. The nucleospin gel column (Nucleospin Gel and PCR Clean-up Kit, Macherey-Nagel) was placed into a 2 ml collection tube and the whole sample was loaded onto it. The sample was centrifuged for 30 sec at 11,000 rpm and the flow-through was discarded. The column

was placed in the same collection tube and 700 µl Buffer NT3 was loaded. The sample was centrifuged for 30 sec at 11,000 rpm and the flow-through was discarded. This step was repeated one more time. The column was centrifuged again to remove all residual buffers and it was placed into a new 1.5 ml test tube. 20 µl of pre-warmed Buffer NE was added and the column was incubated at room temperature for 3 min. Finally, the sample was eluted by centrifuging for 1 min at 11,000 rpm.

3.5.14. Sequencing Analysis

Purified DNA samples were sent to Macrogen Inc. (Korea) for sequencing and DNA sequences were analysed using Vector NTI (Invitrogen) software.

3.6. Generation of a Conditional Allele of *CG7985* by CRISPR/Cas9

3.6.1. sgRNA Design

To generate a conditional allele of *CG7985*, our aim was to insert two attP recombination sequences in a reverse direction to the upstream of 5'UTR and the downstream of 3'UTR of *CG7985*. To do so, we sought to find the best possible target sequences at the intergenic region between *CG7985* and the upstream gene *SSDP* and between *CG7985* and the downstream gene *CG14314*. We designed sgRNA target sites by using Optimized CRISPR Design Tool which is an online tool designed by the Massachesetts Institute of Technology. The tool designs $GN_{18}GG$ sgRNA sequences from a given DNA sequence and scores them by blasting each sequence to the *Drosophila* genome. The sgRNA sequence with a score 100 shows the uniqueness of the sequence in the *Drosophila* genome. For both upstream and downstream sgRNA sequences we chose sequences with a score 100 to prevent off-target effects. The chosen upstream sgRNA sequence is GGCGTTGCCACGGTCGCCTAAGG and the downstream sgRNA sequence is GGTCGTGAGGCCGCGATGCGTGG.

3.6.2. Construction of plasmids

3.6.2.1. Construction of Plasmid Expressing sgRNA. A 700 bp DNA block that contains a U6-promoter sequence followed by the upstream sgRNA, a directed repeat, the downstream sgRNA, a directed repeat, and a transcription termination sequence was ordered from Integrated DNA Technologies (IDT). The directed repeat sequence was taken from the CRISPR locus of *Streptococcus pyogenes* genome without modification so that the transcription of sgRNA would mimic the original type II CRISPR adaptive immune system. The DNA block was inserted to a pBluescript II vector backbone that was prepared by digestion with EcoRV restriction enzyme to generate blunt ends. For this purpose, the pBluescript II vector was incubated with 1 U EcoRV in 1X NEBuffer 3.1 (New England Biolabs) for 1 hour and the corresponding DNA band was purified from the gel. The DNA was designed in a way that it contains 50 bp DNA sequence that is common to the upstream and downstream of EcoRV restriction site of the cevtor. 120 ng linearized pBlueScript II vector was mixed with 240 ng of DNA block and the volume was added up to 10 µl with dH_2O. Then, 10 µl Gibson Assembly mastermix (New England Biolabs) was added to 10 µl DNA mix. The reaction was incubated for 2 hours in a thermo cycler at 50°C. After incubation, the reaction mix was put on a dialysis membrane which floats on dH_2O for 1 hour to get rid of all salt content of the reaction. Electroporation (Section 3.5.8.2.) was performed and 100 µl of transformed bacteria were plated on an agar plate containing ampicillin. On the next day, several colonies were picked and a colony PCR was performed (Section 3.5.10.3) to evaluate the presence of the insert in the plasmid. Positive colonies were selected and 5 ml of LB was inoculated with each positive colony. On the next day, plasmids were isolated by MiniPrep (Section 3.5.2.1) and sent to Macrogen Inc. (Korea) for sequencing using M13 forward and reverse primers. The colonies in which DNA block was inserted properly and contained no mutation were selected for injection.

3.6.2.2 Targeting Plasmid Construction. All PCRs were performed with Q5 high-fidelity DNA polymerase (New England Biolabs) unless otherwise stated. The targeting vector for the upstream integration event contains two 1500 bp homology arms that flank the upstream target site and a cassette in the form of 3xP3-GFP-attP in between. Similarly, the targeting vector for the downstream integration event contains two 1500 bp homology

arms that flank the downstream target site and a cassette in the form 3xP3-dsRED-attP in between. Therefore, the final targeting vectors contain an attP recombination sequence for site-directed recombination for subsequent modifications of the targeted locus, homology arms for homologous recombination and reporters with eye-specific 3xP3 promoter that drives expression of GFP and dsRED in the eye. To generate the homology arms, first 3000 bp regions containing the target sites in the middle were amplified from flies that were later used for injection purposes. Then, primers with 50 bp overhangs were used to amplify ~ 1500 bp homology arms by two-step PCR (Section 3.5.10.2.) in which the integrated 50 bp sequence corresponds to the region in the vector backbone and 3xP3-reporter-attP cassette. These 50 bp common regions were later used to assemble the vector by Gibson Assembly. 3xP3-reporter-attP cassettes and the pBluescript II vector backbone were amplified from a pre-made vector (Gift from Bassem Hassan, Catholic University of Leuven, Leuven, Belgium). For the assembly of both upstream and downstream targeting vectors, 120 ng of two homology arms, 3xP3-reporter-attP cassette, and pBluescript II vector backbone were mixed and the volume was adjusted to 10 µl with dH_2O. 10 µl of Gibson Assembly mastermix was added to the 10 µl of the final DNA mix. The reaction was incubated for 2 hours in a thermo cycler at 50°C. After incubation, the reaction mix was pipetted onto a dialysis membrane floating on dH_2O for 1 hour to remove all salts present in the reaction. Electroporation (Section 3.5.8.2.) was performed and 100 µl of transformed bacteria were plated on an agar plate with ampicillin. On the next day, several colonies were picked and a colony PCR was performed (Section 3.5.10.3) to evaluate the presence of homology arms and 3xP3-reporter-attP cassette inside the plasmid. Positive colonies were selected and 5 ml of LB was inoculated with each positive colony. On the next day, plasmids were isolated by MiniPrep (Section 3.5.2.1) and sent to Macrogen Inc. (Korea) for sequencing. The colonies containing homology arms and 3xP3-reporter-attP cassette sequences and having no mutations were selected for injection.

3.6.3. Generation of *vasa*-Cas9 Line

y, *vasa*-Cas9, U6-tracrRNA flies were used as a Cas9 source (Gift from Bassem Hassan, Catholic University of Leuven, Leuven, Belgium). Briefly, in a 3xP3-EGFP/vasa-$\Phi C31^{NLS}$attB plasmid (Basler *et al*., 2007) the ΦC31 coding sequence was replaced with

an *Xba*I-containing multiple cloning site through amplification of the *vasa* regulatory elements and plasmid backbone. The Cas9 coding sequence was amplified as an *Xba*I-flanked fragment from pX330 (Cong *et al*., 2013). It was then ligated into *Xba*I site of the modified 3xP3-EGFP/vasa-ΦC31^{NLS}attB plasmid. The resulting 3xP3-EGFP/vasa-Cas9 plasmid was injected to embryos of *y* flies by ΦC31-mediated integration. Positive recombinanats were selected according to GFP fluorescence in their eyes. Finally, *y*,*vasa*-Cas9, U6-tracrRNA flies were crossed with *lig4*^{169} flies to generate *yw*, *vasa*-Cas9, U6-tracrRNA, lig4^{169}, which were later used for injection.

3.6.4. Embryo Injection

Preblastoderm embryos were injected through their chorion membrane by following a standard injection protocol. Embryos were injected at 18°C and immediately shifted to 25°C. U6-sgRNA_upstream, U6-sgRNA_downstream, pBSII-3xP3-GFP-attP, and pBSII-3xP3-dsRED-attP vectors were injected to 300 embryos of *yw*, *vasa*-Cas9, U6-tracrRNA, *lig4*^{169} flies at a concentration of 100ng/µl of each. All injection mixtures were prepared in water.

3.6.5. Screening of Recombinants

Viable G0 *vasa*-Cas9, U6-tracrRNA flies, which developed from embryos injected with gRNA and pBSII-3xP3-reporter-attP plasmids were crossed individually to *w*^{1118} flies. The G1 generation was screened 10 days after the cross. Flies were individually screened under a fluorescence dissection microscope for GFP and/or dsRED expression in their eyes. Double positive flies were selected, counted and their percentage was calculated after screening process. Each double positive fly was crossed to balancer flies to establish individual stocks. Finally, PCR was performed on each population to determine the presence of the transgenes at the desired genomic position.

3.7. Experiments for Functional Analysis

3.7.1. Knockdown Analysis of *CG7985* in the Eye

To specifically downregulate the expression of *CG7985* in the eye, the eye-specific Gal4 line, *ey*-Gal4, was crossed with the UAS-*CG7985*RNAi line.

$$yw; \frac{ey-Gal4}{ey-Gal4}; \frac{TM2}{TM6B} \quad X \quad yw; \frac{UAS-CG7985RNAi}{UAS-CG7985RNAi}; \frac{TM2}{TM6B}$$

Figure 3.1. Eye specific downregulation of *CG7985* by *ey*-Gal4 driver.

3.7.2. Generation of Whole Eye Mutants by Protein Trap Line

The protein trap line specific for *CG7985* has been recombined with *FRT82B* and EGUF/hid method was used to generate whole eye mutants. The technique is explained in detail in section 1.5.3.

$$yw; ey-Gal4, UAS-flp; \frac{FRT82B, GMR-hid}{TM2} \quad X \quad yw; \frac{sp}{cyo}; \frac{FRT82B, P.Trap}{TM6B}$$

$$\downarrow$$

$$yw; \frac{ey-Gal4, UAS-flp}{sp\ or\ cyo}; \frac{FRT82B, GMR-hid}{FRT82B, P.Trap}$$

Figure 3.2. EGUF/hid method to generate whole eye mutants in terms of *CG7985* by using protein trap line recombined to *FRT82B*.

3.7.3. Generation of Mutant Clones by Protein Trap Line

The protein trap line specific for *CG7985* has been recombined with *FRT82B* and crossed with a line, which displays PR-specific RFP reporter expression, *GMR*-RFP, and is located on a *FRT82B* chromosome. The technique is explained in section 1.5.3 in detail.

$$yw; ey-Gal4, UAS-flp; \frac{FRT82B, GMR-RFP}{TM2} \quad X \quad yw; \frac{sp}{cyo}; \frac{FRT82B, P.Trap}{TM6B}$$

$$yw; \frac{ey-Gal4, UAS-flp}{sp\ or\ cyo}; \frac{FRT82B, GMR-RFP}{FRT82B, P.Trap}$$

Figure 3.3. Generation of mutant clones of *CG7985* by FRT/Flp mitotic recombination

4. RESULTS

4.1. Bioinformatic Analysis of CG7985

4.1.1. *CG7985* is a Member of the Highly Conserved Hexosaminidase Branch

Drosophila melanogaster has four different hexosaminidases, which have been defined in the CAZy database as being members of the hexosaminidase family 20 under the superfamily of glycosyl hydrolase 20. Phylogenetic analysis of hexosaminidases collected from different species, including four *Drosophila* hexosaminidases, has revealed that the hexosaminidase family 20 has two major branches. While human lysosomal α and β subunits, nematode HEX-1 and three *Drosophila* hexosaminidases (Hexo1, Hexo2, and Fdl) belong to the same sub-family of the hexosaminidase family 20, the other four members of nematode hexosaminidases (HEX-2, HEX-3, HEX-4, HEX-5), human HexDC and *Drosophila* CG7985 are grouped together in another branch (Gutternigg *et al*., 2007).

To carry out the phylogenetic analysis of CG7985, we collected hexosaminidase sequences by blasting the CG7985 protein sequence to different genomes using NCBI protein blast. The phylogenetic tree was generated from protein sequences that were aligned by ClustalW using Mega5 software. The reliability of the constructed tree was evaluated using the bootstrap method. Figure 4.1 shows the phylogenetic tree of the subfamily of hexosaminidase family 20, including *Drosophila* CG7985. The fidelity of the branching points was very high except one branching point between *C.porcellus* and the major branch of primates. CG7985 and nematode HEX-2 were segregated into individual branches and vertebrate HexDC proteins and CG7985 appear to have diverged from a common protein sequence. The phylogenetic tree resembles the evolutionary history of speciation and although it is not included in the tree, protein blast of CG7985 reveals several bacterial proteins with high similarity. It suggests that the branching event between two sub-families of the hexosaminidase family 20 has an ancient origin.

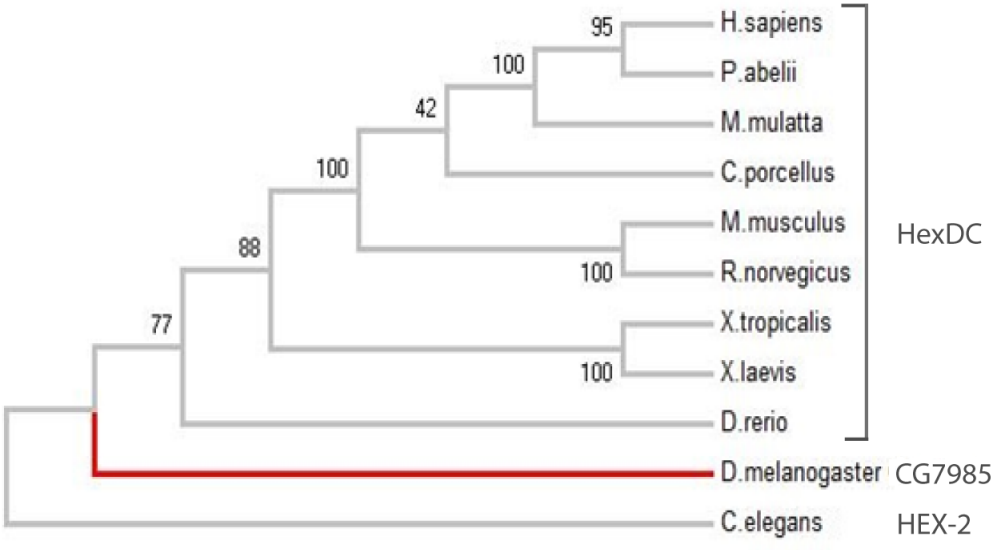

Figure 4.1. Phylogenetic tree for CG7985 based on the bootstrap algorithm. The tree shows that CG7985 is the homolog of vertebrate HexDC and *C-elegans* HEX-2.

A phylogenetic tree shows the relative evolutionary distance between DNA or protein sequences from different species, however, it fails to show in which regions there is conservation between the sequences under comparison. During evolution, gene sequences are subject to change by mutations, which is directly reflected in the amino acid sequence of proteins. However, mutation rates are usually very low in regions related to the activity of proteins. In order to evaluate the degree of conservation between CG7985 and other members from the same sub-family of hexosaminidases and to reveal possible active sites of CG7985, we performed multiple sequence alignments using the amino acid sequence of CG7985 and a range of homologous sequences from *T. adherens* to *H. sapiens*. Figure 4.2 shows the result of such a multiple sequence alignment. Black boxes indicate the direct conservation of amino acid identity, while gray boxes indicate conservation at the level of the nature of amino acids. It is clear that there is a high conservation between CG7985 and the other members of the same sub-family at the protein level. One important point to note is that CG7985 and the other homologous proteins have a His/Asn-Xaa-Gly-Ala/Cys/Gly/Met-Asp-Glu-Ala/Ile/Leu/Val motif in common, which previously has been shown to execute hexosaminidase activity. The glutamate residue of this motif is the key amino acid involved in the catalytic activity of hexosaminidases (Hou *et al*., 2001).

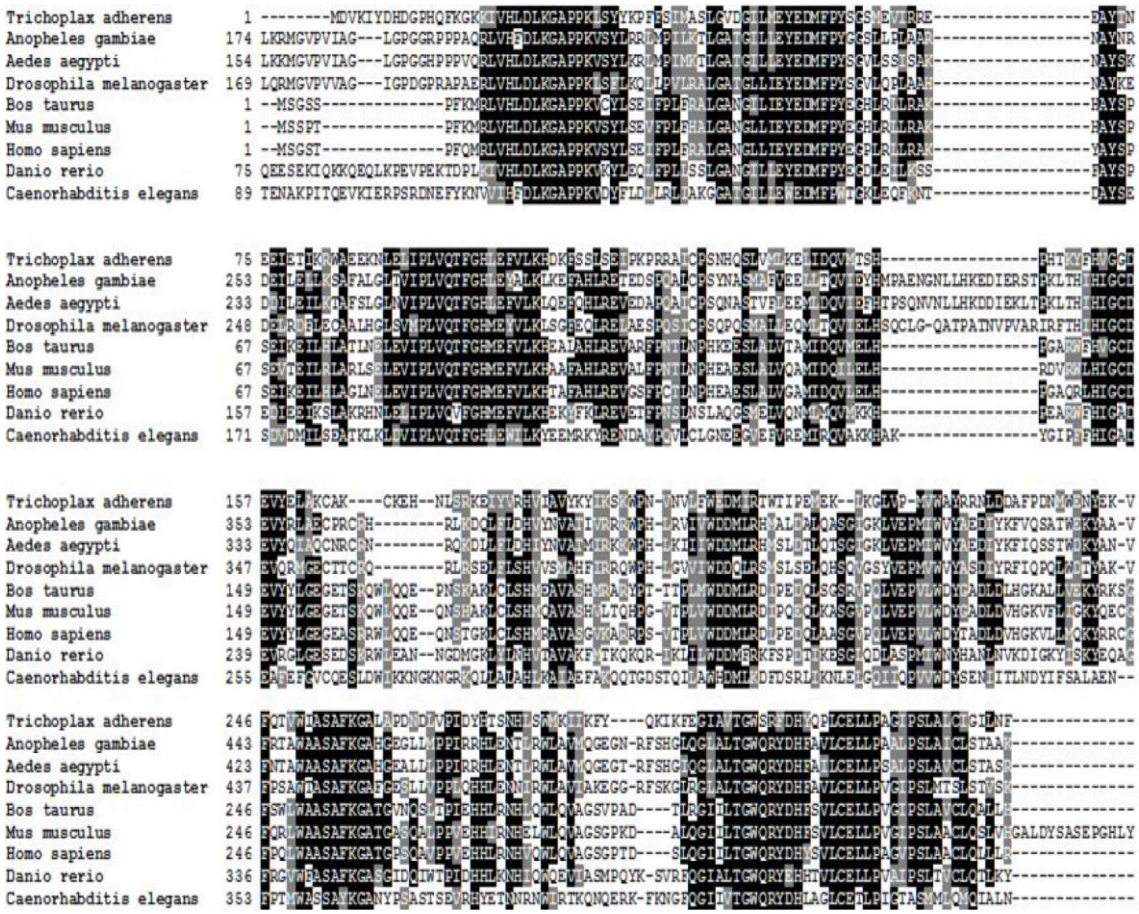

Figure 4.2. Multiple sequence alignment of CG7985 and the homologous protein sequences from different species. Black regions indicate the same amino acid sequences between aligned protein sequences and grey regions show the conservation of amino acids of similar nature.

4.1.2. CG7985 Contains a Putative Transmembrane Domain

The type of the protein and its subcellular localization is an important indication of its possible functions. Transmembrane proteins are embedded into the lipid bilayer and located in the plasma membrane or other membranous organelles. Here, they are involved in critical interface functioning like communication between cells or organization of signalling events. Cytoplasmic proteins, on the other hand, are free agents inside the cell with roles in important intracellular molecular events or modification of other proteins. Recently, recombinant forms of murine and human HexDC have been molecularly characterized. They have been shown to act as nucleocytoplasmic enzymes and specifically remove N-acetylgalactosamine but not N-acetylglucosamine (Gutternigg *et al.*, 2009).

There is 35% identity between *Drosophila* CG7985 and human HexDC on the protein level and these proteins share a specific motif for hexosaminidase function (Figure 4.2). However, using a tool for the prediction of transmembrane helices in proteins (TMHMM Server v. 2.0), we have shown that CG7985 contains a highly hydrophobic putative transmembrane domain between amino acids 13 and 35 with a probability of 0.99879 (Figure 4.3). Therefore, unlike the murine and human forms of HexDC, CG7985 is not expected to be a cytosolic protein.

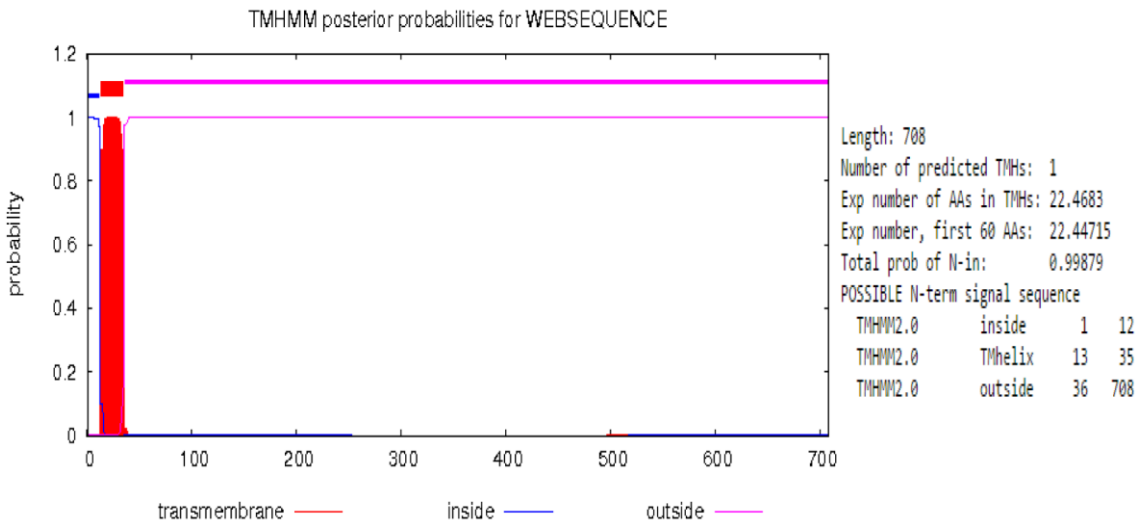

Figure 4.3. Transmembrane domain prediction of CG7985 using the TMHMM Server v. 2.0. CG7985 contains a putative transmembrane domain between amino acids 13 and 35 with a probability of 0.99879.

4.2. *CG7985* is Expressed in Photoreceptor R7 in the Enhancer Trap Line AC887

Enhancer-trap elements are modified P-element transposons that contain a minimal promoter and a Gal4 element. The minimal promoter is incapable of inducing transcription itself. However, if after transposition, it is inserted into a region under the influence of local enhancer elements, the activity of the minimal promoter will cause the expression of Gal4 that will directly reflect the enhancer activity pattern (Ward *et al.*, 2002).

In her post-doc study, Dr. Çelik generated an enhancer-trap library using a PiggyBac transposable element. This element contained a minimal promoter upstream of a Gal4

sequence. Later, the characterization of a subset of these lines has been done by Arzu Öztürk (A.Öztürk, 2010) leading to the identification of the line, AC887, in which insertion of the PiggyBac element has been mapped to the first intron of *CG7985* (Figure 4.4.).

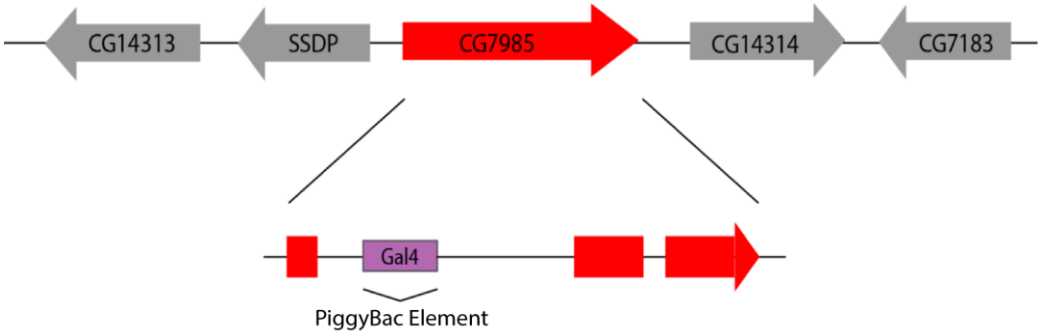

Figure 4.4. Schematic view of the insertion of the PiggyBac transposable element into the first intron of *CG7985*.

The Gal4/UAS system was used to visualize the enhancer activity in combination with an UAS-GFP reporter line with a nuclear localization signal. Whenever the expression of Gal4 is induced by nearby enhancer elements, Gal4 will be expressed and the Gal4 protein will bind to UAS to trigger the expression of GFP. The nuclear localization signal will cause the transport of the GFP to the nucleus and allow the co-localization with other markers that are transcription factors and are localized to the nucleus. To reveal the expression pattern of *CG7985*, we performed immunohistochemical analysis on third instar larval eye imaginal discs using anti-GFP antibody and an antibody against the pan-neuronal marker Elav. Additionally, specific markers for photoreceptors were used to co-stain GFP-positive cells and uncover their identity. The GFP signal was observed in a single photoreceptor cell in each ommatidium starting in the 8^{th} row after the morphogenetic furrow. Co-staining with the R7-specific marker Prospero revealed that *CG7985* is specifically expressed in photoreceptor R7. However, the onset of the GFP signal was 3-4 rows posterior to the onset of the Prospero signal. This delay in the GFP signal might be the result of time lag caused by the interaction between the Gal4 protein and UAS. Moreover, it is important to note that Prospero additionally stains 4 cone cells in each ommatidium. The location of Prospero-positive R7 cells was inferred from its co-localization with Elav-positive cells. Therefore, triple co-localization of Elav, Prospero, and GFP revealed the expression of *CG7985* in photoreceptor R7 (Figure 4.5).

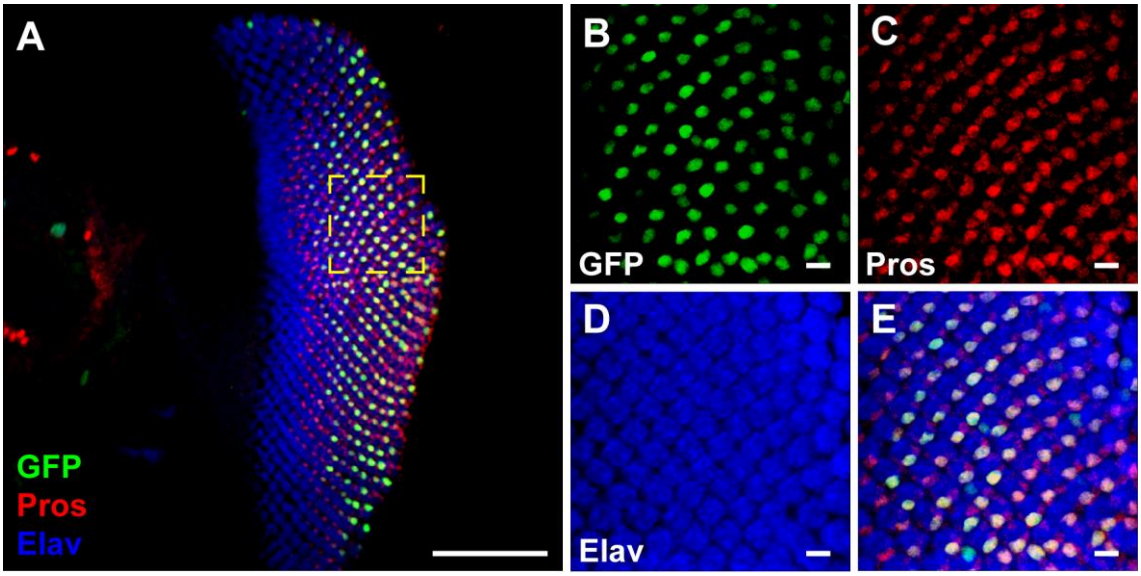

Figure 4.5. The enhancer-trap line AC887 inserted in *CG7985* shows specific expression in photoreceptor R7 A: Triple immunostaining of third instar larval eye imaginal disc with antibodies against GFP, Prospero and Elav. B, C, D, and E: Close view of GFP, Prospero, and Elav immunostainings. Note the co-localization of Prospero and GFP signals.

4.3. Protein Localization of CG7985

Enhancer-trap lines can give an initial idea about the expression pattern of a particular gene. However, there are two drawbacks of using an enhancer trap to reveal the expression pattern of a gene. First, enhancer traps do not show where the protein is localized after the corresponding mRNA is translated and second, the enhancer elements that activate the minimal promoter of the P-element might not reflect the whole repertoire of enhancer elements of the gene of interest. To overcome these hurdles two different tools have been generated, an eGFP-tagged CG7985 construct was produced by BAC recombineering (G.Kaçmaz, 2013) and a peptide antibody against CG7985. Additionally, a protein-trap line inserted into CG7985 from a public database has been investigated in detail.

4.3.1. Protein Localization of CG7985 by CG7985::eGFP (BAC) Line

In BAC recombineering, a BAC vector containing the complete coding region of the

gene of interest and a reasonable part of upstream and downstream DNA sequences is selected from a publicly available BAC library and a DNA sequence encoding eGFP is introduced before the stop codon of the gene to produce a fusion protein. After integration of the construct into the fly genome by site-specific recombination, the fusion protein will be expressed from its endogenous regulatory sequences introduced with the construct.

To analyze the protein localization of CG7985, we performed immunofluorescence stainings with antibodies against GFP, Prospero, and Elav on third instar larval eye imaginal discs of the CG7985::eGFP BAC transgenic line (Figure 4.6).

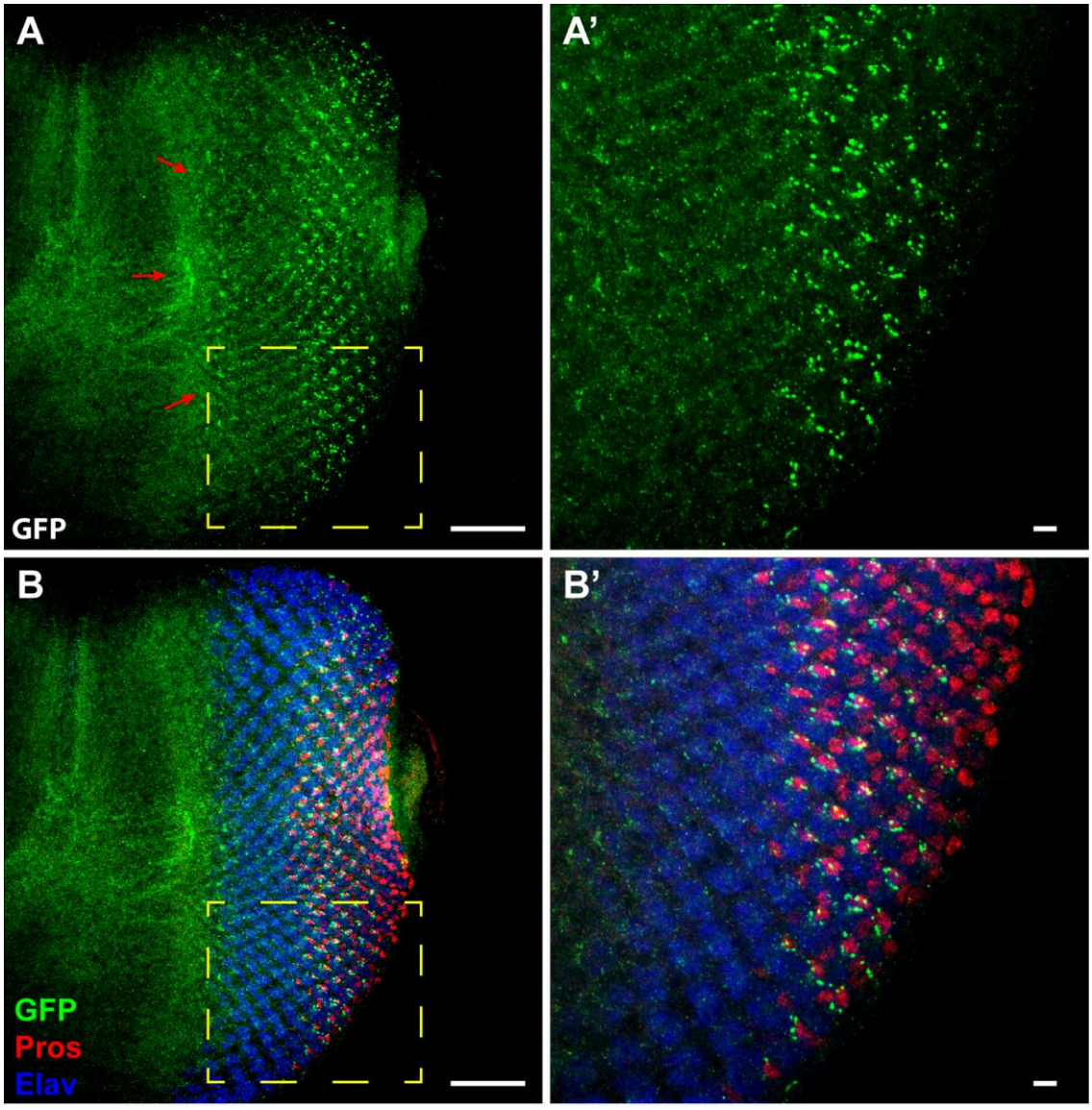

Figure 4.6. CG7985 is localized to photoreceptor R7, in and anterior to the morphogenetic furrow in the CG7985::eGFP BAC line.

In line with the photoreceptor R7-specific expression in the enhancer trap line, we observed dot-like GFP signals surrounding Prospero-positive photoreceptor R7 nuclei. However, additional GFP signals were observed anterior to and within the morphogenetic furrow (Figure 4.6 red arrows). The R7-specific staining in the BAC transgenic line starts at the same time as Prospero expression. While this observation seems to contrast what was observed in the Gal4 line, it is well known that Gal4 expression appears delayed when compared to endogenous expression.

4.3.2. Subcellular Localization of CG7985 by CG7985::eGFP BAC Line

Determination of the subcellular localization of CG7985 was important in order to make more accurate predictions about its function. Previously, other *Drosophila* hexosaminidases have been shown to function in N-Glycan biosynthesis within the Golgi apparatus (Gutternigg *et al*., 2009; Rosenbaum *et al.*, 2014). However, no hexosaminidases functioning in the glycosphingolipid degradation pathway have been identified in *Drosophila*. One pre-requisite for an enzyme functioning in this pathway would be to be localized in the endosomal/lysosomal pathway.

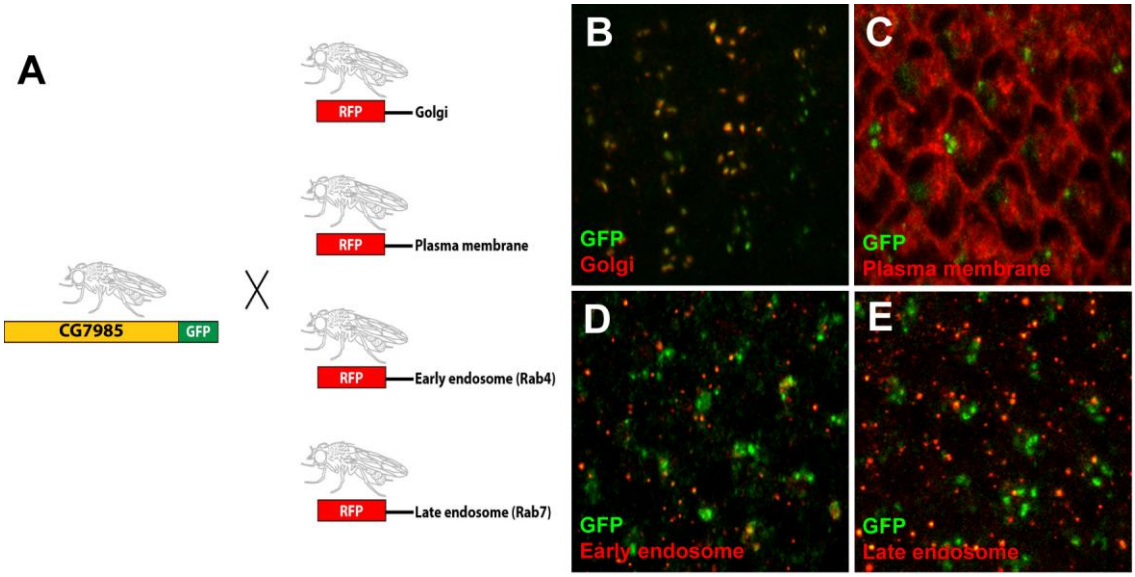

Figure 4.7. CG7985 is localized to the Golgi apparatus and partially to early endosomes and late endosomes.

To analyze the subcellular localization of CG7985, we crossed the CG7985::eGFP BAC line with different reporter lines that label different cellular compartments with red fluorescent protein (RFP) (Figure 4.7a). In these reporter lines signaling peptides specific to each compartment have been fused to RFP and the RFP protein localizes to particular organelles depending on the signaling peptide it contains. Four different reporter lines displaying localization to the Golgi apparatus, plasma membrane, early endosome, and late endosome have been used in this study. Examination of co-localization between the GFP and the RFP signal showed that CG7985 is mainly localized to the Golgi apparatus. However, additional signals of co-localization are observed with early and late endosomes. No localization to the plasma membrane has been observed (Figure 4.7b).

The subcellular localization of CG7985 did not allow a conclusion on whether CG7985 plays a role in N-Glycan biosynthesis or the glycosphingolipid degradation pathway. According to the KEGG pathway database, an online bioinformatics tool that assigns roles to the proteins role in distinct metabolic pathways, CG7985 might have roles both in N-Glycan biosynthesis and in the degradation of gangliosides. Combining this information with the localization results, it can be suggested that CG7985 functions in both pathways.

4.3.3. Protein Localization of CG7985 Using a Protein Trap Line

Although using a BAC line is promising to reveal the localization of a protein, it also has its weaknesses. Since the BAC construct is inserted in another location of the genome, together with the activity of the endogenous gene, the number of transcripts is doubled generating an overexpression line. Also, it is not clear if the expression of the gene in another location of the genome will directly reflect the activity in its endogenous locus especially as it is not 100% clear if the chosen upstream and downstream sequences included in the construct represent all the regulatory regions.

About a decade ago, a protein trap library with the purpose of tagging genes in their endogenous loci has been generated. This strategy uses the same principle as in enhancer trapping. However, the P-element construct does not contain a minimal promoter, instead,

it contains a GFP coding region flanked by splicing acceptor (SA) and donor sites (SD). Basically, the GFP construct behaves as an exon and is spliced into the mRNA eventually producing a protein with a GFP tag (Morin *et al.*, 2001). As explained in section 1.5.2 in detail, two outcomes are possible when the GFP construct is inserted upstream of the first coding exon. It might either generate a protein tag at the N-terminus or it splices with some cryptic exons from sequences inside the P-element. In the latter case, a 25-30 kDa protein with GFP coding region is generated, and it has been shown that this truncated protein localizes similar to the endogenous protein. The reason for this phenomenon is thought to be that the transcription of the GFP construct is mediated by the gene's own promoter elements (Quinones-Coello *et al.*, 2006).

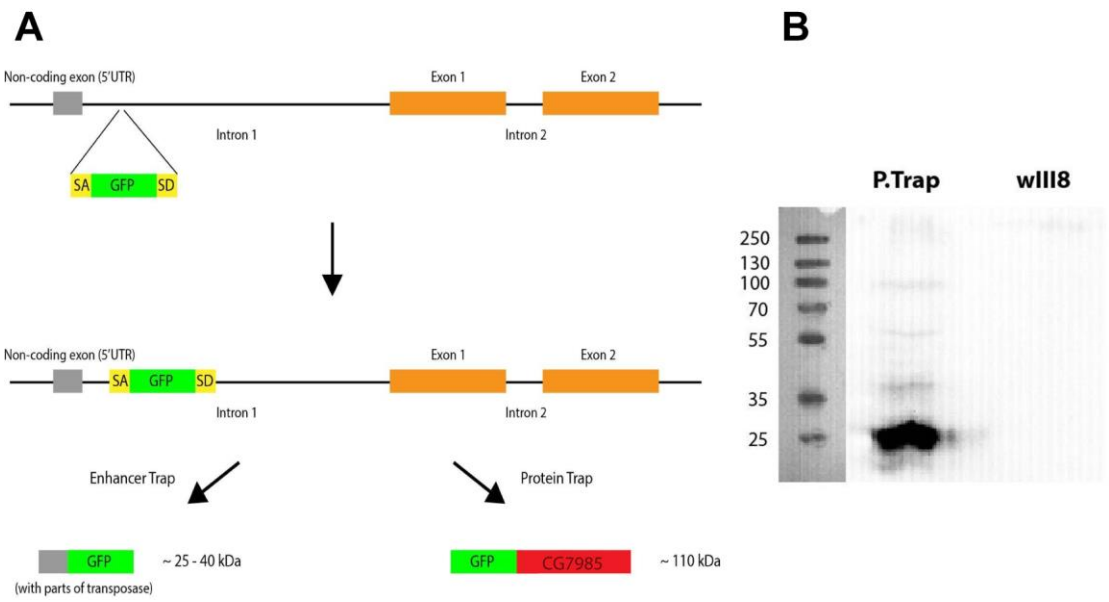

Figure 4.8. GFP insertion in CG7985 specific protein trap line generates a truncated protein containing GFP. A: Possible outcomes of SA-GFP-SD insertion into the first intron of the *CG7985* gene. B: Western blot analysis of CG7985-specific protein trap line with anti-GFP antibody. A protein of ~ 25 kDa was detected. w^{1118} line was used as negative control. SA:splice acceptor, SD: splice donor.

In the case of the CG7985-specific protein trap line ($CG7985^{CPTI100032}$), the GFP construct is inserted about 1 kb downstream of the 5' UTR and hence upstream of the first coding exon (Figure 4.8a). To reveal the nature of the protein trap line, Western blot analysis using an antibody against GFP was performed. If the GFP construct generates an

N-terminus tag of CG7985 protein, a protein of about 110 kDa is expected. Otherwise, a protein of about 25-30 kDa will be observed. Western blotting analysis showed that the GFP insertion does not generate a protein tag, but instead it generates a truncated protein with GFP (Figure 4.8b). As expected in a wild-type fly line (w^{1118}) that was used as a control no GFP expression was observed. Western blotting analysis showed that the GFP insertion does not generate a protein tag, but instead it generates a truncated protein with GFP in it.

To analyse protein localization in the protein trap line CG7985^{CPTI100032} in third instar larval eye imaginal discs, immunofluorescence analysis with an antibody against GFP was performed. Analysis revealed a dot-like pattern of protein localization around photoreceptor R7 nuclei, within and anterior to the morphogenetic furrow (Figure 4.9a).

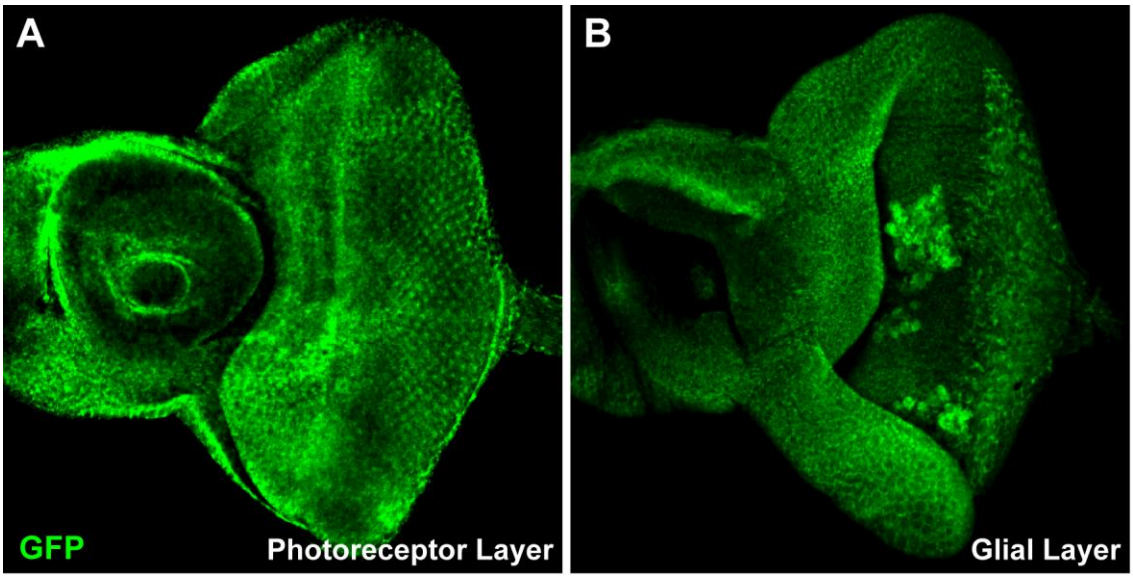

Figure 4.9. Protein localization of CG7985 in third instar eye imaginal discs of the protein trap line CG7985^{CPTI100032}. A: Protein localization of CG7985 around photoreceptor R7 nuclei, within and anterior to the morphogenetic furrow at the photoreceptor layer . B: Third instar eye imaginal discs of the protein trap line also show protein localization of CG7985 in the glial layer.

The observed pattern of GFP localization was strikingly similar to the pattern observed with the CG7985::eGFP BAC line. However, unlike the expression pattern of the enhancer trap line and the protein localization of CG7985::eGFP BAC line, expression

in the glial layer of the eye imaginal disc was observed (Figure 4.9b). In the third instar eye imaginal disc, glial cells are located at the apical part of the disc and move toward the nascent photoreceptors at the same pace as the movement of the morphogenetic furrow. Although the exact role of glia in the development of the eye imaginal disc is mostly unknown, a glial overmigration phenotype has been linked to a defect in the growth of the eye imaginal disc (Yuva-Aydemir *et al.,* 2011).

4.3.4. Generation and Characterization of an Antibody against CG7985

The most reliable and direct way to analyse the localization of a protein is to use an antibody against it. Since there is no commercially available antibody against CG7985, we attempted to generate an antibody against CG7985. For this purpose a specific, 15 amino acid long peptide sequence near the C-terminus of the CG7985 protein has been selected (Figure 4.10a) and a synthetic peptide was synthesized and used to immunize rabbits by the company Innovagen AB®. Serum samples were analysed between each booster injection by ELISA assays. The sera were also analysed by Western blotting of protein isolated from wild-type (w^{1118}) tissues. Several bands were observed on the Western blots including bands of expected size suggesting that the sera contain anti-CG7985 antibodies. Pre-immune serum was used as a control. After a final boost the antibody was affinity-purified.

Western blot performed after affinity purification revealed the presence of several bands of about 50 kDa, 80 kDa, and 130 kDa. In order to minimize non-specific binding, the antibody was pre-adsorbed with larval tissues dissected from the protein-trap line. This line was shown to represent a mutant for *CG7985* (see Section 4.4.1). The pre-adsorbed antibodies were used in comparison with the non-adsorbed antibody and, it was shown that pre-adsorption significantly increased the specificity of the staining and all bands except for one were significantly reduced (Figure 4.10b). Surprisingly however, the single band observed on the blot using the pre-adsorbed antibody did not match the annotated size of CG7985 protein, which is 82 kDa. Observation of a higher molecular weight band for CG7985 might be the result of post-translational modifications. To evaluate this hypothesis and reveal the identity of this band it will be analysed by mass spectrometry.

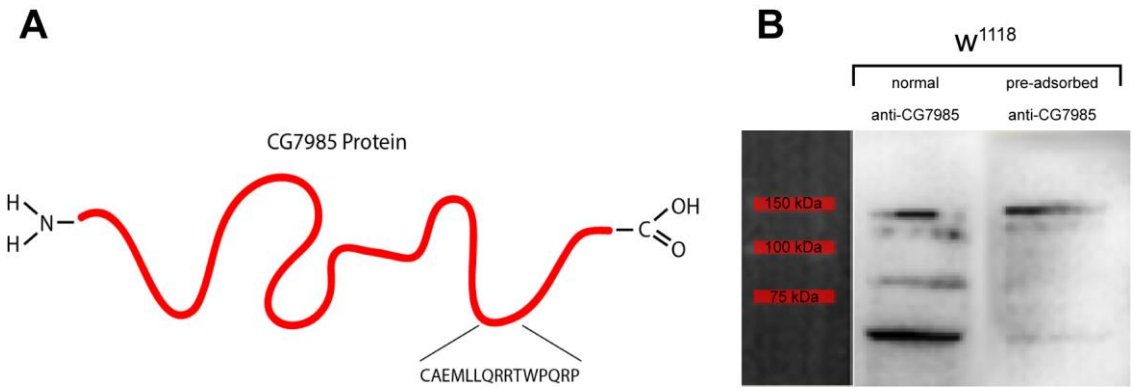

Figure 4.10. Western blot analysis of normal and pre-adsorbed CG7985 antibody. A: Schematic view of the selected peptide sequence to generate a CG7985-specific antibody. B: Comparison of the specificity of normal and pre-adsorbed CG7985 antibody by Western blotting. Only one band persisted and other bands disappeared largely.

4.3.5. Protein Localization of CG7985 by anti-CG7985 Antibody

The pre-adsorbed CG7985 antibody was later used in immunofluorescence stainings of wild-type third instar eye discs. These analyses revealed a localization of CG7985 that is similar to the protein trap in third instar eye imaginal discs. Although weak, a dot-like signal at the photoreceptor level and also in the glial layer (Figure 4.11) was revealed.

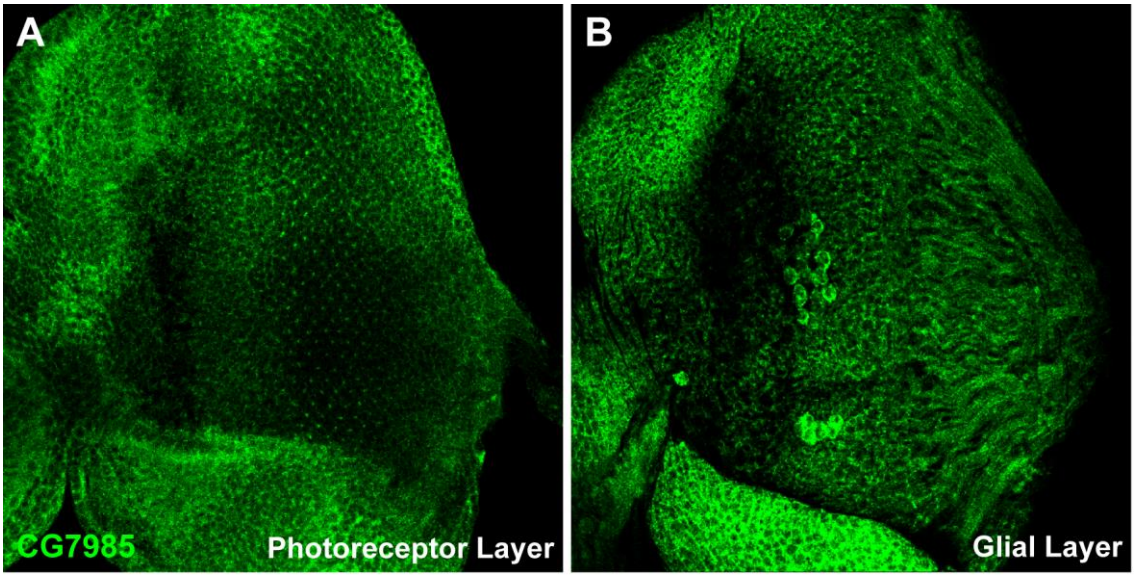

Figure 4.11. Protein localization of CG7985 in wild type third instar eye imaginal discs using pre-adsorbed CG7985 antibody. Signals in both photoreceptor and glial cell layer are similar to GFP signals in protein trap third instar eye imaginal disc.

Taking together all localization data, overlapping signals of the CG7985 antibody and the protein trap line *CG7985*^{CPTI100032} and also to some extent in the CG7985::eGFP BAC line revealed that CG7985 is localized to photoreceptor R7, within the morphogenetic furrow, anterior to the morphogenetic furrow as well as glial cells in the third instar eye imaginal disc.

4.4. Mutant Analysis of *CG7985* Using the Protein Trap Line

4.4.1. Transcription of *CG7985* is Blocked in the Protein Trap Line

Enhancer-trap and protein-trap lines using P-elements have been generated to ease the analysis of the expression pattern and localization of proteins of interest, respectively. However, an unexpected outcome of this strategy came with the realization of a positional bias of insertion of transposable elements towards the 5' region of target genes during transposition events. Analysis of many lines showed that insertions happen in or near the 5' untranslated region (5'UTR) and cause loss-of-function mutations by preventing the initiation of transcription (Aleksic *et al*., 2009).

In the case of CG7985 specific protein trap line *CG7985*^{CPTI100032}, the insertion of the GFP construct is about 1 kb downstream of the 5'UTR. To evaluate if this particular insertion prevents the transcription of *CG7985*, we performed a reverse transcription-PCR (RT-PCR). PCR was performed on cDNA samples obtained from wild-type (w^{1118}) and the protein trap line *CG7985*^{CPTI100032} using two primer pairs to amplify exon 1 and exon 2 of *CG7985* and a control primer pair to amplify β-actin (Figure 4.12a). To eliminate potential contamination by genomic DNA on PCR results especially in the *CG7985*^{CPTI100032} protein trap line, one of the primers was chosen from the exon-exon junction, which is present in the mRNA sequence but not the genomic sequence of *CG7985*. While the expected PCR fragments of 1300 bp for exon 1, 700 bp for exon 2 and 400 bp for a specific region of β-actin gene were observed in the wild-type line, in case of the protein trap line only a band for β-actin was observed. Thus, it appears that the transcription of *CG7985* is blocked by

the insertion of the GFP construct in the protein trap line and the protein trap line represents a mutant for *CG7985* (Figure 4.12b).

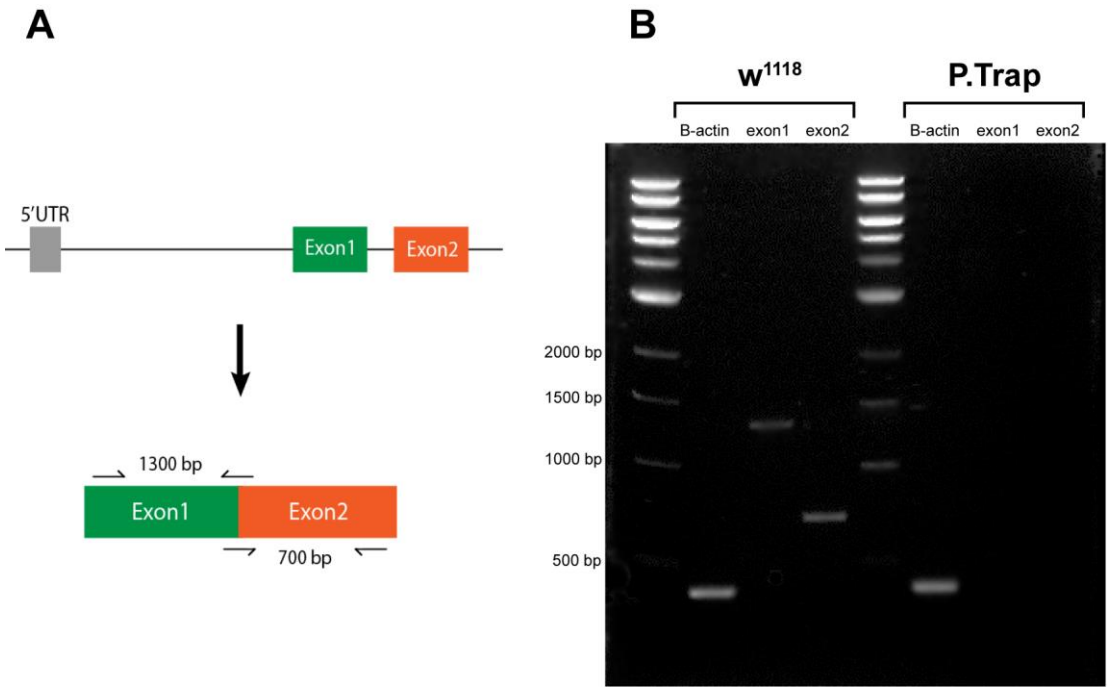

Figure 4.12. Transcription of *CG7985* is blocked by the insertion of a GFP construct in the protein trap line $CG7985^{CPTI100032}$. A: Schematic view of the position of primers and the corresponding size of PCR products. B: Comparison of PCR results on cDNA samples of w^{1118} and protein trap line. No transcript of *CG7985* is present in the protein trap line, while control PCR with β-actin gives the expected band (400 bp).

4.4.2. $CG7985^{null}$ Mutants are Lethal at the Late Third Instar Larval Stage

The protein trap line was shown to represent a mutant of *CG7985* as no mRNA is produced (Figure 4.12) and will from now on be referred to as $CG7985^{null}$. The line is homozygous viable until the late third instar stage of larval development and was used to analyse the phenotypic consequences of *CG7985* deletion. Initial examination of this line showed the presence of aggregations of melanotic masses just beneath the larval cuticle and over the fat body at the late third instar larval stage causing lethality before puparium formation (Figure 4.13a). In *Drosophila*, the melanization reaction is an essential component of the cell-mediated immune response and wound healing and is preceded by capsulation of parasitic invaders or disintegrated self-tissues, which is mediated by immune cells known as hemocytes. The activity of hemocytes increases in response to

parasitic, fungal or bacterial attack, and in such cases the cell-mediated defence system no longer recognizes the body tissues as self (Rizki and Rizki, 1980). The phenotype observed in *CG7985* mutant resembles a well-known melanotic tumor mutant, *tumor*^{w} (*tu*^{w}), in which the caudal fat body cells start to disintegrate at the third instar larval stage prior to hemocyte aggregation and melanization to encapsulate them. This indicates that the abnormality of fat body tissue maintenance is an underlying factor for the encapsulation reaction (Rizki and Rizki, 1974). In *CG7985* mutant larvae, a dissociation of fat body cells all over the body in the beginning of the third instar larval stage accompanied by the formation and melanization of capsules was also observed (Figure 4.13b).

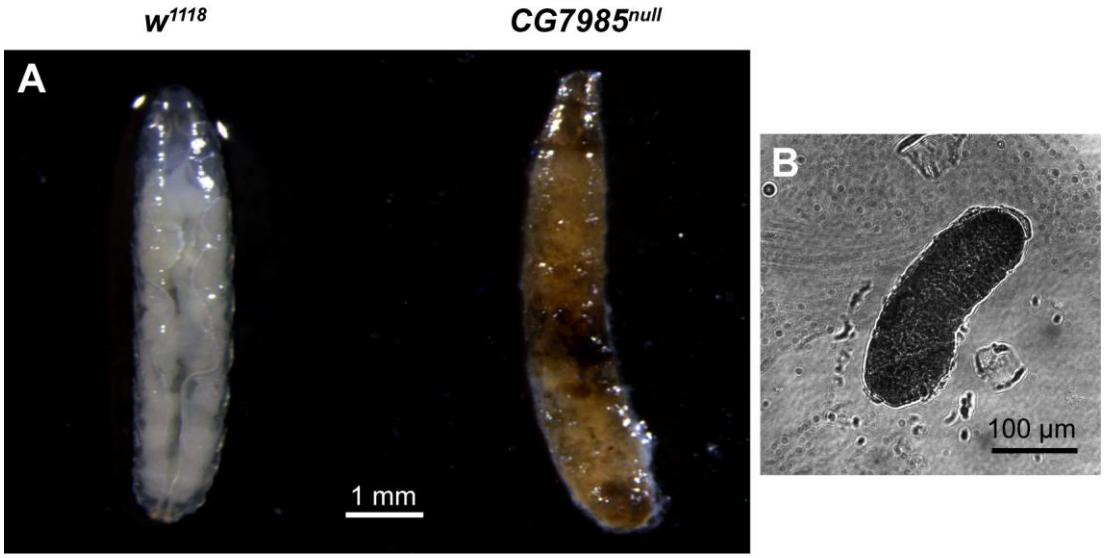

Figure 4.13. *CG7985*^{null} mutant larvae are lethal at the late third instar stage. A: Comparison of wild type (*w*^{1118}) and *CG7985*^{null} mutant larvae. Melanized capsules are present all over the larval body. B: Example of a melanized capsule dissected from *CG7985* mutant larvae.

4.4.3. *CG7985*^{null} Mutants Show Overgrowth in the Eye Imaginal Disc

The development of the eye imaginal disc starts at the embryonic stage by setting aside a small number of cells. Throughout larval development, the number of cells and their proliferation pattern are kept under strict control by several metabolic pathways. At the end of the third larval instar stage, about 6400 photoreceptor cells form the final structure of the eye imaginal disc, which differentiated from epithelial cells by the activity

of differentiation factors. Any impairment of the biological processes such as cell division, growth, death, and polarity likely cause an imbalance in the number of differentiated and undifferentiated cells, disrupting the general morphology of the eye imaginal disc (Kumar *et al*., 2011).

Because of our special interest in the eye and the specific expression of *CG7985* in the eye, the eye imaginal disc was analysed for abnormal phenotypes. Comparison of the general morphology of wild type and *CG7985*^{null} mutant eye imaginal discs revealed a tumor-like tissue overgrowth phenotype in *CG7985*^{null} mutant eye imaginal discs (Figure 4.14). In almost all *CG7985* mutant eye imaginal discs that were examined, overgrowth was especially observed at the anterior part of the eye imaginal discs, which manifested itself as foldings of the tissue.

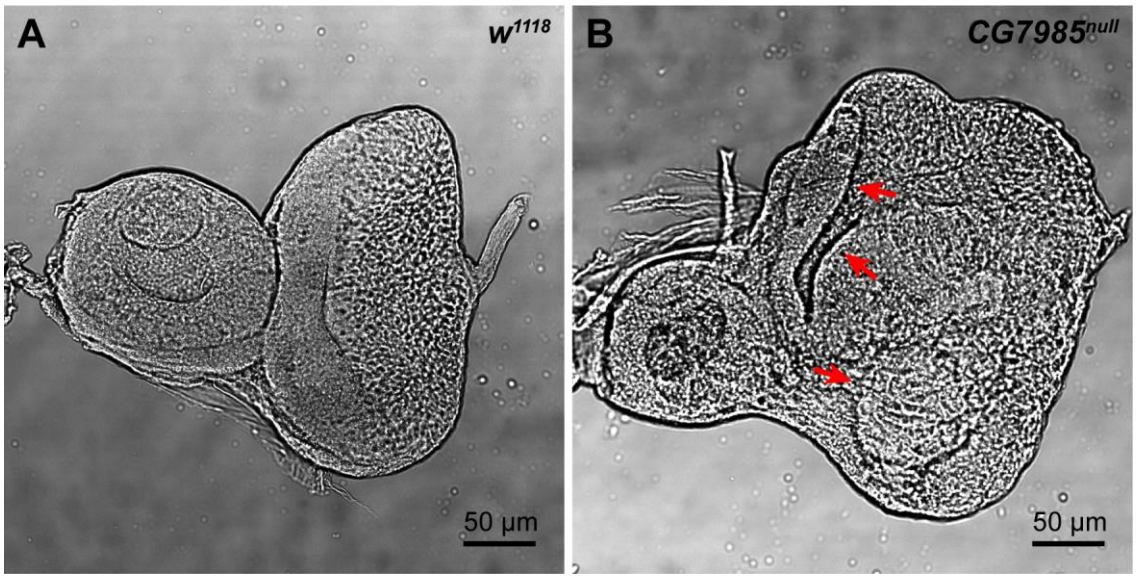

Figure 4.14. Comparison of wild type (*w*^{1118}) and *CG7985*^{null} mutant third instar eye imaginal discs. Loss of function of *CG7985* causes overgrowth of the eye imaginal disc. Note the larger size and folding of the tissue (red arrows).

4.4.4. *CG7985*^{null} Mutant Eye Imaginal Discs Exhibit Excessive Photoreceptor Loss

The overgrowth phenotype observed in *CG7985*^{null} mutant eye imaginal discs suggests an imbalance in the proliferation pattern of eye imaginal disc cells. In a normal developmental context, two successive cycles of cell division, called first and second

mitotic waves, form an appropriate number of cells, which later differentiate to photoreceptors and accessory cells. Moreover, a strict spatiotemporal control of cell divisions is necessary so that cells receive the correct differentiation signals and become neurons. In *Drosophila* eye development, members of signalling pathways including Notch and EGFR as well as the endocytic machinery have been linked to the control of cell division and growth. Therefore, mutations in these genes give rise to hyperplastic or neoplastic growth phenotypes (Baker *et al*., 2001; Gilbert and Moberg, 2006).

To analyse the differentiation and photoreceptor number of the *CG7985*^{null} mutant eye imaginal disc, we performed immunohistochemical analysis with an antibody against the neuronal marker Elav. As judged by analysing the Elav staining, the number of photoreceptors in *CG7985*^{null} mutant eye imaginal discs is significantly reduced compared to wild-type discs. Although the number of photoreceptors in *CG7985*^{null} mutant eye imaginal discs varies from one disc to another, the number of labelled neurons is always lower than in wild-types. Successfully differentiated photoreceptors are mainly located at the posterior edge of the eye imaginal discs, which likely indicates that there is a detrimental effect at the anterior part of the *CG7985*^{null} eye imaginal discs (Figure 4.15).

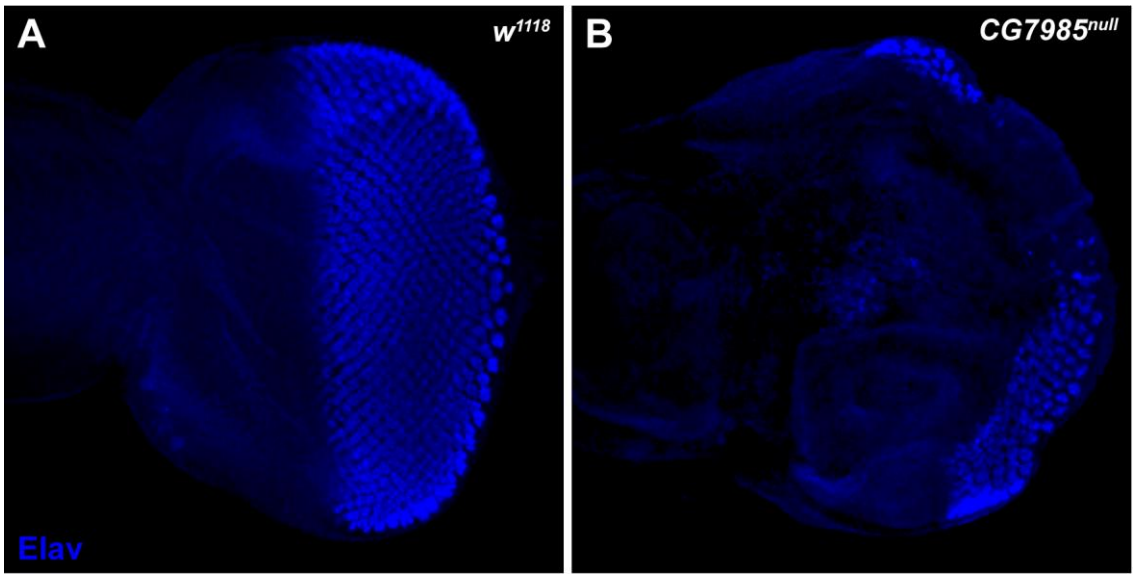

Figure 4.15. Comparison of photoreceptor differentiation between wild type (w^{1118}) and *CG7985*^{null} mutant eye imaginal discs with the neuronal marker Elav. A: Normal pattern and number of differentiated photoreceptors in a wild type (w^{1118}) eye imaginal disc. B: *CG7985*^{null} mutant eye imaginal disc exhibits significant photoreceptor loss.

4.4.5. Whole-eye *CG7985* Mutants Show Photoreceptor Loss in Adult Eye

The death of *CG7985*^{null} mutant larvae at the late third instar stage renders the observation and analysis of adult *CG7985*^{null} mutant eyes impossible. To overcome this difficulty, we used a method called EGUF/hid which allows the generation of eyes that are composed of cells exclusively homozygous for the mutation of interest in an otherwise heterozygous fly (Stowers and Schwarz, 1999). To make use of this system, the allele containing the mutation had to be recombined onto a chromosome carrying the appropriate FRT sequence in the location 82B (FRT82B). FRT82B is located on the third chromosome of *Drosophila* where *CG7985* and thus the mutant protein trap line (*CG7985*^{null}) is located. Since the generation of whole mutant eyes in the EGUF/hid method depends on the mitotic recombination between chromosome arms bearing FRT sequences at the same location, recombination of the *CG7985*^{null} mutation and the GMR-hid transgene eventually generates three distinct populations of cells in the eye in which the only surviving cells are the ones carrying the *CG7985*^{null} mutation in a homozygous state.

The analysis of adult eyes in *CG7985*^{null} whole mutant eyes revealed that the photoreceptor loss phenotype observed in larvae is present in adult eyes as well. Compared to wild type adult eyes, we observed a loss of eye tissue and also the formation of a melanized tumor-like tissue mass (Figure 4.16).

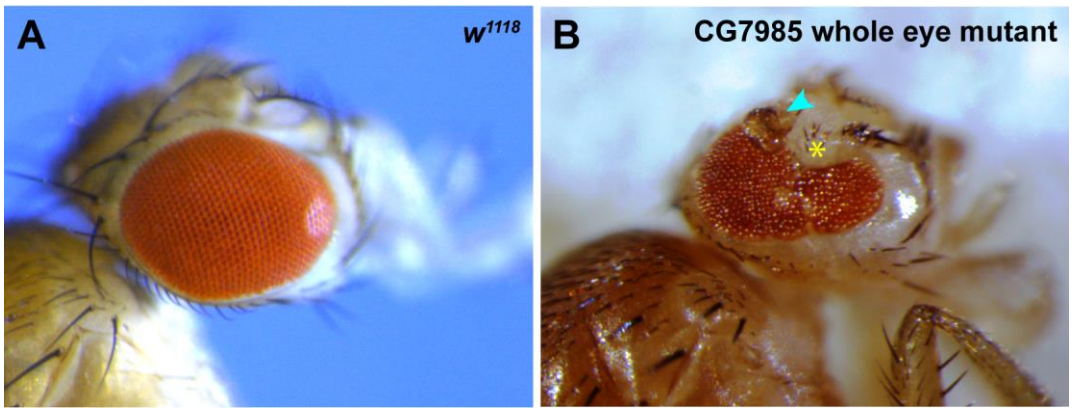

Figure 4.16. Comparison of wild type (*w*^{1118}) and *CG7985*^{null} whole mutant adult eyes. A: Wild type adult eye. B: *CG7985*^{null} whole eye mutant in an otherwise heterozygous animal. Tissue loss in the eye, formation of head tissue and bristles in place of eye tissue (asterisk), and melanized tumor-like mass (arrowhead) are visible.

4.4.6. Loss of CG7985 Function Induces Apoptosis in the Eye Imaginal Disc

Programmed cell death or apoptosis is a genetically controlled mechanism that is important for the development and homeostasis of multicellular organisms. However, apoptosis is also induced by various stress events. One common feature shared by *Drosophila* and other organisms is the activation of caspases in the cell death program (Fan and Bergman, 2008). A high degree of homology between vertebrate and *Drosophila* caspases made use of cleaved-Caspase-3 antibody, raised against human Caspase-3, very popular in *Drosophila* apoptosis research. In *Drosophila*, it is assumed that human Caspase-3 antibody recognizes two cleaved effector caspases, DRICE and DCP-1 (Fan and Bergman, 2010).

Observation of photoreceptor loss in *CG7985*^{null} discs led to the idea that the elimination of cells might be the result of increased caspase activity and hence an increase in apoptotic cell number. To analyse apoptotic activity in *CG7985*^{null} eye imaginal discs, we performed co-staining of cleaved Caspase-3 (Cas3) and the neuronal marker Elav.

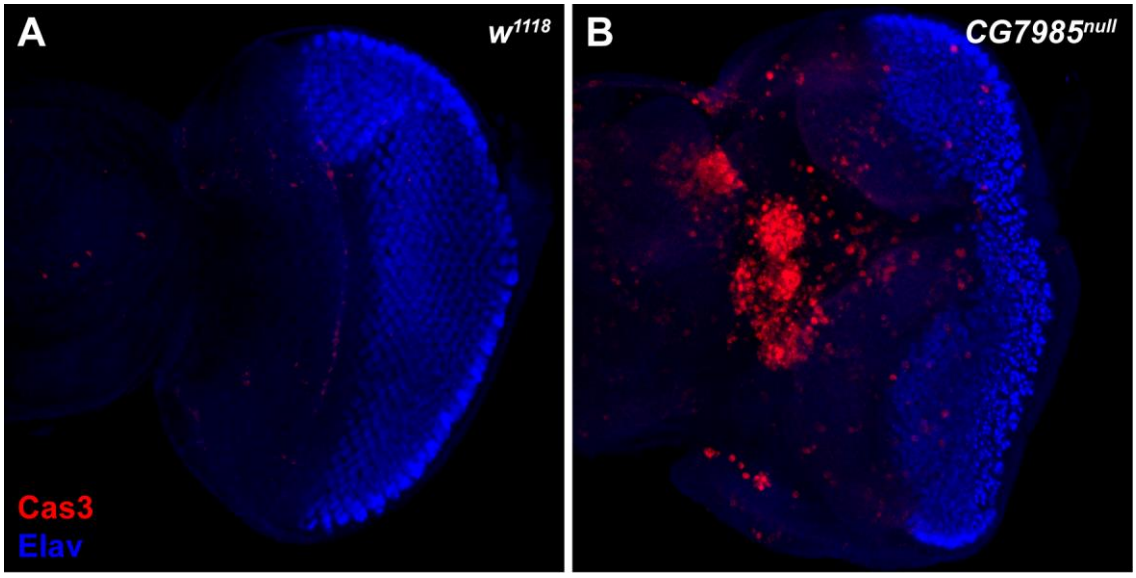

Figure 4.17. Comparison of apoptotic activity in wild-type (w^{1118}) and *CG7985*^{null} mutant eye imaginal discs by cleaved Caspase-3 (Cas3) antibody. A: Wild-type eye imaginal disc have no apoptotic activity. B: Apoptotic activity is highly increased at the anterior part of the *CG7985*^{null} mutant eye imaginal disc. Note that there are only few apoptotic neuronal cells that are labelled with Elav.

This staining is expected to show general apoptotic activity, the relative positions of dying cells, and all the differentiated photoreceptors. As a result of this experiment, it was shown that apoptotic activity was increased at the anterior, undifferentiated part of the *CG7985*^{null} mutant eye imaginal discs compared to wild type discs (Figure 4.17). Interestingly, almost no apoptotic neuronal cells were observed, which likely shows that the decreased number of photoreceptors is a result of a depletion of the pool of cells that are normally recruited to differentiate into photoreceptors.

4.4.7. Loss of CG7985 Function Causes Lipid Accumulation and Lysosomal Enlargement

Lysosomal storage disorders are characterized by the excess accumulation of lipids and other lipid raft components in lysosomes. As stated before in the introduction part, loss of function of hexosaminidases results in defects in the degradation of glycosphingolipids including gangliosides. However, the accumulation of one component of lipid rafts also triggers the accumulation of other components in lysosomes. In several types of lysosomal storage disorders, disruption of the cholesterol mechanism and functioning of signalling cascades has been shown as the result of secondary accumulations of cholesterols and transmembrane proteins, respectively (Ceresa and Schmid, 2000).

In order to understand if the loss of CG7985 function results in lipid accumulation, we used a specific dye, called LipidTOX^{TM} Phospholipidosis and Steatosis Detection Stain, which has been specifically designed to stain large accumulations of phospholipids known as phospholipidosis. The aim was to visualize the phospholipid staining together with Elav antibody to reveal the status of photoreceptor differentiation. However, it appeared that LipidTOX^{TM} staining was not compatible with a two-day procedure of immunofluorescence staining and appeared to diffuse out of the cells. Thus, the phospholipid staining of wild-type and *CG7985*^{null} mutant eye imaginal discs were compared and showed the presence of large accumulations of phospholipids in *CG7985*^{null} mutant eye imaginal discs (Figure 4.18b). The lack of signal in wild type

tissue (Figure 4.18a) does not indicate a problem in the staining procedure. As stated before, LipidTOX™ Phospholipidosis and Steatosis Detection Stain does not bind individual phospholipids. It has been specifically designed to recognize phospholipid accumulations.

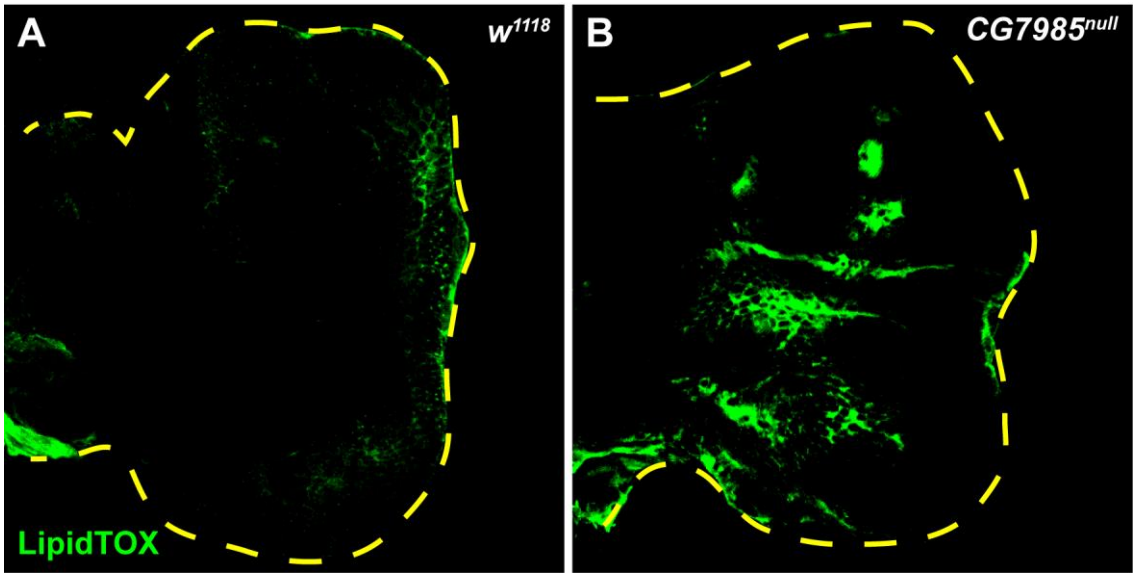

Figure 4.18. Phospholipid accumulation in *CG7985*^{null} mutant eye imaginal discs. A: LipidTOX™ Phospholipidosis and Steatosis Detection Stain in wild type eye imaginal disc. No accumulation observed. B: LipidTOX™ Phospholipidosis and Steatosis Detection Stain in *CG7985*^{null} mutant eye imaginal disc. Large accumulations observed at anterio-middle region of the eye imaginal disc.

The observation of lipid accumulation in *CG7985*^{null} mutant eye imaginal discs is the first indication for a putative function of CG7985 in the glycosphingolipid degradation pathway. Considering the symptoms of lysosomal storage disorders in *Drosophila* and vertebrates, it was necessary to analyse the status of lysosomes. Generally, excess accumulation of lipids and other components in lysosomes due to defects in degradation pathways causes swelling, and in extreme cases bursting of lysosomes. In an attempt to reveal the morphological status of lysosomes, an acidotropic dye, namely Lysotracker, which stains acidic compartments, including lysosomes and autolysosomes was used.While its name Lysotracker implies that it stains all lysosomes, the high detection threshold of this dye doesn't allow to stain lysosomes in their normal morphological states. Instead, it stains enlarged lysosomes like autolysosomes that arise when phagosomes

combine with lysosomes. Alternatively, it is used to reveal the diseased state of lysosomes like in lysosomal storage disorders (Edgar *et al*., 2009).

The lysotracker staining of wild-type and *CG7985*^{null} mutant eye imaginal discs revealed that the number and size of lysosomes in *CG7985*^{null} mutant eye imaginal discs is dramatically increased compared with the wild type. The region of cells with enlarged and numerically increased lysosomes was also accompanied with photoreceptor loss (Figure 4.19). This result implies that disruption of lysosomal morphology might be the reason for neuronal loss.

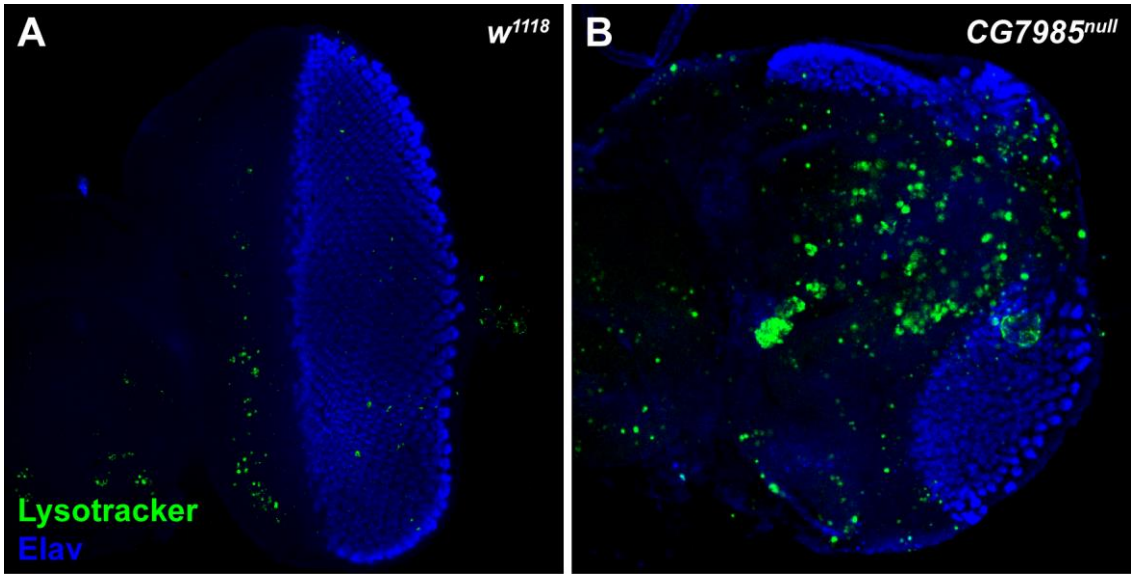

Figure 4.19. Comparison of the number and size of lysosomes in wild-type (w^{1118}) and *CG7985*^{null} mutant eye imaginal discs by Lysotracker. The number and size of lysosomes are dramatically increased in *CG7985*^{null} mutant eye imaginal disc.

Lipid accumulation and lysosomal enlargement were observed in separate experiments, thus, it was important to show if lipid accumulations are the reason of lysosomal enlargements. For this purpose, we used Lysotracker and LipidTOX™ Phospholipidosis and Steatosis Detection Stain together to evaluate if co-localization of signals can be observed. Stainings on *CG7985*^{null} mutant eye imaginal discs revealed that Lysotracker and LipidTOX phospholipid stains co-localized at many points (Figure 4.20a', b', c' blue arrows). Once more, this result supports the role of CG7985 in the glycosphingolipid degradation pathway.

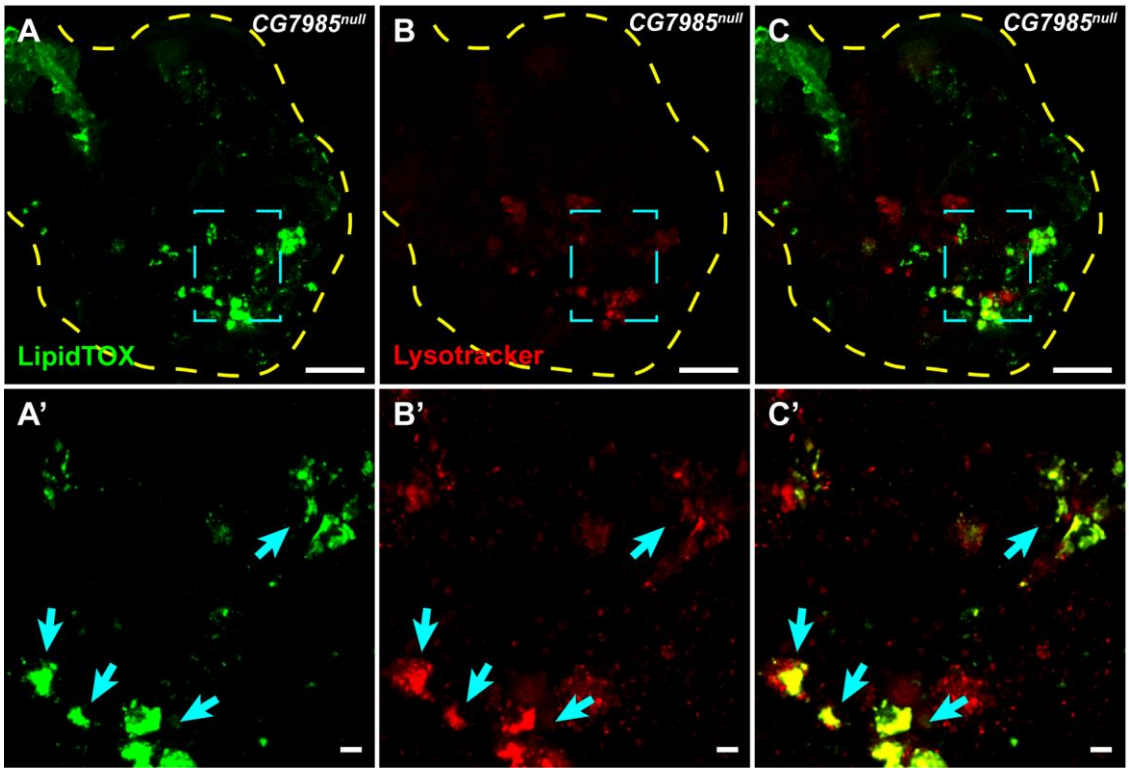

Figure 4.20. Lipid accumulations result in lysosomal enlargements in *CG7985*^{null} mutant eye imaginal disc. Co-localized signals of Lysotracker and LipidTOX^{TM} phospholipid stains prove that lipid accumulations are the reason of lysosomal enlargement.

4.4.8. Enlarged Lysosomes Trigger Apoptosis

Previously, we showed that Cas3-positive apoptotic cell number was dramatically increased in *CG7985*^{null} mutant eye imaginal discs. Previously, several groups have tried to link apoptosis to the dysfunction of lysosomes (Aits and Jaattela, 2013; Appelqvist *et al*., 2011; Boya and Kroemer, 2008). These studies revealed that excessive accumulation of waste products and the eventual increase in size and number of lysosomes results in so-called “leaky lysosomes”, from which harmful hydrolytic enzymes leak into the cells and trigger apoptosis. In such cases, swelling of lysosomes increases the permeabilization of the lysosomal membrane in a way that it can no longer hold the hydrolytic enzymes inside. Cathepsins have been put forward as the primary responsible molecules in triggering apoptosis since they mediate dramatically increased proteolysis after they leak into the cytosol (Aits and Jaattela, 2013).

We hypothesized that the enlargement of lysosomes that were observed in *CG7985*^{null} mutant eye imaginal disc might be the reason for the large number of Cas3-positive apoptotic cells. In order to confirm this hypothesis, co-staining with cleaved Cas-3 antibody and Lysotracker was performed. Although not a complete co-localization of Cas3 and Lysotracker signals was observed, the localization of the two signals appeared to be highly correlated. Therefore, it still appears plausible that lysosomal enlargement is the reason for triggering an apoptotic signal in cells that are mutant for *CG7985*.

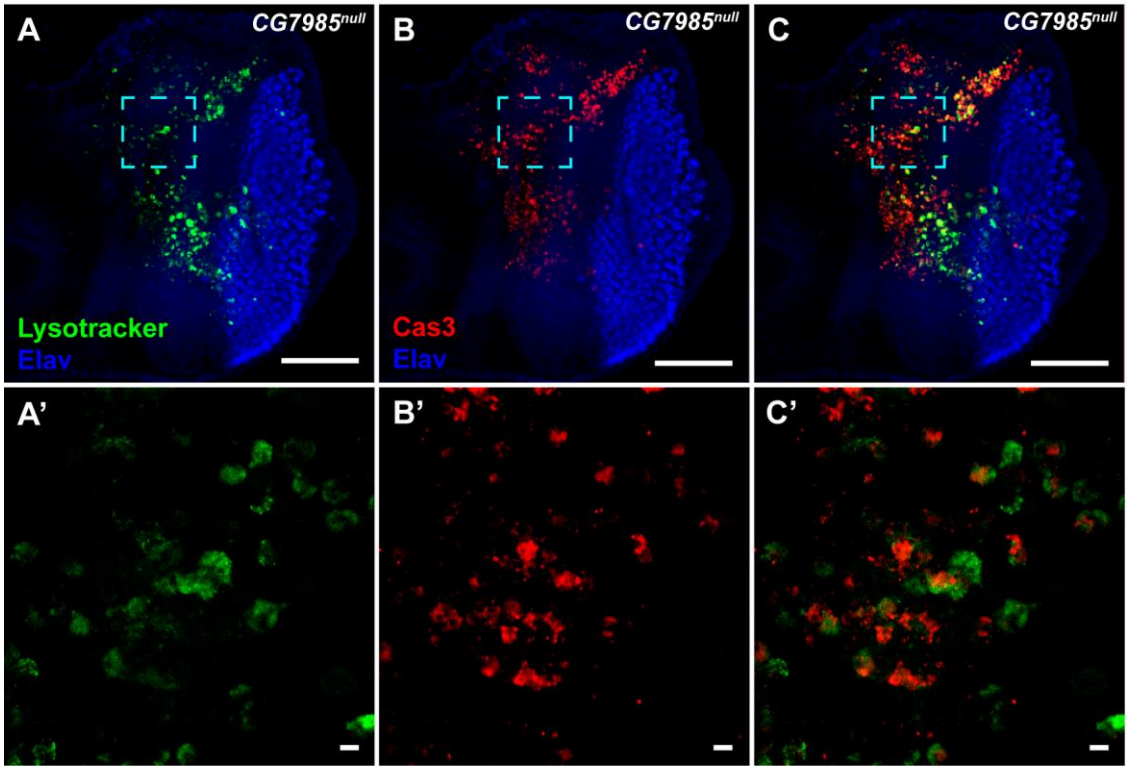

Figure 4.21. Apoptotic signal is triggered by enlarged lysosomes. A and A': Lysotracker staining of *CG7985*^{null} mutant eye imaginal disc. B and B': Anti-cleaved Cas3 staining of *CG7985*^{null} eye imaginal discs. C and C': Location of Lysotracker and cleaved Cas3 antibody signals are largely correlated in the cells of *CG7985*^{null} mutant eye imaginal disc.

4.4.9. Apoptotic Cells Trigger Compensatory Proliferation in Neighboring Cells

In Figure 4.14 it was shown that the loss of function of CG7985 causes overgrowth of eye imaginal discs, which appears as a general increase in size and formation of tumor-like tissue foldings. This result seems to contradict the observation that the Cas3-positive

apoptotic cell number is dramatically increased in *CG7985*^{null} mutant eye imaginal discs (Figure 4.17). An intensive literature survey helped in finding a possible explanation for this apparent dilemma. In *Drosophila* and vertebrates, proapoptotic proteins – mostly caspases – have been shown to induce compensatory proliferation in neighboring cells in an attempt to replace them with dying cells to maintain tissue homeostasis (Ryoo and Bergman, 2012). Thus, in the next experiment proliferation in eye imaginal discs in *CG7985*^{null} mutants was investigated. For this purpose, an antibody against phospho-histone H3 (anti-pH3), which marks proliferating cells at the M phase, was used. In wild-type eye imaginal discs, cells divide synchronously just before the MF (Figure 4.22a), whereas the number of dividing cells in *CG7985*^{null} mutant eye imaginal discs is greatly increased and the proliferation pattern is disrupted (Figure 4.22b).

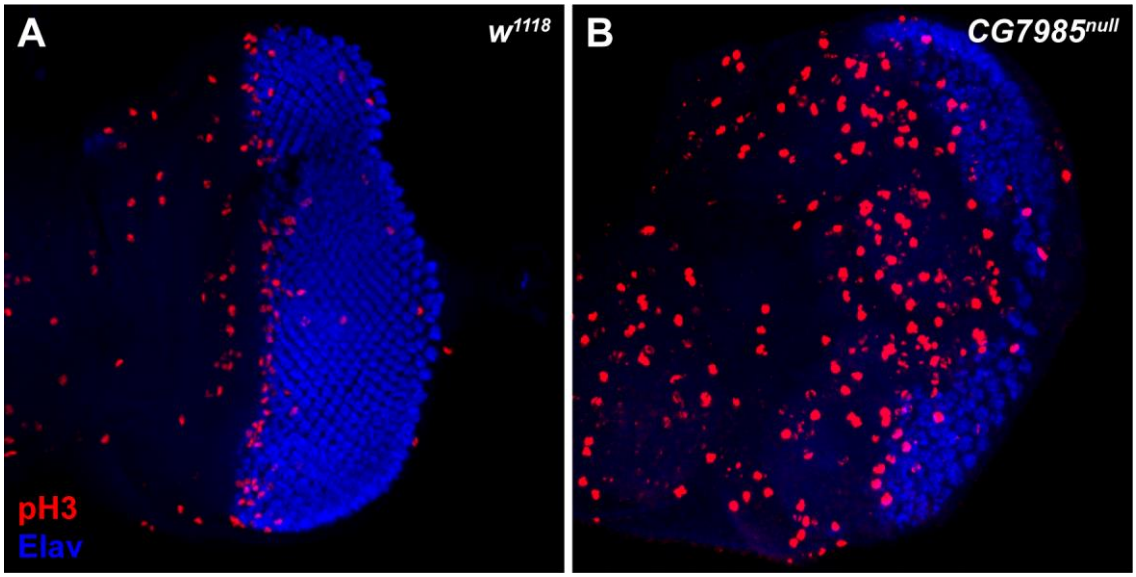

Figure 4.22. Comparison of the number of proliferating cells in wild-type (*w*^{1118}) and *CG7985*^{null} mutant eye imaginal discs. Proliferating cells were labelled with anti-phosphohistone H3 (pH3) antibody. Although cells divide synchronously just before the MF in the wild-type disc, the number of proliferating cells is dramatically increased and the normal proliferation pattern is disrupted in *CG7985*^{null} mutant eye imaginal disc.

To analyse the localization of proliferating cells in comparison to the location of apoptotic cells, a co-localization experiment was planned. However, antibodies against pH3 and cleaved Cas3 are raised in the same host and we couldn't obtain antibodies that react with the corresponding *Drosophila* proteins and are raised in different hosts to

perform this experiment. Therefore, we used an indirect way using Lysotracker together with anti-pH3 antibody. Since we previously showed that Lysotracker-positive cells were co-localized with anti-cleaved Cas3-positive cells, we hypothesized that we would obtain the same result.

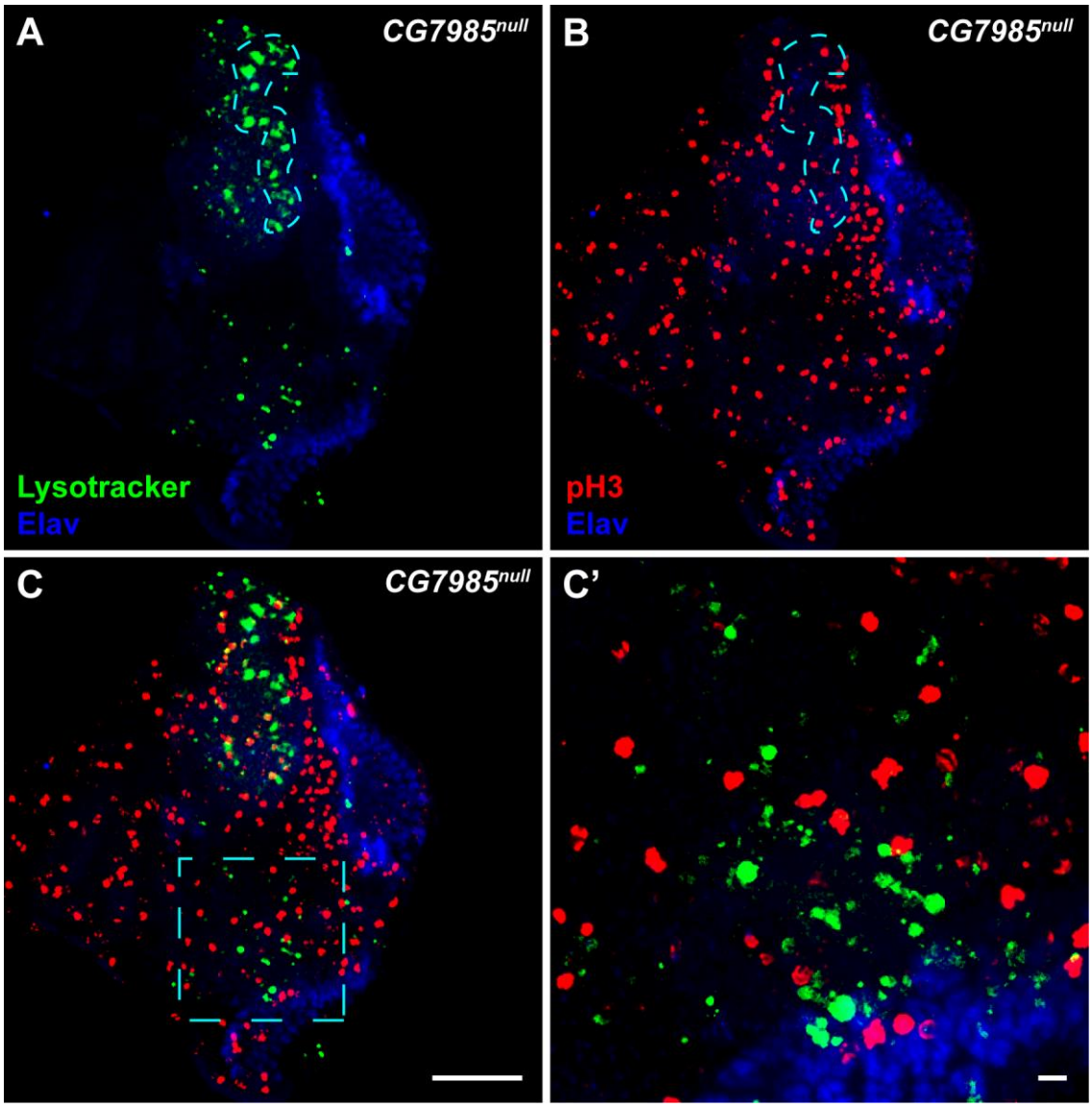

Figure 4.23. Proliferating cells are localized around the cells with enlarged lysosomes. Imaginal discs were stained with Lysotracker and anti-pH3 antibody. A and B: The territory with high number of Lysotracker-positive cells are devoid of proliferating cells. C and C': Lysotracker positive cells do not co-localize with proliferating cells.

Double staining of Lysotracker and anti-pH3 showed that the number of proliferating cells around the territory of Lysotracker-positive cells, which are cells with enlarged

lysosomes and hence apoptotic are increased (Figure 4.23a and b). Also, in a close view, it can be observed that Lysotracker-positive cells do not co-localize with pH3-positive proliferating cells (Figure 4.23c'). Therefore, it appears that apoptotic dying cells promote proliferation of their neighboring cells.

4.4.10. Wingless Signalling Mediates Compensatory Proliferation

In *Drosophila*, Decapentaplegic (Dpp) and Wingless (Wg) are growth factors secreted in growing tissues (Perez-Garijo *et al*., 2011). Therefore, in several studies, they were proposed to have a role in compensatory proliferation. In our study, we have shown that apoptotic dying cells promote proliferation of neighboring cells. In the next few experiments we set out to investigate if this compensatory proliferation is mediated by a growth signal and which one of the growth signalling pathway is involved.

Several pathways are known to promote tissue growth and proliferation. In some of them like in the Notch signalling pathway, membrane-bound receptors and ligands are in direct contact on the plasma membranes of two opposing cells to initiate the signalling cascade. In others, the pathway is triggered in a distance by diffusible signalling molecules.

In $CG7985^{null}$ mutants, compensatory proliferation was triggered in cells that were several cell diameters away from the nearest apoptotic cell. Thus, we hypothesized that the signal emitted from the apoptotic cells must be diffusible. Therefore, we focused on Wingless signalling and analysed its general tissue distribution using an anti-Wingless antibody in wild-type and $CG7985^{null}$ mutant eye imaginal discs.

The analysis showed that Wingless is localized to the anterio-lateral parts of the wild-type eye imaginal disc (Figure 4.24a). Normally, the movement of the MF is faster at the anterio-lateral parts of the eye imaginal disc due to its shape. By localizing to those parts, Wingless signalling forms an inhibitory loop with Dpp signalling, which promotes the movement of the MF and prevents the formation of ectopic eye tissue (Ma and Moses, 1995). Compared to the wild-type control, the localization of Wingless is distributed over a broader range in $CG7985^{null}$ mutant eye imaginal disc. Especially, an additional intense

Wingless signal at the anterio-middle region was apparent. This region corresponds exactly to the region in which the ectopic proliferation was previously observed and suggests that Wingless signalling mediates compensatory proliferation in *CG7985*^{null} mutant eye imaginal discs (Figure 4.24b red arrow).

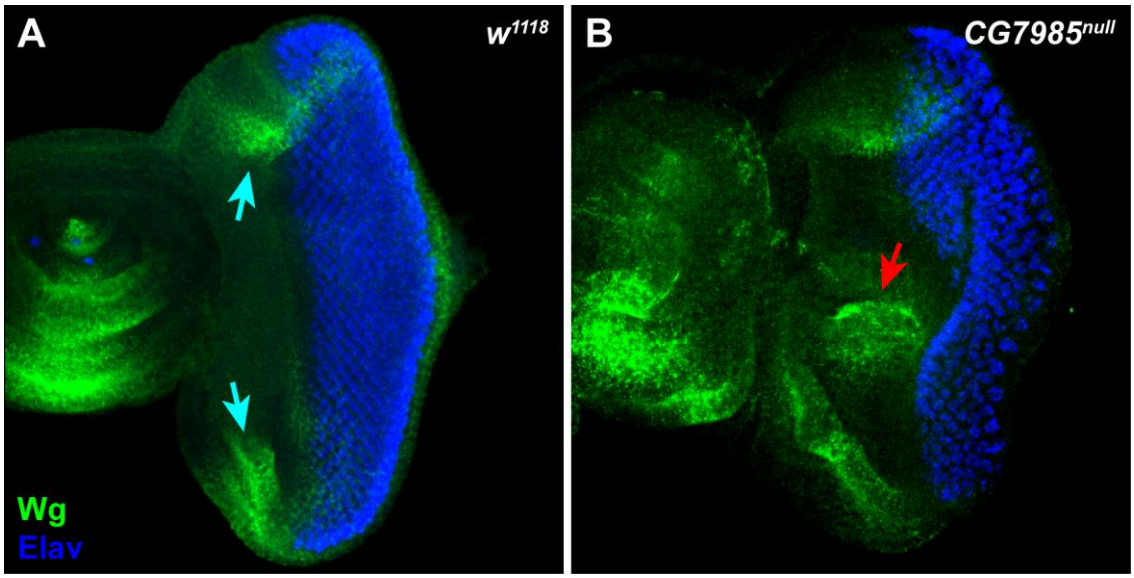

Figure 4.24. The distribution of Wingless (Wg) in wild-type (*w*^{1118}) and *CG7985*^{null} mutant eye imaginal discs. A: In wild-type, Wg is localized to anterio-lateral parts of the eye imaginal disc (blue arrows). B: In *CG7985* mutant eye imaginal disc, in addition to its normal distribution in anterio-lateral regions, ectopic expression of Wg in anterio-middle region is also observed (red arrow).

4.5. Tissue-specific Knockdown Analysis of *CG7985*

4.5.1. Eye-Specific Knockdown of *CG7985* Shows Similar Results to Mutant Analysis

Knockdown analysis of a gene by means of RNA interference (RNAi) is an alternative strategy to mutant analysis. While in mutants the function of the gene is lost in all cells where it is expressed, RNAi allows for more specific analysis by particular downregulation in specific tissues or even cell types.

To further support the function of CG7985 in *Drosophila* eye development obtained

by analyzing *CG7985*^{null} mutants, we crossed the eye-specific Gal4 driver *ey*-Gal4 to UAS-CG7985RNAi that encodes for a double-stranded RNA to downregulate the expression of *CG7985*. The combination of *ey*-Gal4 and UAS-CG7985RNAi resulted in knockdown of *CG7985* specifically in the eye.

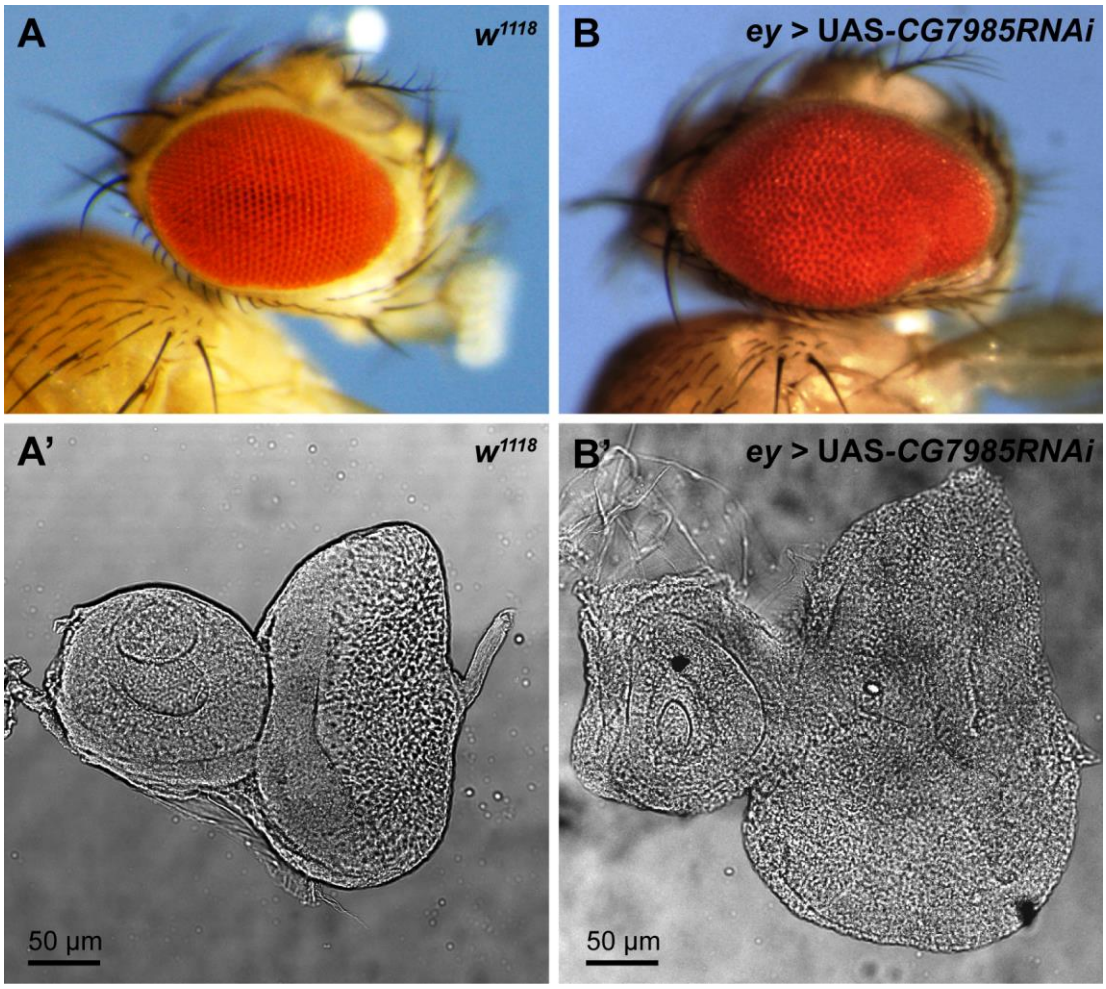

Figure 4.25. Eye-specific knockdown of *CG7985* results in overgrowth of the eye. A and A': Wild-type adult eye and eye imaginal disc. B and B': Adult eye and eye imaginal disc of ey > UAS-CG7985RNAi line. The overgrowth phenotype is similar to the mutant phenotype, except for the photoreceptor differentiation phenotype that was not observed to a large extent.

Similar to the results obtained in the null mutant analysis, knockdown of *CG7985* in the eye resulted in overgrowth of the eye imaginal disc. As a reflection of overgrowth in the eye imaginal discs, we also observed overgrowth in the adult eyes. Although eye imaginal discs were enlarged in both *CG7985* mutant and knockdown, unlike the results

obtained with whole-eye mutants of *CG7985*, no photoreceptor loss was observed in adult eyes of *CG7985* knockdown (Figure 4.25). Additionally, the effect of *CG7985* downregulation on the growth of the eye varied from individual to individual resulting in overgrowth of the adult eyes to different extents.

To analyse the differentiation of photoreceptors, immunofluorescence analysis of *CG7985* knockdown eye imaginal discs with anti-Elav antibody was performed. This analysis revealed that photoreceptors differentiated almost normally, although the apical cell polarity of photoreceptors in ommatidia were disrupted and there were some positional problems in the location of photoreceptors near the anterior side of the eye imaginal disc. This phenotype might result from a problem in the movement of the MF.

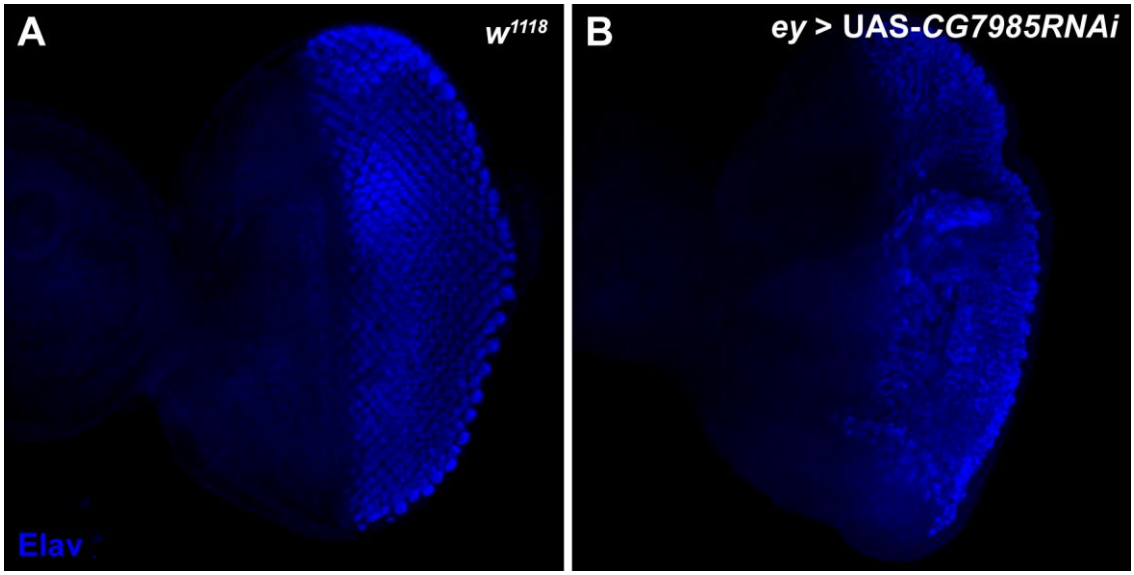

Figure 4.26. Comparison of photoreceptor differentiation between wild type (w^{1118}) and ey > UAS-CG7985RNAi knockdown eye imaginal discs using the neuronal marker Elav. A: Normal pattern and number of differentiated photoreceptors in a wild type (w^{1118}) eye imaginal disc. B: ey > UAS-CG7985RNAi knockdown eye imaginal disc does not exhibit significant photoreceptor loss. However, the localization of photoreceptors is disrupted.

Lysotracker staining was performed to evaluate the number and size of lysosomes in *CG7985* knockdown eye imaginal discs. This analysis revealed an increase in the number of lysosomes, however the effect was milder than the effect observed in the $CG7985^{null}$ mutants (Figure 4.27a).

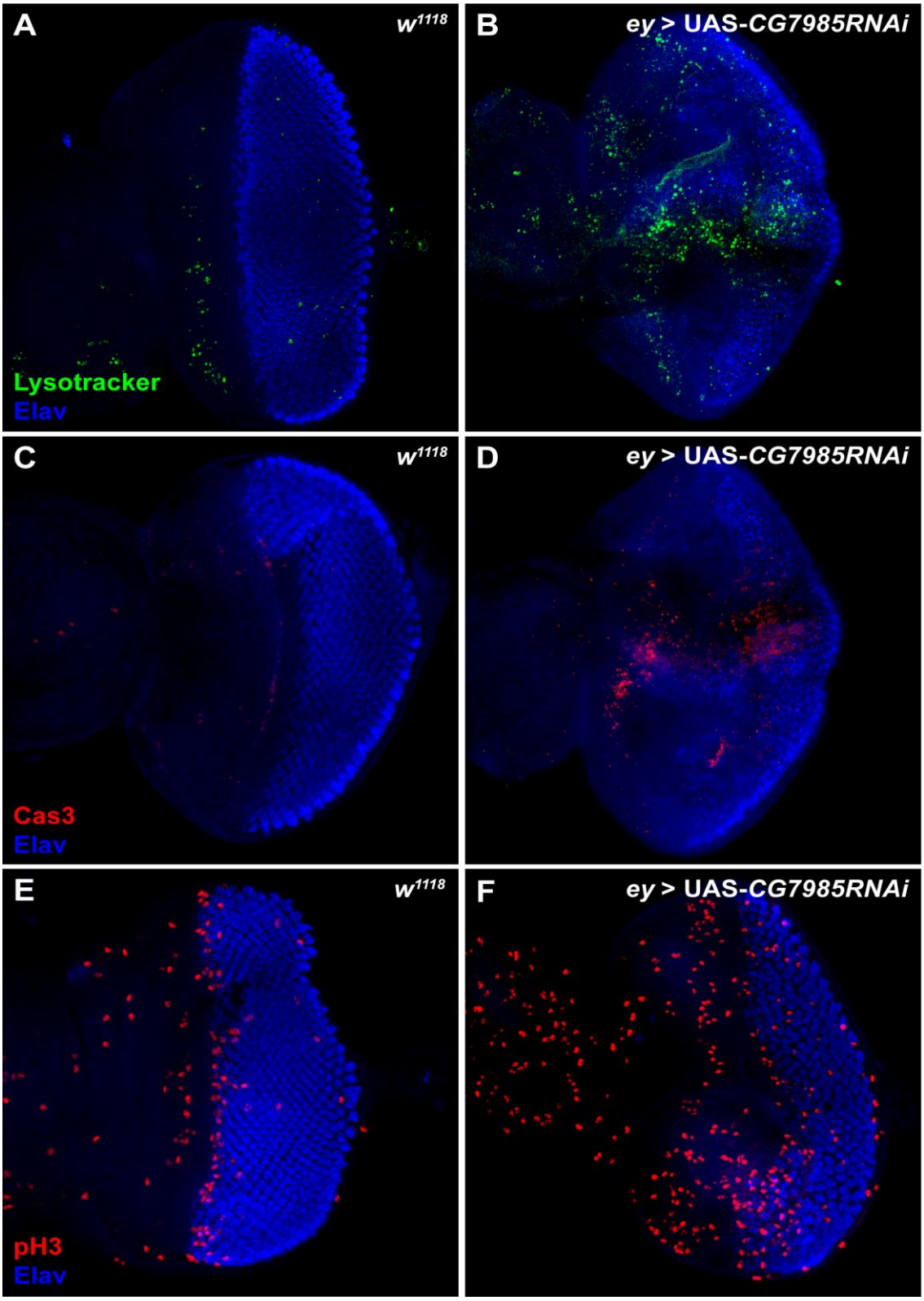

Figure 4.27. Eye-specific knockdown of *CG7985* results in phenotypes that are similar to those observed in $CG7985^{null}$. A and B: The number of lysosomes is increased when CG7985 is downregulated. C and D: Apoptotic activity is increased when CG7985 is downregulated. E and F: The number of proliferating cells is increased when CG7985 is downregulated.

In order to evaluate the number of apoptotic cells, anti-cleaved Cas3 antibody was used. Compared to wild-type control, the apoptotic activity was higher. However, when the results were compared to the results obtained in the mutant, clearly the number of apoptotic cells was fewer in *CG7985* knockdown eye imaginal discs. This result also correlates with the milder effect of *CG7985* knockdown on lysosomes (Figure 4.27b).

Lastly, the number of proliferating cells using anti-pH3 antibody was evaluated. Compared to the control, the number of proliferating cells was dramatically increased. However, unlike the milder effects that were observed in Lysotracker and anti-cleaved Cas3 immunostainings, the effect of knockdown of *CG7985* on the proliferation state of cells was similar to that observed in the null mutant (Figure 4.27c).

4.6. Generation of *CG7985* Conditional Allele by CRISRP/Cas9

4.6.1. Strategy Overview

The development of CRISPR/Cas9 technology was one of the breakthroughs in genome-engineering of model organisms. Although, in the beginning, the use of this technology was limited to the mutation of a few genes that give visible phenotypes that can easily be scored such as white and yellow genes, nowadays it has become the gold standard in genome editing.

CRISPR/Cas9 technology enables the efficient introduction of double-stranded breaks (DSB) that can either be used directly to generate frameshift mutations in exons by the error-prone nonhomologous end-joining (NHEJ) pathway or to integrate foreign DNA sequences into the genome by the homology-directed repair (HDR) pathway (Gratz *et al.*, 2014). In this study, a two-step strategy combining CRISPR-mediated HDR was combined with a recombinase-mediated cassette exchange (RMCE). In the first step, we aimed to integrate two attP recombination sites in opposite orientations into the intergenic regions between *CG7985* and its upstream and downstream genes, together with visible eye markers 3xP3-GFP and 3xP3-dsRED. These visible markers were followed by stop codons and a SV40 polyA terminator sequence. In brief, the aim was to flank the genomic locus of

CG7985 with two attP recombination sites in opposite directions and to integrate two different visible markers (GFP or dsRED under the control of eye-specific 3xP3 promoters) to trace the homologous recombination events separately, by visualizing GFP and dsRED fluorescence in the eyes of putative positive recombinants.

In the second step, after the successful integration of the two recombination constructs would result in the integration of attP recombination sites into the genome, RMCE would be applied to replace the genomic locus of *CG7985* with any DNA of choice.

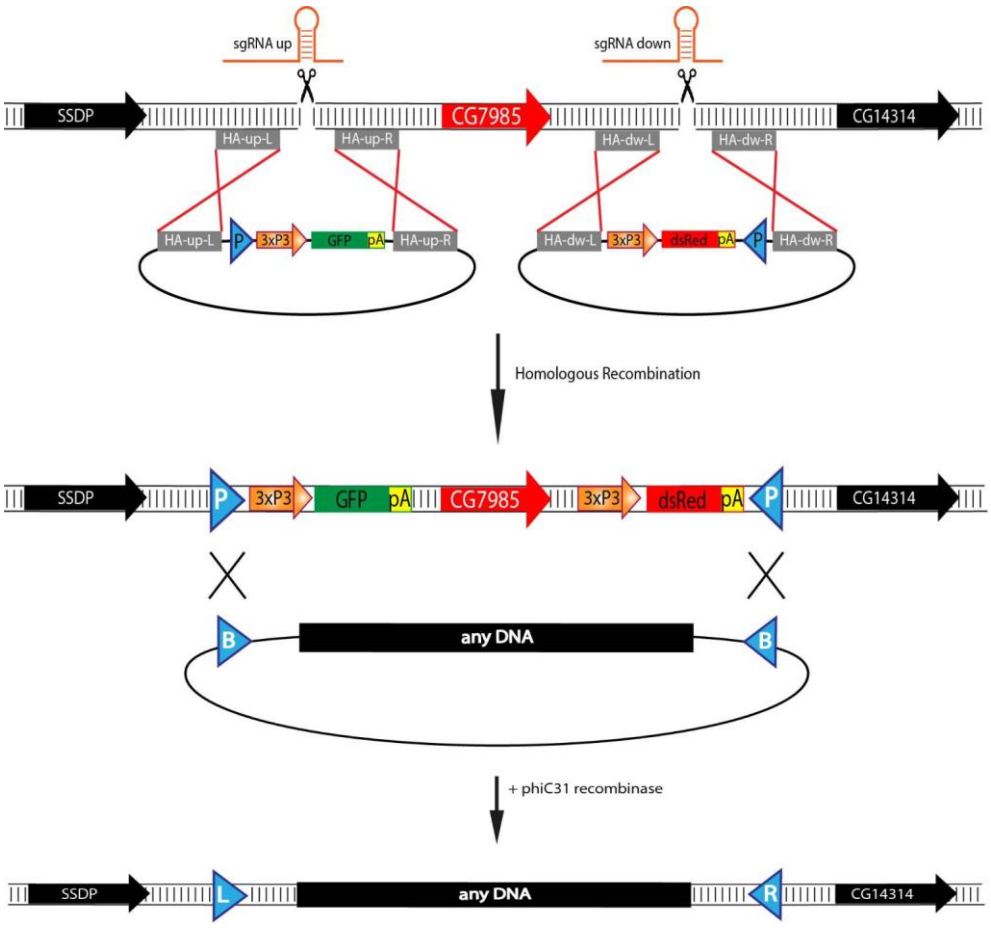

Figure 4.28. Schematic overview of the two-step genome editing process of the genomic locus of *CG7985* by CRISPR/Cas9 and RMCE. In the first phase, sgRNAs generate DSBs and two separate homologous recombination events take place to introduce attP recombination sites and markers into the genome. In the second phase, the genomic locus of *CG7985* can be replaced with any DNA between the two attB sites in a replacement cassette by RMCE.

To do so, embryos of positive recombinants would be injected with replacement cassettes containing two attB recombination sites in opposite orientations flanking any DNA of choice. In theory, ΦC31 recombinase would induce site-directed recombination between the recombination sites attP and attB thereby replacing the genomic locus of *CG7985* with the DNA sequence flanked by the attB sites in the replacement casettes (Figure 4.28). It has been reported that recombination between attP and attB sites leaves a minimal scar in the genome, namely attR and attL sites, which however do not interfere with gene function. In our strategy we nevertheless chose target sites in intergenic regions several kb upstream and downstream of the genomic locus of *CG7985* to avoid that any scar sequence would interfere with the function of the *CG7985* gene.

Overall, using such a two-step process to edit the genomic locus of *CG7985* would allow us to perform various genome modifications, including the addition of protein tags, point mutations, exon deletions or any other desired changes in the genomic locus of *CG7985*. However, our main aim was to use this system to generate different mutants of *CG7985* and tag it with different fluorescent markers in its endogenous locus.

4.6.2. SgRNA and Targeting Plasmid Design and Cloning

In the first phase of the two-step process, CRISPR/Cas9 is used to introduce attP recombination sites and fluorescent markers into the genome. For this purpose, a sgRNA plasmid was generated, from which two separate sgRNAs were transcribed to generate DSBs at defined positions in the upstream and downstream of the genomic locus of *CG7985*. To construct the sgRNA plasmid, we used the Gibson assembly method. Using this method, a pBlueScript II vector linearized by *EcoRV* and a synthetic DNA block which contain upstream and downstream targeting sequences, directed repeats (DR) to separate these like in the original CRISPR locus in *Streptococcus pyogenes* genome, and a *Drosophila* U6 promoter (dmU6) to induce their transcriptions were assembled (Figure 4.29a). After transformation of the assembled plasmid, several bacterial colonies were selected to test for the presence of the plasmid by colony PCR. Colony PCR was performed with one primer located within the synthetic DNA block and one primer located within the vector backbone. The expected band size was 1.3 kb and the colony PCR result

showed that all the colonies that were tested were positive (Figure 4.29b). After sequencing, one of colonies carrying no mutations was selected and used for injection into embryos.

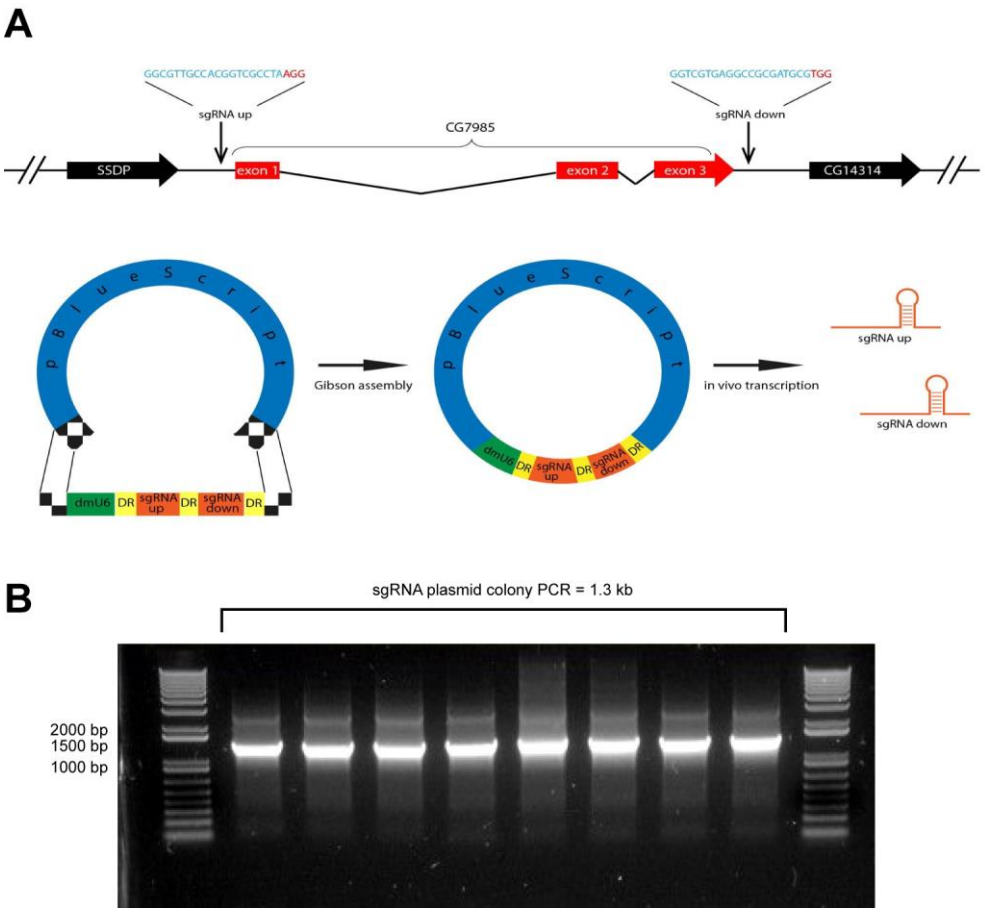

Figure 4.29. Cloning of the sgRNA plasmid using Gibson assembly. A: Schematic view of the positions of target sequences and construction of sgRNA plasmid using Gibson assembly. B: Colony PCR result to check the presence of sgRNA plasmid in 8 different colonies. All selected colonies were positive displaying the expected 1.3 kb band.

We followed a similar strategy to construct two different targeting plasmids for the upstream and downstream integration events. However, in the targeting plasmids, 3xP3-GFP-attP and 3xP3-dsRED-attP transgenes were flanked by 1.5 kb long homology arms in order for homologous recombinations to take place (Figure 4.30a and b). Here, a pBlueScript II vector backbone, two homology arms, and the transgene were assembled using Gibson assembly.

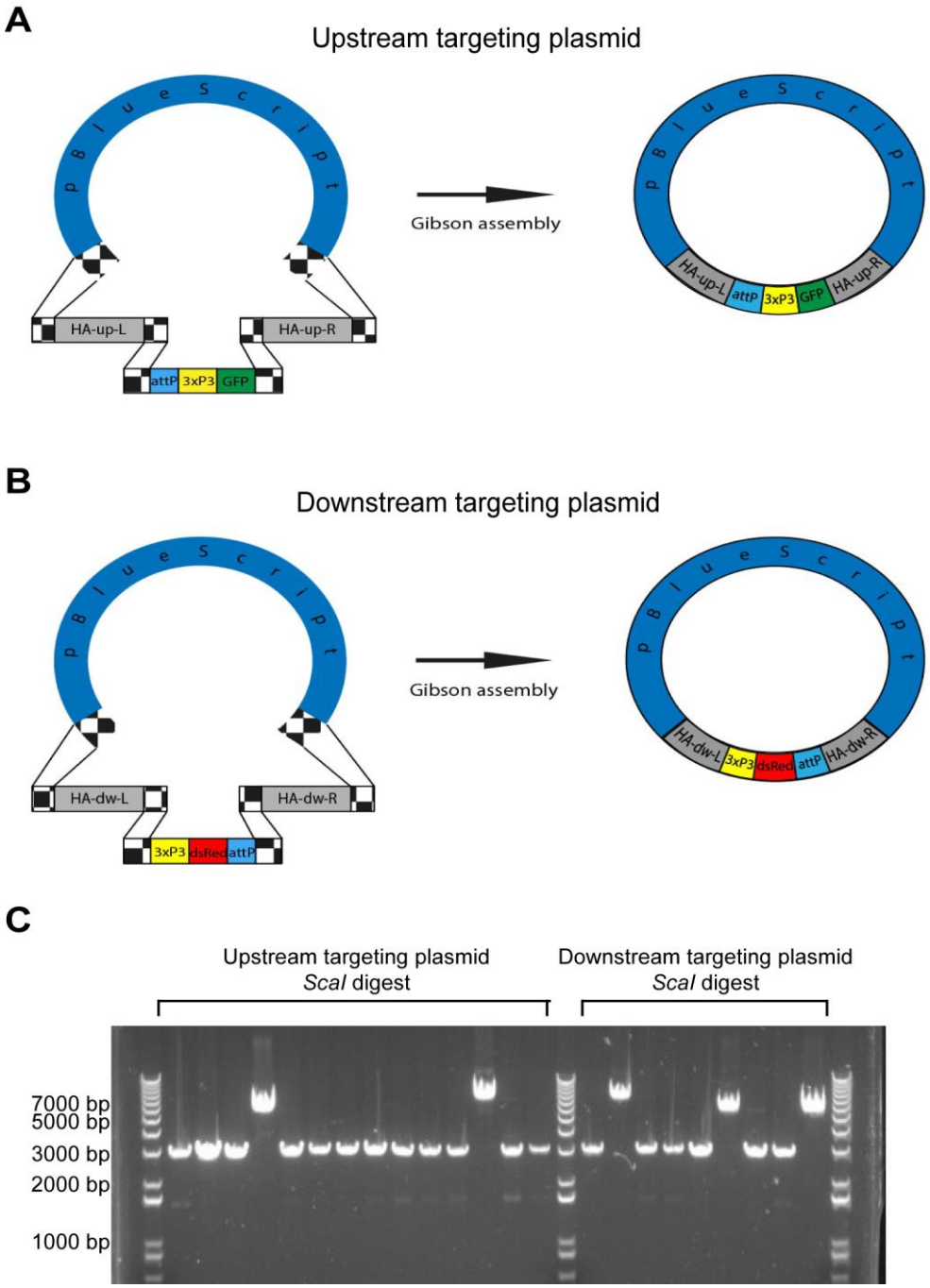

Figure 4.30. Cloning of upstream and downstream targeting plasmids by Gibson assembly. A and B: Schematic view of the construction of targeting plasmids by Gibson assembly. Grey bars correspond to homology arms which flank the 3xP3-GFP-attP and 3xP3-dsRED-attP transgenes. C: Restriction digestion result of putative assembled plasmids with *ScaI* enzyme. The ones with size around 7 kb were sent to sequencing.

However, this time the presence of the assembled plasmid was tested by restriction digestion with *ScaI* enzyme. The enzyme cuts within the transgenes and the size of the

plasmid together with its homology arms and transgene is about 7.5 kb. Figure 4.30c shows that some of the colonies were positive for both upstream and downstream targeting plasmids. After isolating and sequencing the DNA from positive colonies, one of each type without mutation was chosen for injection into embryos.

4.6.3. Injection of Embryos and Selection of Positive Recombinants

Although CRISPR/Cas9 is a very efficient genome editing tool, it still suffers from high lethality rate of injected embryos and low germline mutation frequency. It has been shown that the lethality rate is extremely high when Cas9 is ubiquitously expressed by an *actin* promoter since mutations in developmentally important cells interfere with the fine-tuned developmental program (Ren *et al*., 2013). In an attempt to generate heritable mutant alleles and decrease the lethality rate, in later studies, germline specific promoters, *nanos* and *vasa*, have been used to express Cas9. Limiting the expression of Cas9 to germ cells dramatically increased germline transmission frequency and decreased the lethality rate (Kondo and Ueda, 2013). In the light of these improvements in the system, we decided to use a transgenic fly line, in which Cas9 is expressed by the germline-specific *vasa* promoter. Moreover, we crossed this transgenic line to a *lig4* mutant line. Ligase4 (Lig4) is the key element in the NHEJ pathway. Thus by using the mutant *lig4* we aimed to block the NHEJ pathway so that cells were forced to use the HDR pathway to repair DSB using the provided targeting plasmids. It was reported that this strategy exhibits a higher rate of HDR than wild-type embryos (Beumer *et al*., 2013).

300 embryos of *yw*, *vasa*-Cas9, U6-tracrRNA, $lig4^{169}$ transgenic line were injected with the mixture of sgRNA and both upstream and downstream targeting plasmids. After incubation at 25°C for 15 days, successfully eclosed adult flies were counted. It turned out that 124 individuals out of 300 were alive. The lethality rate was 58.6%, which was higher than expected. Since putative homologous recombination events took place in the germ cells of the injected embryos, these flies were crossed individually to w^{1118} flies to transmit the putative mutant allele to the next generation. After 15 days, the progeny was screened by looking at the GFP and dsRED fluorescence in their eyes.

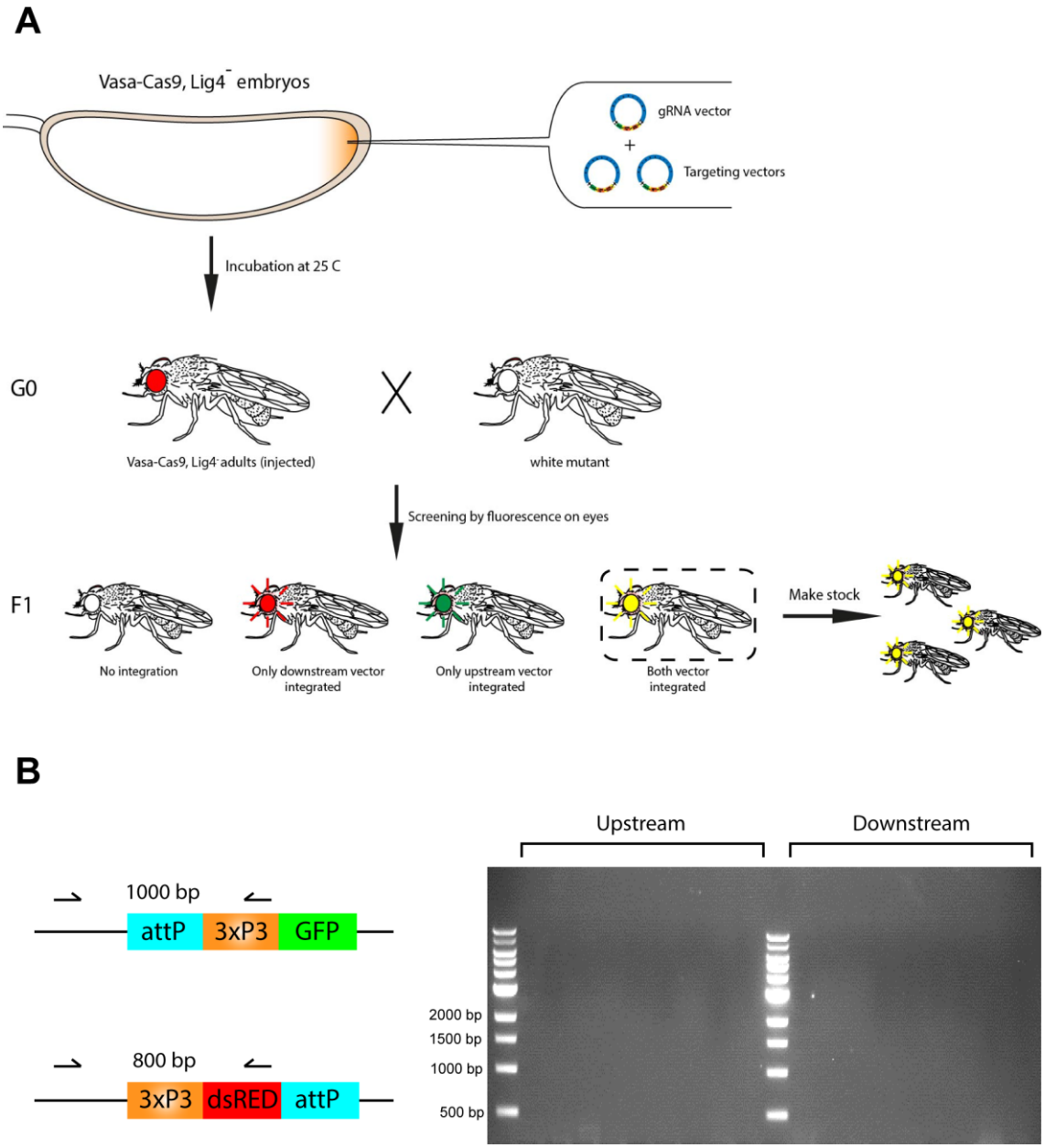

Figure 4.31. Schematic view of injection of plasmids and selection of positive recombinants, and PCR result to evaluate the integration events. PCR is performed with one primer inside the genome near the putative insert and one primer inside the construct. Gel image shows that none of the integration events took place.

Although 3xP3 is a strong eye promoter (promoter of Pax6) and widely used, no strong GFP and dsRED signals were observed. Instead, we observed very weak GFP signal and no dsRED signal at all. 9 individuals displaying a weak GFP signal were selected and individual populations were generated by crossing these with w^{1118} flies. Finally, 2 flies from each population were selected and their genomic DNA was isolated to evaluate the

presence of the transgenes by PCR. We picked one primer complementary to a genomic sequence near the putative insert and one primer inside the construct for both upstream and downstream inserts. It turned out that we failed to introduce both upstream and downstream construct at defined positions in the genome (Figure 4.31b).

5. DISCUSSION

Many human disorders are caused by the malfunction of cellular activities such as proliferation, apoptosis, establishment of cellular and planar polarity, differentiation, and migration. A number of model systems have been used extensively to study normal and abnormal cellular and metabolic processes to understand the details of pathogenesis. Among them the *Drosophila* eye has come to the forefront because it has a sequential developmental program in which several metabolic processes and signaling cascades work in harmony to form the delicate structure of the adult fly eye. So far, several successful attempts have been made to use the *Drosophila* eye as a model for human disorders, including neurodegenerative disorders and carcinogenesis. The functional conservation of proteins in the aforementioned metabolic processes between human and *Drosophila* gives important insights about disease mechanisms and allows us to unravel the pathology of human disorders and paves the way for the development of cures.

Defects in membrane trafficking and degradation of cellular constituents for a healthy turnover of monomers are the hallmarks in most neurodegenerative disorders and several other disease states. Such defects generally result in the accumulation of undegraded molecules, including proteins and lipids due to aberrant lysosomal degradation and endosomal sorting. In the framework of this study, we, for the first time, tried to functionally characterize a novel hexosaminidase called CG7985 using the *Drosophila* eye as a model. Previously, hexosaminidases have been shown to have a role in the glycosphingolipid degradation pathway and thus their deficiency results in aberrant lysosomal degradation causing lysosomal storage disorders. However, in *Drosophila* and other invertebrates, no study so far has been attributed to the analysis of hexosaminidase function in the glycosphingolipid degradation pathway to the best of our knowledge. Most of the studies investigating the function of hexosaminidases in *Drosophila* and other invertebrates, including *C.elegans* focus only on their role in the N-glycan biosynthesis pathway. In this study, our investigation of CG7985 function mainly focused on its involvement in the glycosphingolipid degradation pathway in *Drosophila*. We tried to do so by examining the defects in the endo-lysosomal degradation pathway and the secondary consequences of these defects by loss-of-function analysis, including mutant and knockdown analysis of *CG7985*.

5.1. CG7985 is a Novel Hexosaminidase in *Drosophila*

The *Drosophila* genome encodes for four different hexosaminidases. Three of them have been studied well and their metabolic activities and functional involvements in different biological processes have been elucidated. Hexo1 and Hexo2 are the hexosaminidases with a role in chitin degradation. They are responsible for cleaving N-acetyl-β-D-glucosamine residues from the long and branched structure of chitin. From this point of view, they have important roles in the degradation of chitin especially when completely developed adult flies eclose from their pupal case (Leonard *et al.*, 2005). Fused lobes, on the other hand, is the principle hexosaminidase in N-glycan biosynthesis. The N-glycan biosynthesis pathway is similar in vertebrates and invertebrates, but at a certain point, Fused lobes cleaves an N-acetyl-β-D-glucosamine residue to form simple, paucimannosidic N-glycans in *Drosophila*. Loss-of-function of Fused lobes causes formation of complex types of N-glycans in *Drosophila* like those in vertebrates. Since the structure of N-glycans has important implications in different steps of development, the loss-of-function of Fused lobes causes pleiotropic developmental effects (Rosenbaum *et al.*, 2014).

In a recent study, all these aforementioned hexosaminidases have been shown to specifically cleave N-acetyl-β-D-glucosamine residues. However, none of them can cleave N-acetyl-β-D-galactosamine residues (Dragosits *et al*., 2014). It has been proven in different studies that hexosaminidases are split into two evolutionary conserved branches. One branch contains Hexo1, Hexo2, and Fused lobes and the other branch contains CG7985 and its vertebrate homolog HexDC and *C.elegans* homolog Hex-2. To show if this branching comes with a functional difference, Gutternigg and his colleagues performed enzymatic assays showing that HexDC and Hex-2 specifically cleave N-acetyl-β-D-galactosamine residues (Gutternigg *et al.*, 2009). Thus, this evolutionary branching of hexosaminidases implies a slight difference in their specificity towards their substrates.

Having vertebrate and invertebrate homologs with specific cleaving activity against N-acetyl-β-D-galactosamine residues, it seems safe to conclude that CG7985 stands as the only N-acetyl-β-D-galactosamine specific hexosaminidase in *Drosophila*. The difference in the enzymatic activity of hexosaminidases in *Drosophila* might cause an important alteration in their functions in different metabolic pathways. In chitin degradation and N-

glycan biosynthesis, N-acetyl-β-D-glucosamine residues must be cleaved and the functional involvement of Hexo1, Hexo2, and Fused lobes have been shown in these metabolic pathways. However, if CG7985 acts on N-acetyl-β-D-galactosamine residues as the activity of its homologs implies, then it would be unfavorable to conclude that it might also have a role in these metabolic pathways. On the other hand, the ganglioside structure in *Drosophila* is similar to that of vertebrates and in vertebrates the role of hexosaminidases in the ganglioside degradation pathway has been described (Werth *et al*., 2001). The key point here is that the structure of GM2 ganglioside contains a terminal N-acetyl-β-D-galactosamine residue, which must be cleaved to degrade it to its simpler GM3 form. As mentioned before, defects in this degradation process cause the accumulation of undegraded gangliosides leading to a specific form of lysosomal storage disorders (Gravel *et al.,* 2001).

In the light of all this information and findings, CG7985 steps forward as the only hexosaminidase in *Drosophila* with a presumed function in the ganglioside degradation pathway. Our observations of lipid accumulation and enlargement of lysosomes, which show similarity to the phenotypes in lysosomal storage disorders, were the major reasons toward analysis of CG7985 in the ganglioside degradation pathway.

5.2. Discrepancies in Expression Pattern and Protein Localization of CG7985

Drosophila melanogaster has been a versatile model organism for over a century. Since it is one of the first model organisms that has been used for revealing gene functions, their expression pattern, and corresponding protein localization, many genetic tools have been generated to manipulate its genome. One of the leading tools to examine expression patterns of genes is enhancer trapping. As mentioned before, the technique depends on the mobility of transposable elements by which transgenes can be introduced into the genome. In enhancer trapping, reporters like LacZ or GFP and later a Gal4 sequence with a minimal promoter have been introduced throughout the genome to trap the activity of enhancers, which normally induce expression of genes. Therefore, the aim of using an enhancer trap is to mimic the expression pattern of a gene, which is normally affected by the same

enhancers. In our study, we used an enhancer trap in which the transposable element (PiggyBac-element) containing a Gal4 sequence was introduced to the first intron of *CG7985*. Crossing this enhancer trap line to a UAS-GFP line revealed a photoreceptor R7 specific expression pattern of *CG7985*.

Although enhancer traps can be very fruitful to show the expression pattern of genes, one of the drawbacks of this system is that one can never be quite sure that the minimal promoter in a transposable element would be affected by all enhancers that normally affect the expression of the corresponding gene. The coverage of the expression pattern of the gene almost entirely depends on the location of the inserted transposable element in the genome. Some physical barriers can interfere with the interaction of enhancers and the minimal promoter. In such a case, one can observe only the partial expression pattern of the gene of interest.

Being aware of this fact about enhancer trapping, we turned our attention to other tools by which we could directly observe the protein localization of CG7985. First, we used a BAC line in which an extra sequence of the genomic locus of *CG7985* together with a GFP coding sequence just before its stop codon was introduced to another location in the genome. Immunohistochemical analysis of eye imaginal discs in this line supported the photoreceptor R7 specific expression pattern observed in the enhancer trap line. However, we detected additional regions of protein localization of CG7985 within and anterior to the MF. Therefore, we concluded that the enhacer-trap line indeed showed only a partial expression pattern of *CG7985*. Although using this BAC line instead of an enhancer-trap line to reveal protein localization of CG7985 seems more reliable, still a BAC line has its own weaknesses. First of all, it is not completely clear if the genomic locus of *CG7985* that was introduced into the genome contains all the enhancer elements that are required. Second, since it was introduced to another position in the genome, the expression pattern of the transgene might be altered due to its new location.

The most direct way to observe the localization of a protein is to use an antibody raised against it. Since we are the first group to work on CG7985, there was no commercially available anti-CG7985 antibody. Previous attempts to express this protein in bacteria and using a baculovirus system were unsuccessful (G. Kaçmaz, 2013). Thus, we

decided to generate a peptide antibody. This antibody was raised against a 15 amino acid long, highly specific region of CG7985 near its C-terminus. The antibody was tested by Western blotting and revealed several bands on the blot. This implied that the raised antibody possibly cross-reacted with other proteins. To minimize non-specific binding and enrich the antibody against CG7985, we performed pre-adsorption with mutant tissues (Protein Trap). Comparison of pre-adsorbed and normal antibody by Western blotting showed that all the bands except one were diminished. Although this process seemed to work well, the remaining band did not exactly match the annotated weight of CG7985. The reason for this result might be possible post-translational modifications on CG7985. Nevertheless, the pre-adsorbed antibody was used in immunofluorescence analysis and revealed a protein localization of CG7985 similar to the localization observed in the BAC line. However, additional signals in the glial layer of the eye imaginal disc were observed.

Support for the specificity of protein localization of CG7985 with pre-adsorbed antibody came from another line, a CG7985-specific protein trap line, in which a GFP construct is transcribed by the promoter elements of *CG7985* producing a ~ 25-30 kDa protein. Although the signal of pre-adsorbed anti-CG7985 antibody was weaker, it recapitulated the distribution of the protein trap line at both the photoreceptor and glial cell layers. Thus, we are quite confident that this represents the actual protein localization of CG7985.

5.3. Loss of Function of CG7985 Causes Lysosomal Cell Death

Lysosomes are the center for cellular recycling containing numerous hydrolases that degrade cellular macromolecules. Therefore, the permeabilization of the lysosomal membrane must be kept under tight control to prevent leakage of hydrolases that might degrade cellular contents if they disperse through the cytoplasm. Increased permeabilization or complete rupture of the lysosomal membrane due to excessive accumulation of undegraded macromolecules causes so-called lysosomal cell death. This form of cell death is generally carried out by cathepsin proteases, which can trigger necrotic, apoptotic cell deaths or apoptosis-like features depending on the extent of leakage (Aits and Jaattela, 2013).

In our study, first of all, we have shown by RT-PCR that the insertion of a GFP construct near the promoter elements of *CG7985* in the protein trap line causes a blockage of transcription of *CG7985*. Therefore, this protein trap line was used for mutant analysis. Since our main focus was to reveal a possible function of CG7985 in the ganglioside degradation mechanism, first, we tried to show if loss-of-function causes accumulation of gangliosides. For this purpose, we intended to use an antibody against GM2-type gangliosides but these experiments gave unreliable thus inconclusive results. Some regions in the eye imaginal discs seemed to have an increased population of GM2 gangliosides but it was not possible to differentiate and compare those regions with the rest of the tissue. To overcome this hurdle, we decided to generate mosaic eye imaginal discs with the help of FRT/Flp recombination. In such an eye imaginal disc, we would be able to show the accumulations in mutant tissue patches by comparing them with the neighboring wild-type tissues patches. However, despite all efforts, we could not obtain such mosaic eye imaginal discs. One possible explanation for this failure is that since mitotic recombination takes place in a small number of cells and functional loss of CG7985 results in apoptosis, these apoptotic cells could have died and been compensated by other cells maintaining tissue homeostasis.

Several studies showed the co-accumulation of lipid raft components if there is a defect in the degradation of one type of the components (Pagano *et al.,* 2000). Thus, we decided to find a general lipid dye that could recognize large accumulations of lipid raft components. We found a dye called LipidTOX^{TM} Phospholipidosis and Steatosis Detection Stain that selectively binds to large accumulations of lipid droplets. The analysis of mutant eye imaginal discs using this dye revealed large lipid accumulations. However, the link between loss-of-function of CG7985 and lysosomal storage disorders has been made by the observation of enlarged lysosomes in which lipids accumulated.

The revelation of the pathophysiological mechanism in lysosomal storage disorders is a demanding task. Since the cellular consequences of substrate accumulation depend on the type of the storage material, the extent of storage, and the type of the cell in which the substrate is accumulated, it is almost impossible to predict all consequences of lysosomal storage disorders. Accumulation can alter several signalling pathways since generally receptors and ligands are also trapped in lysosomes upon accumulation of other cellular

membrane components. Also, it can alter the intracellular calcium homeostasis affecting the function of channel proteins. However, one of the well-known mechanisms that is impaired upon lysosomal storage is autophagy. The lysosomes play a major role in autophagy-mediated cellular turnover of proteins and organelles. During autophagy, a large portion of cytosol is sequestered in autophagosomes and then degraded upon fusion with lysosomes. In lysosomal storage disorders, however, the fusion between autophagosomes and lysosomes is impaired, leading to undegraded accumulation of organelles like mitochondria and also polyubiquitinated proteins (Ballabio and Gieselmann, 2009).

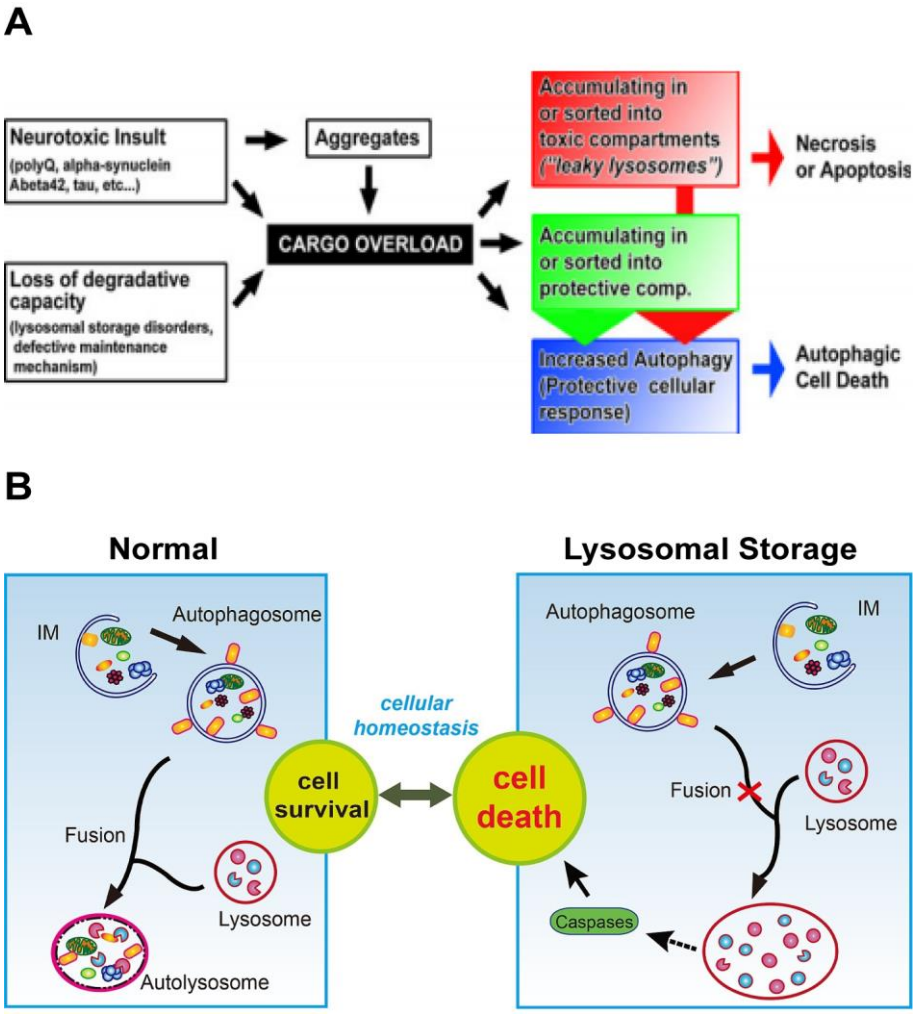

Figure 5.1. Possible outcomes of lysosomal storage. A: Cargo overload due to loss of degradative capacity results in necrosis, apoptosis or autophagic cell death (adapted from Wang *et al*., 2013). B: The impairment of fusion between lysosomes and autophagosomes in lysosomal storage results in the activation of caspases (adapted from Jung *et al*., 2015).

Loss of degradative capacity of lysosomes due to defects in one or more of the hydrolytic enzymes causes cargo overload which can trigger necrosis, apoptosis or autophagic cell death through different mechanisms (Figure 5.1a). Also, the impairment of fusion between autophagosomes and lysosomes in lysosomal storage disorders can result in the activation of caspases, which drives cells to apoptosis (Figure 5.1b). In light of this information, we evaluated the survival state of the cells with enlarged lysosomes in *CG7985* mutant eye imaginal discs and observed that most of them were apoptotic.

The number of apoptotic cells in *CG7985* mutant tissue was evaluated with anti-cleaved Cas3 antibody and showed that apoptotic activity was highly increased. However, autophagic cell death, which can be traced by autophagy-related protein Atg8a, an ubiquitin-like protein required for the formation of autophagosomal membrane could not be traced. Since we couldn't obtain anti-Atg8a antibody that reacts with the corresponding protein in *Drosophila*, we used a mCherry-tagged Atg8a transgene with UAS. However, the need for combination of this transgene with a Gal4 line and the necessity to make the protein trap line homozygous made the genetics so complicated that we couldn't establish the necessary line to evaluate autophagic cell death in *CG7985* mutant eye imaginal discs.

5.4. Lysosomal Cell Death Triggers Compensatory Proliferation

Apoptosis is a highly conserved mechanism, which has evolved due to its positive effects on organismal survival. It is not only important in development, but also in eliminating damaged and potentially cancerous cells (Renehan *et al*., 2001). Although eliminating harmful cells is already beneficial to organisms, recently, several evidences have suggested that apoptotic cells can induce proliferation of neighboring cells to replace dying cells and hence maintain tissue homeostasis (Ryoo and Bergmann, 2012).

In our study, at the first glance, the observations of increased apoptotic cell number and overgrowth of *CG7985* mutant eye imaginal discs seemed to contradict each other. We showed that the number of proliferating cells was also dramatically increased. However, further investigation revealed that proliferating cells were mostly located near apoptotic cells. It was obvious that the effect of the CG7985 mutation was non-autonomous.

Although the effect of the mutation results in cell death, indirectly, dying cells trigger proliferation in neighboring cells. Once again, the generation of mosaic eye imaginal discs would be helpful to show this non-autonomous effect in which we would expect to observe apoptotic cells in mutant tissue patches and proliferating cells in wild-type neighboring cells. However, we still could show that apoptotic cells were not co-localizing with proliferating cells.

There are two well-known types of overgrowth phenotypes; hyperplastic growth and neoplastic growth. Hyperplastic growth is observed when the apoptotic effect of the mutation is restricted to one region of the tissue from which dying cells emit growth and survival signals to induce compensatory proliferation in surrounding unaffected tissue. On the other hand, in neoplastic growth, the effect of the mutation is autonomous and it directly triggers proliferation in the same affected cells causing overgrowth of the tissue.

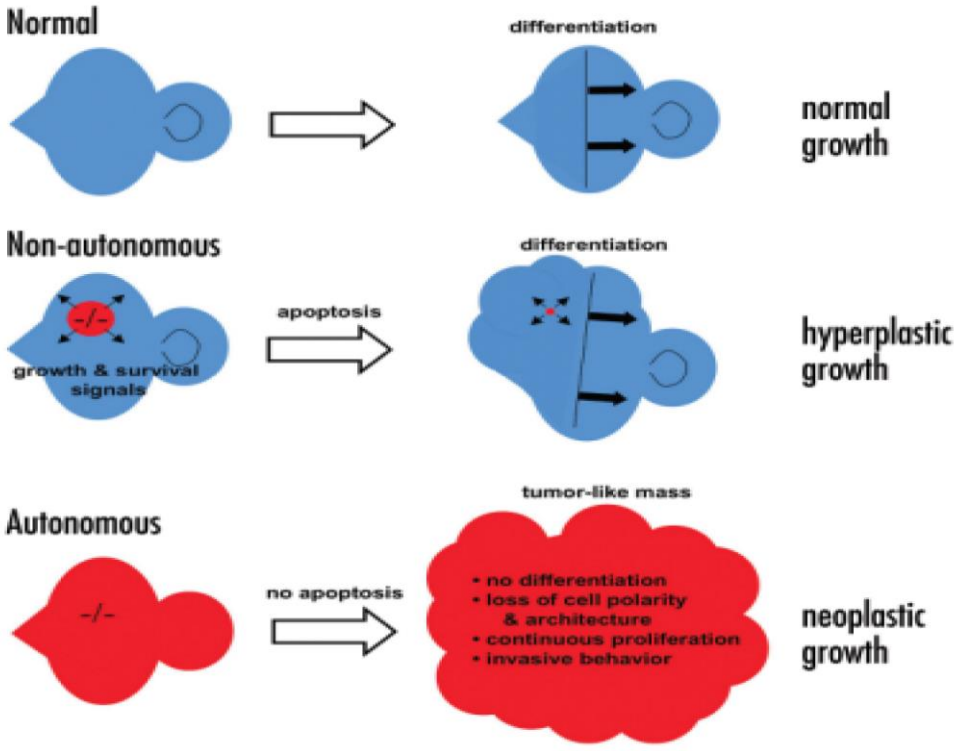

Figure 5.2. The effect of different types of mutations on the growth of the eye imaginal disc. The mechanism underlying the observed effects of loss-of-function of CG7985 on the growth of the eye imaginal disc is similar to the middle figure. Apoptotic cells at a certain region of the eye imaginal disc trigger proliferation in neighboring cells by emitting growth and survival signals (adapted from Gilbert and Moberg, 2006).

When it comes to eye imaginal discs, hyperplastic growth affects the differentiation of photoreceptor to different extents but it doesn't completely prevent differentiation. However, in neoplastic growth, no differentiation could be observed (Gilbert and Moberg, 2006) (Figure 5.2). In our case, the apoptotic effect of CG7985 mutation was almost always observed at the anterio-middle part of the eye imaginal disc, but proliferating cells were found dispersed at distant regions. Moreover, we have always observed photoreceptor differentiation to different extents which were located at the posterior tip of the eye imaginal discs.

The compensatory proliferation that resulted in hyperplastic growth of the *CG7985* mutant eye imaginal discs must have been mediated by growth signals emitted from apoptotic cells. Since proliferating cells were dispersed to distant regions of the eye imaginal discs, it was easy to conclude that the growth signal must have been a diffusible signal. Previously, Dpp and Wg have been shown to be emitted from apoptotic cells in *Drosophila* (Morata *et al*., 2010). Taking this fact into account, we have shown the ectopic dispersal of Wg through the anterio-middle region of the *CG7985* mutant eye imaginal discs. Collectively, our data exactly meet the criteria of hyperplastic growth through a non-autonomous proliferative effect of apoptotic cells.

5.5. Knockdown of *CG7985* Shows Milder Effects Than Mutants

Although knockdown and mutant analysis can be used interchangeably for the functional characterization of most of the genes, in most other cases including ours, knockdown of genes results in milder effects compared to the effects of their complete mutants. Previously, it has been shown that the knockdown of *CG7985* by a ubiquitous Gal4 driver downregulates its expression about 70% (G. Kaçmaz, 2013). This implies that there is still a residual activity of *CG7985* in the eye imaginal disc when the eye-specific *ey*-Gal4 driver is used to downregulate its expression in the eye.

The decrease in the amount of a functional protein may exert different effects. In some cases, removing a functional protein does not affect the metabolic pathway it plays a role in. However, some others may exert effects to different extents upon a gradual

removal of the protein. This phenomenon depends on the presence of other proteins that play similar roles to compensate the removal of the protein or if the protein functions in a dose-dependent manner. According to the results that we observed both in mutant and knockdown analysis, CG7985 functions in a dose-dependent manner. Both mutant and knockdown of *CG7985* exert the same effects, including the increase of lysosomes in both number and size, the increase in apoptotic cell number, and also the increase in proliferating cell number. However, the effect on lysosomal morphology and the apoptotic activity was much milder in knockdown than in the mutant. One important observation to note that the number of proliferating cell was similar in both cases. To explain this observation we suggest that, in the knockdown, it takes more time for the apoptotic cells to die and they emit the growth signal for a longer time than the apoptotic cells in the mutant. The immunostainings of the growth factors, Wg and Dpp, in the knockdown eye imaginal discs supported this hypothesis. In both cases, we observed broader distribution of growth factors and also an increase in the intensity of the signals that might show their overproduction (Appendix B, Figure B.1).

As mentioned before, the accumulation of one type of plasma membrane component might sequester the other components in the lysosomes, including cholesterol and transmembrane proteins. This explains the pleiotropic effect of lysosomal storage disorders. For example, the sequestration of receptors and ligands in lysosomes might affect the signalling pathways to different extents. In such a case, it has been shown that the accumulation of Notch in the late endosomes and lysosomes resulted in the ectopic activation of Notch signalling in a ligand-independent manner (Vaccari *et al*., 2009). In the framework of our study, we also identified the accumulation of both Notch and its receptor Delta especially around the MF in knockdown eye imaginal discs (Appendix B, Figure B.2). It is worth to keep in mind that the ectopic activation of Notch signalling upon the accumulation of Notch receptor and its ligand Delta might also contribute to the overgrowth phenotype that we observed in knockdown eye imaginal discs. However, the time frame of this study was too short to analyse this phenomenon further.

In conclusion, the similar effects that we observed in both mutant and knockdown eye imaginal discs further proved the role of CG7985 in lysosomal degradation.

Considering its putative enzymatic activity, this degradative role presumably exerts itself in the ganglioside degradation pathway.

5.6. The Problems in the Generation of *CG7985* Conditional Allele by CRISPR/Cas9

Although it is a new technique, CRISPR/Cas9 has been used in several model organisms to generate simple mutants by NHEJ or to introduce changes by HDR. In *Drosophila*, although several attempts have been made to find the optimum conditions for the system to work, there is still no consensus about which way is the most efficient. To use NHEJ pathway to generate frameshift mutants, Cas9 was either injected as plasmid from which it is transcribed inside the cells, directly injected as mRNA, or provided from a transgenic source. In our system, we used a transgenic *Drosophila* line in which Cas9 was expressed from a germ-line specific *vasa* promoter. In this way, we aimed to increase the heritable mutation rate and decrease the lethality rate by preventing its expression in developmentally important cells. We also combined this transgenic, germ-line specific Cas9 source with a mutation in *lig4* gene, which is an important component of the NHEJ pathway. The purpose of using a *lig4* mutant *Drosophila* line was to prevent NHEJ pathway so that the only possible repair pathway left for cells was HDR.

Here, we aimed to combine CRISPR/Cas9 with RMCE. In the first step, we decided to edit the genome by introducing attP recombination sites in a way that they would flank the genomic locus of *CG7985*. In the second step, by the injection of replacement casettes with attB recombination sites and any DNA sequence in between, we planned to generate different *Drosophila* lines with changes in the genomic locus of *CG7985* using site-directed recombination between attP and attB recombination sites. The success of the first phase of the system depends on two different homologous recombination events to take place. For this purpose, we generated one sgRNA plasmid from which two different sgRNAs would be transcribed and two different repair plasmids supplied with homology arms that cells would use to repair DSBs. We constructed the repair templates with attP recombination sites, and GFP and dsRED reporters with the eye-specific promoter 3xP3. This would allow us to easily trace positive recombinants following the GFP and dsRED

fluorescence in the eyes of flies after homologous recombination took place. However, in the screening process, it turned out that we could observe a weak GFP signal in some individuals but no dsRED signal at all. This might mean that homologous recombination didn't take place so that we couldn't obtain the transgenic line or a closed chromatin structure near the insertion site prevented the activation of the 3xP3 promoter.

After failing to select putative double-positive recombinants by GFP and dsRED signals in their eyes, we decided to evaluate the individuals with a weak GFP signal by PCR. However, this selection was quite laborious since it depends on the quality of extracted genomic DNA and the compatibility of selected primers. Through the optimization process with several different extraction methods and different sets of primers, interestingly, we could detect the presence of 3xP3-reporter-attP constructs in the genome but the attempts to localize this construct in the genomic locus of *CG7985* yielded no result. It can be concluded from this data that the homologous recombination took place to insert 3xP3-reporter-attP into the genome but not exactly at the position that we have planned.

As mentioned before, the NHEJ pathway is used to generate frameshift mutations to simply produce non-functional proteins. Since we currently only have the protein trap line as a mutant line and the above mentioned CRISPR did not work so far, we attempted to generate a simple mutation by NHEJ. Unfortunately, it was not possible to use NHEJ to generate a frameshift mutation in the remaining time of this study, but it will be used to generate a mutant as a future perspective of this study.

5.7. A Proposed Working Model

The excessive storage of waste products due to defects in hydrolytic enzymes impairs the endolysosomal system jeopardizing the survival of cells. Increase in the lysosomal membrane permeabilization and consequent lysosomal rupture result in autolysis and eventual cell death. It has been proposed that the release of Cathepsins from ruptured lysosomes activates Caspases to trigger apoptosis (Chwieralski *et al*., 2006). Although endolysosomal degradation is a ubiquitous mechanism that is

necessary for the survival of all cell types, a dysfunctional degradation mainly affects the cells with a high substrate turnover rate like neurons (Wang *et al*., 2012).

The loss-of-function of *CG7985* results in very similar symptoms to lysosomal storage disorders. Enlargement of lysosomes and subsequent apoptotic activity inside these cells suggest that it has a role in the endolysosomal degradation pathway. One of the key observations to show its importance for the organism was neuronal loss in the eye imaginal discs of *CG7985* mutants. At first glance, the reason of the neuronal loss phenotype seems to be directly related to increased apoptotic activity. However, so far, we didn't observe any apoptotic activity inside Elav-positive neurons. Instead, the apoptotic cells were located at the anterior part of the eye imaginal disc, which is the location for neuronal precursor cells that differentiate later as photoreceptors upon receiving correct differentiation signals. As mentioned before, the number of cells in the eye imaginal disc before differentiation begins at the third instar stage is spatiotemporally controlled by several signaling pathways. At certain points in the development of the eye imaginal disc, waves of proliferation ensure the correct number of cells located at the anterior side of the eye imaginal disc. Upon the movement of the MF, those cells receive differentiation signals to produce about 800 ommatidia harboring 8 photoreceptors each. Therefore, any unbalance in the number of these cells will result in over- or underproduction of photoreceptors.

The attempts to observe the protein localization of CG7985 has revealed that it is localized to photoreceptor R7, within the MF, and at its anterior side. The role of CG7985 in the development of photoreceptor R7 is still unknown since we didn't observe a specific removal of R7 photoreceptors. However, the lysosomal enlargement and emergence of apoptotic cells were located at the anterior part of the eye imaginal discs. Therefore, we can deduce that the loss-of-function of CG7985 at the anterior part of the eye imaginal disc results in apoptosis and eventual cell death. Since neuronal precursors are located in this part of the eye imaginal disc, we conclude that the neuronal loss phenotype is the result of depletion in the number of neuronal precursors.

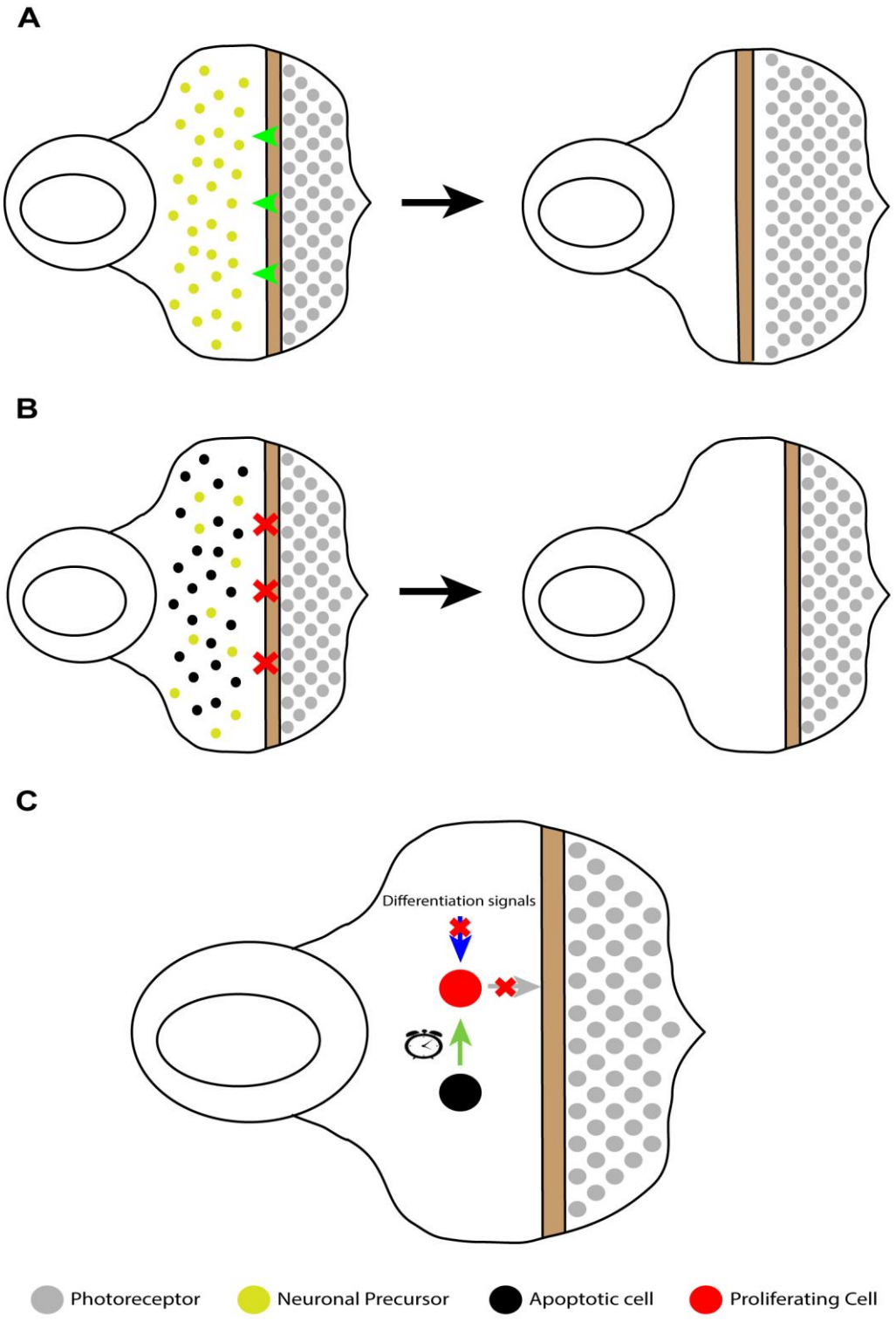

Figure 5.3. A proposed model to explain the effects of the loss-of-function of CG7985 in the development of the eye. A: Neuronal precursors differentiate as photoreceptors through the movement of the MF. B: The depletion of neuronal precursors result in fewer differentiated photoreceptors in *CG7985* mutants. C: Newly proliferating cells cannot receive the differentiation signal due to time elapsed through the emittance of diffusible growth signals by apoptotic cells.

The hyperplastic growth that we observed due to the non-autonomous proliferative effect of apoptotic cells does not compensate the neuronal loss. Normally, apoptotic cells emit growth signals to trigger proliferation in neighboring cells in an attempt to replace dying cells and maintain tissue homeostasis. However, in the eye imaginal disc, cells must receive differentiation signals in a strict temporal period to become photoreceptors. Therefore, we propose that newly proliferating cells miss a critical time point to differentiate as photoreceptors since emittance of diffusible growth factors by apoptotic cells, the time that is needed for the diffusion of these growth factors, and the division process take time. However, it is important to note that, alternatively, Wingless signalling, which normally inhibits Dpp signalling to prevent movement of the MF at the anterio-lateral sides of the eye imaginal disc, might be the reason for the cessation of the movement of the MF. Since it diffuses through the anterio-middle region, here, it might exert its effect as an inhibitor for the movement of the MF preventing photoreceptor differentiation.

APPENDIX A: VECTOR MAPS

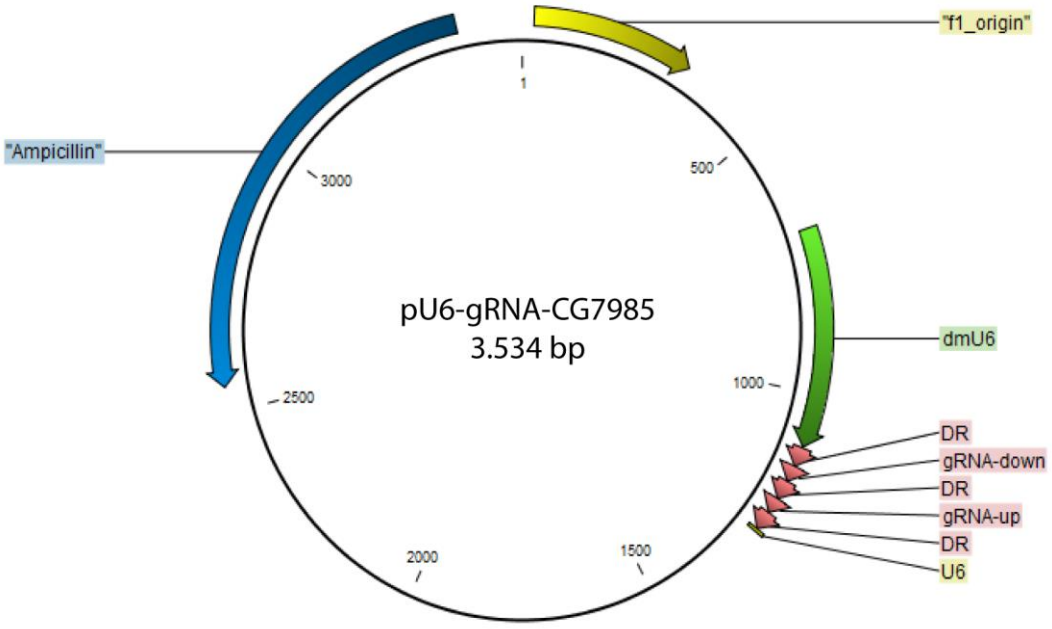

Figure A.1. Vector map of pU6-gRNA-CG7985.

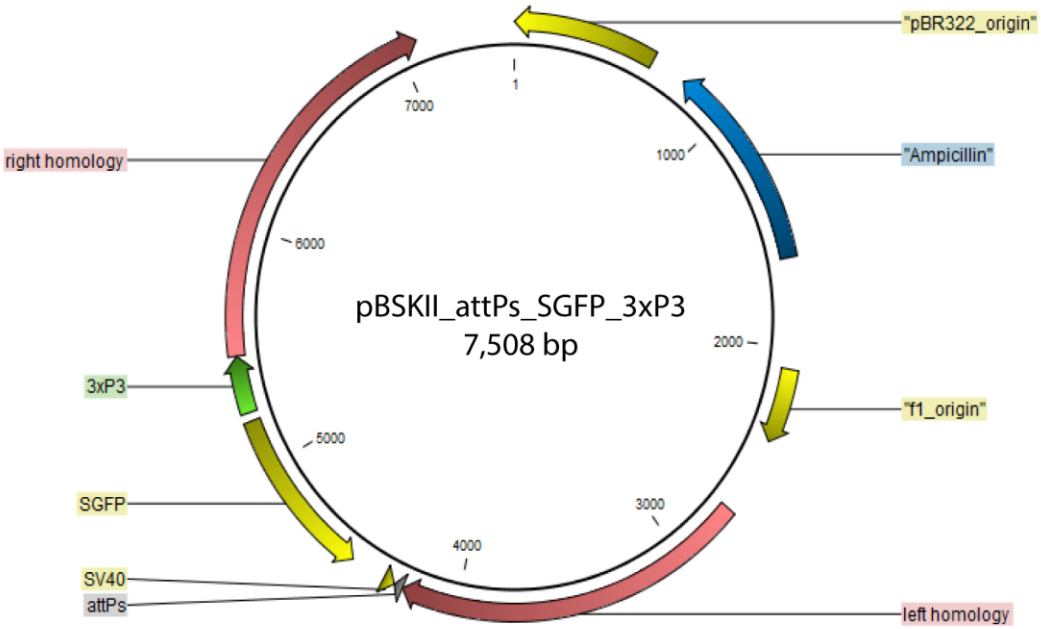

Figure A.2. Vector map of pBSKII_attPs_SGFP_3xP3.

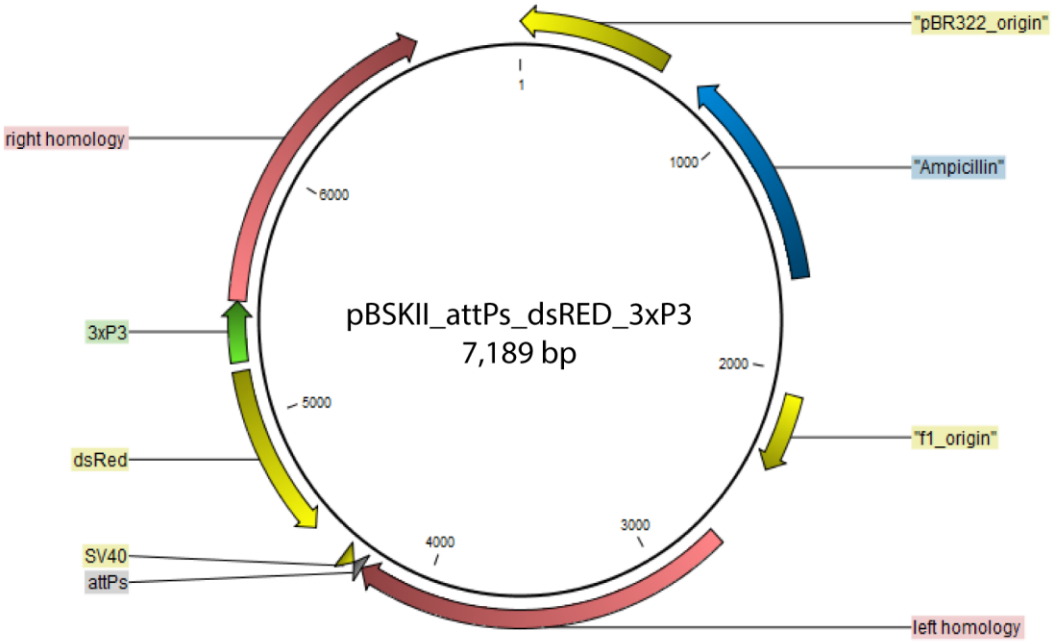

Figure A.3. Vector map of pBSKII_attPs_dsRED_3xP3.

APPENDIX B: IMMUNOHISTOCHEMISTRY OF *CG7985* KNOCKDOWN EYE IMAGINAL DISCS

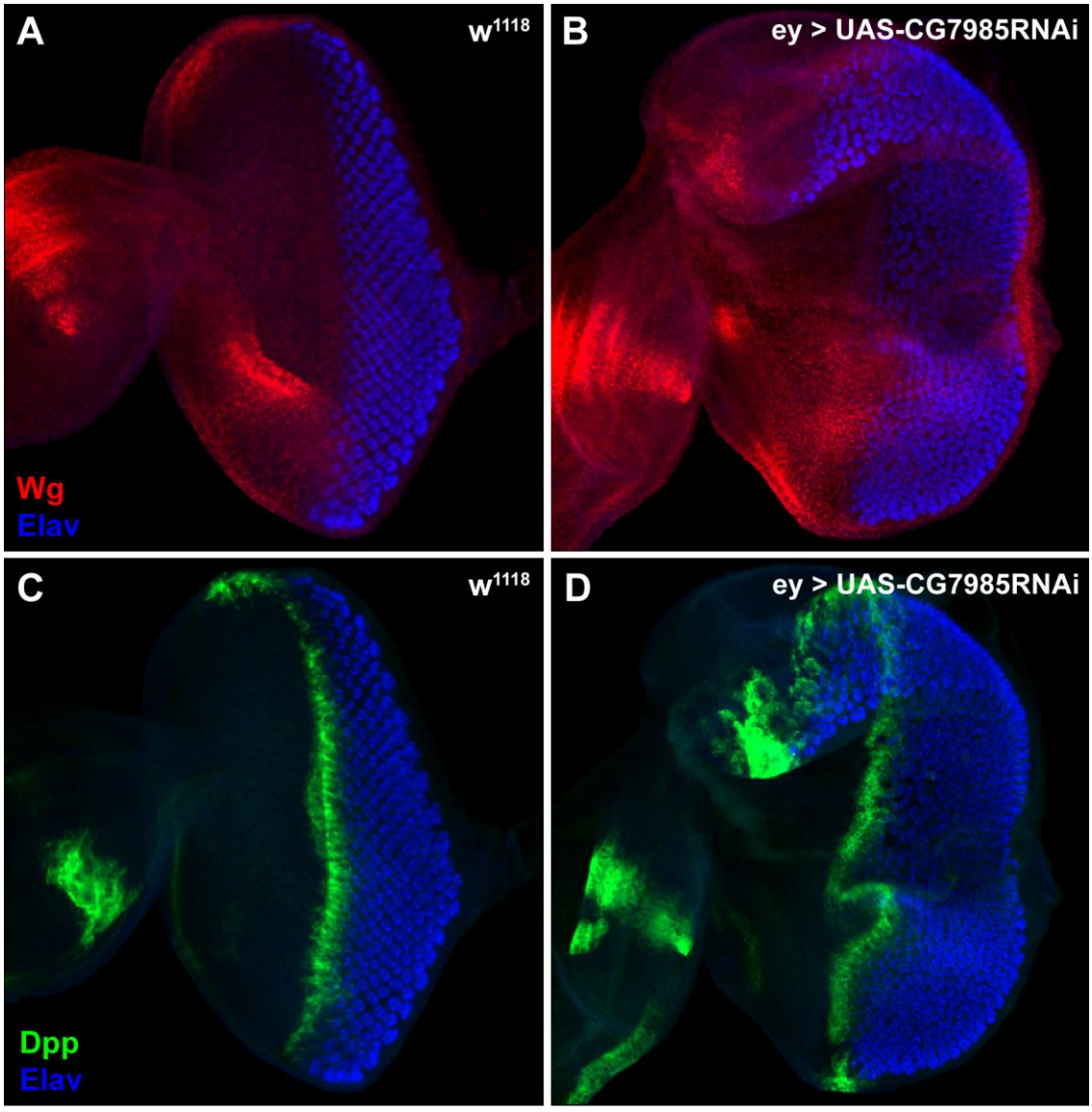

Figure B.1. Distribution of Wg and Dpp in wild-type and *CG7985* knockdown eye imaginal disc. A: Wg is located at the anterio-lateral sides of the wild-type eye imaginal disc. B: Wg is dispersed through anterio-middle region of the *CG7985* knockdown eye imaginal disc. C: Dpp is located on the MF of the wild-type eye imaginal disc. D: Dpp has a broader distribution in the *CG7985* knockdown eye imaginal disc.

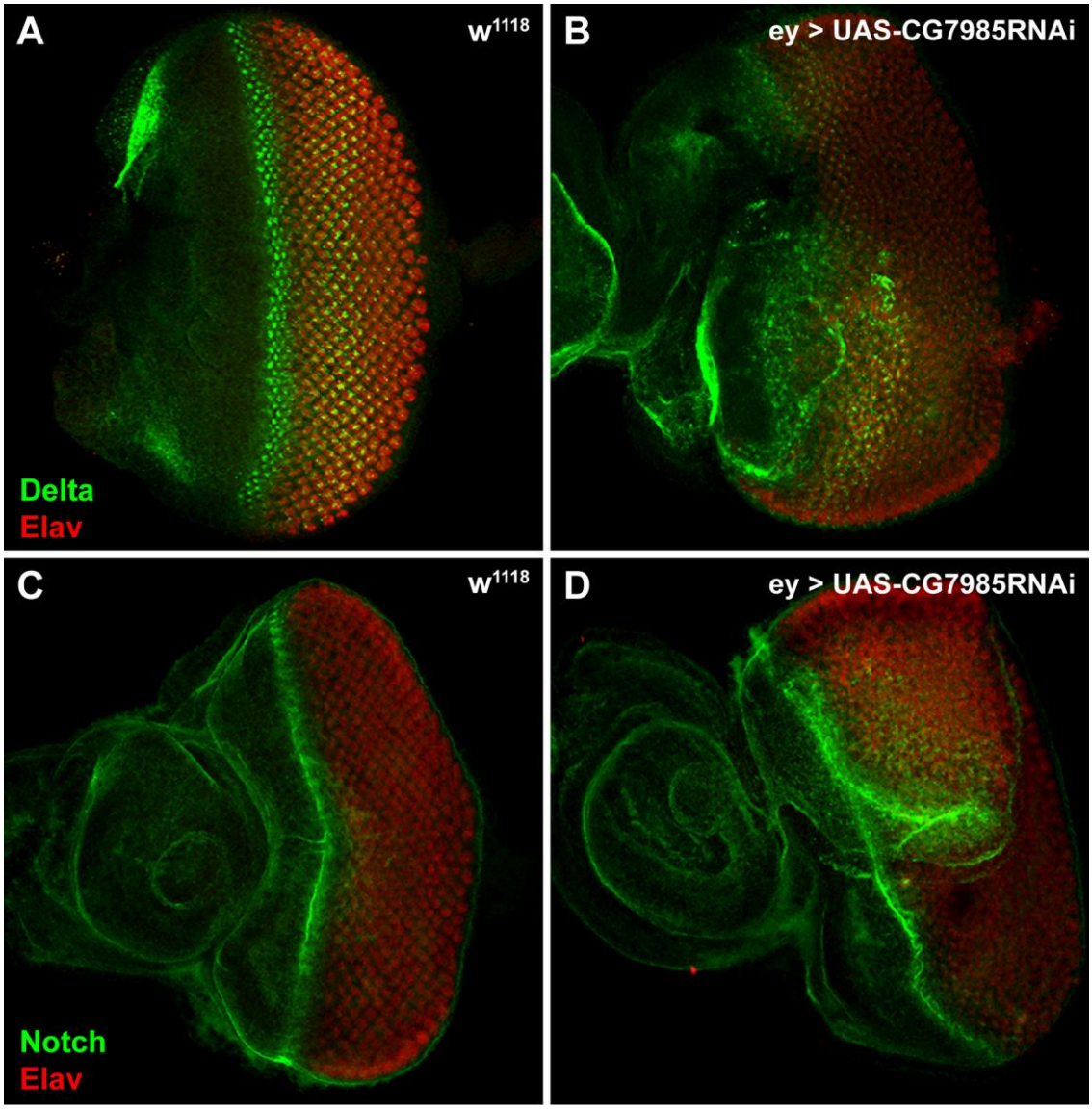

Figure B.2. Distribution of Notch and Delta in the wild-type and *CG7985* knockdown eye imaginal discs. A: Delta is located on and posterior to the MF in the wild-type eye imaginal disc. B: Delta deviates from its normal localization and is accumulated at some regions of the *CG7985* knockdown eye imaginal disc. C: Notch is localized on the MF of the wild-type eye imaginal disc. D: Notch is accumulated at several regions on the MF of the *CG7985* knockdown eye disc.

REFERENCES

Aits, S., and M. Jäättelä, 2013, "Lysosomal Cell Death at a Glance.", *Journal of Cell Science*, Vol. 126, No. 9, pp. 1905–1912.

Aleksic, J., R. Lazic, I. Müller, S. R. Russell, and B. Adryan, 2009, "Biases in Drosophila Melanogaster Protein Trap Screens.", *BMC Genomics*, Vol. 10, pp. 249.

Appelqvist, H., C. Nilsson, B. Garner, A. J. Brown, K. Kågedal, and K. Ollinger, 2011, "Attenuation of the Lysosomal Death Pathway by Lysosomal Cholesterol Accumulation.", *The American Journal of Pathology*, Vol. 178, No. 2, pp. 629–639.

Baker, N. E., 2001, "Cell Proliferation, Survival, and Death in the Drosophila Eye.", *Seminars in Cell & Developmental Biology*, Vol. 12, No. 6, pp. 499–507.

Ballabio, A., and V. Gieselmann, 2009, "Lysosomal Disorders: From Storage to Cellular Damage.", *Biochimica et Biophysica Acta*, Vol. 1793, No. 4, pp. 684–696.

Beumer, K. J., J. K. Trautman, K. Mukherjee, and D. Carroll, 2013, "Donor DNA Utilization during Gene Targeting with Zinc-Finger Nucleases.", *G3 (Bethesda, Md.)*, Vol. 3, No. April, pp. 657–664.

Bischof, J., R. K. Maeda, M. Hediger, F. Karch, and K. Basler, 2007, "An Optimized Transgenesis System for Drosophila Using Germ-Line-Specific phiC31 Integrases.", *Proceedings of the National Academy of Sciences of the United States of America*, Vol. 104, No. 9, pp. 3312–3317.

Blair, S. S., 2003, "Genetic Mosaic Techniques for Studying Drosophila Development.", *Development*, Vol. 130, No. 21, pp. 5065–5072.

Bonini, N. M., W. M. Leiserson, and S. Senzer, 1993, "The Eyes Absent Gene : Genetic Control of Cell Survival and Differentiation in the Developing Drosophila Eye", *Cell*, Vol. 72, pp. 379–395.

Boya, P., and G. Kroemer, 2008, "Lysosomal Membrane Permeabilization in Cell Death.", *Oncogene*, Vol. 27, No. 50, pp. 6434–6451.

Branch, D., and K. Diseases, 1999, "A Vital Role for Glycosphingolipid Synthesis during Development", *Proceedings of the National Academy of Sciences of the United States of America*, Vol. 96, No. August, pp. 9142–9147.

Caciotti, A., S. C. Garman, Y. Rivera-Colón, E. Procopio, S. Catarzi, L. Ferri, C. Guido, P. Martelli, R. Parini, A. Morrone, 2011, "GM1 Gangliosidosis and Morquio B Disease: An Update on Genetic Alterations and Clinical Findings.", *Biochimica et Biophysica Acta*, Vol. 1812, No. 7, pp. 782–790.

Ceresa, B. P., and S. L. Schmid, 2000, "Regulation of Signal Transduction by Endocytosis", *Current Opinion in Cell Biology*, Vol. 12, No. 2, pp. 204–210.

Chao, J.-L., Y.-C. Tsai, S.-J. Chiu, and Y. H. Sun, 2004, "Localized Notch Signal Acts through Eyg and Upd to Promote Global Growth in Drosophila Eye.", *Development*, Vol. 131, No. 16, pp. 3839–3847.

Chern, J. J., and K. Choi, 2002, "Lobe Mediates Notch Signaling to Control Domain-Specific Growth in the Drosophila Eye Disc" *Development*, Vol. 4013, pp. 4005–4013.

Cheyette, B. N. R., P. J. Green, K. Martin, H. Carren, V. Hartenstein, and S. L. Zipursky, 1994, "The Drosophila Sine Oc & Locus Encodes a Homeodomain-Containing Protein Required for the Development of the Entire Visual System", *Genetics*, Vol. 12, pp. 977–996.

Chwieralski, C. E., T. Welte, and F. Bühling, 2006, "Cathepsin-Regulated Apoptosis.", *Apoptosis : An International Journal on Programmed Cell Death*, Vol. 11, No. 2, pp. 143–149.

Dermaut, B., K. K. Norga, A. Kania, P. Verstreken, H. Pan, Y. Zhou, P. Callaerts, and H. J. Bellen, 2005, "Aberrant Lysosomal Carbohydrate Storage Accompanies Endocytic Defects and Neurodegeneration in Drosophila Benchwarmer.", *The Journal of Cell Biology*, Vol. 170, No. 1, pp. 127–139.

Dominguez, M., D. Ferres-Marco, F. J. Gutierrez-Aviño, S. a Speicher, and M. Beneyto, 2004, "Growth and Specification of the Eye Are Controlled Independently by Eyegone and Eyeless in Drosophila Melanogaster.", *Nature Genetics*, Vol. 36, No. 1, pp. 31–39.

Dragosits, M., S. Yan, E. Razzazi-Fazeli, I. B. H. Wilson, and D. Rendic, 2015, "Enzymatic Properties and Subtle Differences in the Substrate Specificity of Phylogenetically Distinct Invertebrate N-Glycan Processing Hexosaminidases.", *Glycobiology*, Vol. 25, No. 4, pp. 448–464.

Ekas, L., G. H. Baeg, M. S. Flaherty, A. Ayala-Camargo, and E. Bach, 2006, "JAK/STAT Signaling Promotes Regional Specification by Negatively Regulating Wingless Expression in Drosophila.", *Development*, Vol. 133, No. 23, pp. 4721–4729.

Fahy, E., S. Subramaniam, H. A. Brown, C. K. Glass, A. H. Merrill, R. C. Murphy, C. R. H. Raetz, D. W. Russell, Y. Seyama, E. Dennis, 2005, "A Comprehensive Classification System for Lipids.", *Journal of Lipid Research*, Vol. 46, No. 5, pp. 839–861.

Fan, Y., and A. Bergmann, 2010, "The Cleaved-Caspase-3 Antibody Is a Marker of Caspase-9-like DRONC Activity in Drosophila.", *Cell Death and Differentiation*, Vol. 17, No. 3, pp. 534–539.

Fan, Y., and A. Bergmann, 2008, "Distinct Mechanisms of Apoptosis-Induced Compensatory Proliferation in Proliferating and Differentiating Tissues in the Drosophila Eye.", *Developmental Cell*, Vol. 14, No. 3, pp. 399–410.

Gilbert, M. M., and K. H. Moberg, 2006, "ESCRTing Cell Proliferation Off the Beaten Path" *Cell Cycle*, No. February, pp. 283–287.

Graham, T. G. W., S. M. A. Tabei, A. R. Dinner, and I. Rebay, 2010, "Modeling Bistable Cell-Fate Choices in the Drosophila Eye: Qualitative and Quantitative Perspectives.", *Development*, Vol. 137, No. 14, pp. 2265–2278.

Gratz, S. J., F. P. Ukken, C. D. Rubinstein, G. Thiede, L. K. Donohue, A. M. Cummings, and K. M. O'Connor-Giles, 2014, "Highly Specific and Efficient CRISPR/Cas9-Catalyzed Homology-Directed Repair in Drosophila.", *Genetics*, Vol. 196, No. 4, pp. 961–971.

Gravel, R., Kaback M., Proia R., Sandhoff K., Suzuki K., Suzuki K., 2001 "The GM2 gangliosidoses", *The Metabolic and Molecular Bases of Inherited Diseases*. Vol 3, pp. 3827-3877.

Gutierrez-Aviño, F. J., D. Ferres-Marco, and M. Dominguez, 2009, "The Position and Function of the Notch-Mediated Eye Growth Organizer: The Roles of JAK/STAT and Four-Jointed.", *EMBO Reports*, Vol. 10, No. 9, pp. 1051–1058.

Gutternigg, M., D. Kretschmer-Lubich, K. Paschinger, D. Rendić, J. Hader, P. Geier, R. Ranftl, V. Jantsch, G. Lochnit, and I. B. H. Wilson, 2007, "Biosynthesis of Truncated N-Linked Oligosaccharides Results from Non-Orthologous Hexosaminidase-Mediated Mechanisms in Nematodes, Plants, and Insects.", *The Journal of Biological Chemistry*, Vol. 282, No. 38, pp. 27825–27840.

Gutternigg, M., D. Rendić, R. Voglauer, T. Iskratsch, and I. B. H. Wilson, 2009, "Mammalian Cells Contain a Second Nucleocytoplasmic Hexosaminidase.", *The Biochemical Journal*, Vol. 419, No. 1, pp. 83–90.

Held L. I., 2002, "Imaginal Discs: The Genetic and Cellular Logic of Pattern Formation.", *Developmental and Cell Biology Series*, No.39, pp. 460.

Hopwood, J., Brooks, D, 1997, "An introduction to the basic science and biology of the lysosome and storage diseases." *Organelle Diseases. Clinical Features, Diagnosis, Pathogenesis and Management*, No.8, pp. 7–36.

Hou, Y., R. Tse, and D. J. Mahuran, 1996, "Direct Determination of the Substrate Specificity of the R -Active Site in Heterodimeric -Hexosaminidase A" *The Biochemical Journal*, Vol. 405, No. 3 pp. 3963–3969.

Hou, Y., D. J. Vocadlo, A. Leung, S. G. Withers, and D. Mahuran, 2001, "Characterization of the Glu and Asp Residues in the Active Site of Human", *The Journal of Biological Chemistry*, Vol. 286, No.25, pp. 2201–2209.

Huang, J., J. M. Trasler, S. Igdoura, J. Michaud, N. Hanai, and R. A. Gravel, 1997, "Apoptotic Cell Death in Mouse Models of G M2 Gangliosidosis and Observations on Human Tay – Sachs and Sandhoff Diseases" *Human Molecular Genetics*, Vol. 6, No. 11, pp. 1879–1885.

Jang, C.-C., 2003, "Two Pax Genes, Eye Gone and Eyeless, Act Cooperatively in Promoting Drosophila Eye Development", *Development*, Vol. 130, No. 13, pp. 2939–2951.

Jemc, J., and I. Rebay, 2007, "Identification of Transcriptional Targets of the Dual-Function Transcription Factor/phosphatase Eyes Absent.", *Developmental Biology*, Vol. 310, No. 2, pp. 416–429.

Jinek, M., K. Chylinski, I. Fonfara, M. Hauer, J. A. Doudna, and E. Charpentier, 2012, "A Programmable Dual-RNA-Guided DNA Endonuclease in Adaptive Bacterial Immunity.", *Science*, Vol. 337, No. August, pp. 816–822.

Jung, M., J. Lee, H.-Y. Seo, J. S. Lim, and E.-K. Kim, 2015, "Cathepsin Inhibition-Induced Lysosomal Dysfunction Enhances Pancreatic Beta-Cell Apoptosis in High Glucose.", *Plos One*, Vol. 10, No. 1, pp. 1-18.

Kaçmaz, G., 2013, "Characterization of a Novel R7-Specific Gene in the Drosophila Visual System", M.Sc. Thesis, Boğaziçi University.

Kondo, S., and R. Ueda, 2013, "Highly Improved Gene Targeting by Germline-Specific Cas9 Expression in Drosophila.", *Genetics*, Vol. 195, No. 3, pp. 715–721.

Kumar, J. P., 2011, "My What Big Eyes You Have: How the Drosophila Retina Grows.", *Developmental Neurobiology*, Vol. 71, No. 12, pp. 1133–1152.

Kumar, J. P., and K. Moses, 2001, "The EGF Receptor and Notch Signaling Pathways Control the Initiation of the Morphogenetic Furrow during Drosophila Eye Development", *Development*, Vol. 2697, pp. 2689–2697.

Lachke, S. A., and W. Hospital, 2001, "Encyclopedia of Life Sciences", *Wiley*, Vol. 25.

Langley, D. B., D. W. S. Harty, N. a Jacques, N. Hunter, J. M. Guss, and C. a Collyer, 2008, "Structure of N-Acetyl-Beta-D-Glucosaminidase (GcnA) from the Endocarditis Pathogen Streptococcus Gordonii and Its Complex with the Mechanism-Based Inhibitor NAG-Thiazoline.", *Journal of Molecular Biology*, Vol. 377, No. 1, pp. 104–16.

Léonard, R., D. Rendic, C. Rabouille, I. B. H. Wilson, T. Préat, and F. Altmann, 2006, "The Drosophila Fused Lobes Gene Encodes an N-Acetylglucosaminidase Involved in N-Glycan Processing.", *The Journal of Biological Chemistry*, Vol. 281, No. 8, pp. 4867–4875.

Ma, C., and K. Moses, 1995, "Wingless and Patched Are Negative Regulators of the Morphogenetic Furrow and Can Affect Tissue Polarity in the Developing Drosophila Compound Eye", *Development*, Vol. 2289, pp. 2279–2289.

Ma, Y., L. Zhang, and X. Huang, 2014, "Genome Modification by CRISPR/Cas9.", *The FEBS Journal*, Vol. 281, pp. 5186–5193.

Mazzoni, E. O., A. Celik, M. F. Wernet, D. Vasiliauskas, R. J. Johnston, T. a Cook, F. Pichaud, and C. Desplan, 2008, "Iroquois Complex Genes Induce Co-Expression of Rhodopsins in Drosophila.", *PLoS Biology*, Vol. 6, No. 4, pp. 84-97.

Morante, J., C. Desplan, and A. Celik, 2007, "Generating Patterned Arrays of Photoreceptors.", *Current Opinion in Genetics & Development*, Vol. 17, No. 4, pp. 314–319.

Morata, G., E. Shlevkov, and A. Pérez-Garijo, 2011, "Mitogenic Signaling from Apoptotic Cells in Drosophila.", *Development, Growth & Differentiation*, Vol. 53, No. 2, pp. 168–176.

Morin, X., R. Daneman, M. Zavortink, and W. Chia, 2001, "A Protein Trap Strategy to Detect GFP-Tagged Proteins Expressed from Their Endogenous Loci in Drosophila.", *Proceedings of the National Academy of Sciences of the United States of America*, Vol. 98, No. 26, pp. 15050–15055.

Moses, K., 2001, *Drosophila Eye : Progressive Neural Development*, Wiley, Vol.33, pp. 1–6.

Neckameyer, W. S., and K. J. Argue, 2013, "Comparative Approaches to the Study of Physiology: Drosophila as a Physiological Tool.", *American Journal of Physiology. Regulatory, Integrative and Comparative Physiology*, Vol. 304, No. 3, pp. R177–188.

Okajima, T., and K. D. Irvine, 2002, "Regulation of Notch Signaling by O -Linked Fucose", *Cell*, Vol. 111, pp. 893–904.

Öztürk, A., 2010, *Characterization of Genes Involved in Photoreceptor Differentiation*, M.Sc. Thesis, Boğaziçi University.

Pagano, R. E., V. Puri, M. Dominguez, and D. L. Marks, 2000, "Membrane Traffic in Sphingolipid Storage Diseases", *Traffic*, Vol. 1, No. 11, pp. 807–815.

Parkinson-Lawrence, E. J., T. Shandala, M. Prodoehl, R. Plew, G. N. Borlace, and D. a Brooks, 2010, "Lysosomal Storage Disease: Revealing Lysosomal Function and Physiology.", *Physiology (Bethesda, Md.)*, Vol. 25, No. 2, pp. 102–115.

Phillips, S. E., E. a Woodruff, P. Liang, M. Patten, and K. Broadie, 2008, "Neuronal Loss of Drosophila NPC1a Causes Cholesterol Aggregation and Age-Progressive Neurodegeneration.", *The Journal of Neuroscience :The Official Journal of the Society for Neuroscience*, Vol. 28, No. 26, pp. 6569–6582.

Quiñones-Coello, A. T., L. N. Petrella, K. Ayers, A. Melillo, S. Mazzalupo, A. M. Hudson, S. Wang, C. Castiblanco, M. Buszczak, L. Cooley, 2007, "Exploring Strategies for Protein Trapping in Drosophila.", *Genetics*, Vol. 175, No. 3, pp. 1089–1104.

Quiring, R., U. Walidorf, U. Kloter, and W. J. Gehringt, 1994, "Homology of the Eyeless Gene of Drosophila to the Small Eye Gene in Mice and Aniridia in Humans", *Science*, Vol. 265, No. August, pp. 785–789.

Ready, D.F., Hanson, T.E. and Benzer, S., 1976, "Development of the *Drosophila* retina, a neurocrystalline lattice", *Developmental Biology*, No.53, pp. 217-240.

Ren, X., J. Sun, B. E. Housden, Y. Hu, C. Roesel, S. Lin, and L. Liu, 2013, "Optimized Gene Editing Technology for Drosophila Melanogaster Using Germ Line-Specific Cas9", *Proceedings of the National Academy of Sciencesof the United States of America*, Vol. 110, No. 47, pp. 19012-19017

Renehan, A. G., C. Booth, and C. S. Potten, 2001, "What Is Apoptosis , and Why Is It Important ?", *BMJ Biology*, Vol. 322, No. June, pp. 1536–1538.

Timothy, M. C., Gonzales, M. B., 2012, "The Cellular Pathology of Lysosomal Diseases", *Wiley*, Vol. 226, No. 2, pp. 241–254.

Reynolds-Kenneally, J., and M. Mlodzik, 2005, "Notch Signaling Controls Proliferation through Cell-Autonomous and Non-Autonomous Mechanisms in the Drosophila Eye.", *Developmental Biology*, Vol. 285, No. 1, pp. 38–48.

Rizk, R. M., 1974, "Topology of the Caudal Fat Body of the Drosophila Melanogaster Tumor^{w} Mutant of Drosophila Melanogaster", *Journal of Invertebrate Pathology*, Vol.24, pp. 37–40.

Rizki, T. M., and R. M. Rizki, 1980, "Developmental Analysis of a Temperature-Sensitive Melanotic Tumor Mutant in Drosophila Melanogaster", *Wilhelm Roux's Archive of Developmental Biology*, Vol. 189, pp. 197-206.

Road, H., and D. Street, 1998, "A Dorsal/ventral Boundary Established by Notch Controls Growth and Polarity in the Drosophila Eye", *Nature*, Vol. 396, No. November, pp. 276–278.

Rosenbaum, E. E., E. Vasiljevic, K. S. Brehm, and N. J. Colley, 2014, "Mutations in Four Glycosyl Hydrolases Reveal a Highly Coordinated Pathway for Rhodopsin Biosynthesis and N-Glycan Trimming in Drosophila Melanogaster.", *PLoS Genetics*, Vol. 10, No. 5, pp 1-20.

Ryoo, H. D., and A. Bergmann, 2012, "The Role of Apoptosis-Induced Proliferation for Regeneration and Cancer.", *Cold Spring Harbor Perspectives in Biology*, Vol. 4, No. 8, pp. 17-26.

Silver, S. J., and I. Rebay, 2005, "Signaling Circuitries in Development: Insights from the Retinal Determination Gene Network.", *Development*, Vol. 132, No. 1, pp. 3–13.

Singh, A., and K.-W. Choi, 2003, "Initial State of the Drosophila Eye before Dorsoventral Specification Is Equivalent to Ventral.", *Development*, Vol. 130, No. 25, pp. 6351–6360.

Sorek, R., C. M. Lawrence, and B. Wiedenheft, 2013, "CRISPR-Mediated Adaptive Immune Systems in Bacteria and Archaea.", *Annual Review of Biochemistry*, Vol. 82, , pp. 237–66.

Stowers, R. S., and T. L. Schwarz, 1999, "A Genetic Method for Generating Drosophila Eyes Composed Exclusively of Mitotic Clones of a Single Genotype" *Genetics*, Vol. 152, No. 4, pp. 1631-1639.

Sugiura, Y., K. Furukawa, O. Tajima, S. Mii, and T. Honda, 2005, "Sensory Nerve-Dominant Nerve Degeneration and Remodeling in the Mutant Mice Lacking Complex Gangliosides.", *Neuroscience*, Vol. 135, No. 4, pp. 1167–1178.

Sweeney, S. T., G. W. Davis, and S. Francisco, 2002, "Unrestricted Synaptic Growth in Spinster - a Late Endosomal Protein Implicated in TGF-β-Mediated Synaptic Growth Regulation", *Neuron*, Vol. 36, pp. 403–416.

Tsai, B., J. M. Gilbert, T. Stehle, W. Lencer, T. L. Benjamin, and T. A. Rapoport, 2003, "Gangliosides Are Receptors for Murine Polyoma Virus and SV40", *EMBO Journal*, Vol. 22, No. 17, pp. 4346-4355.

Ungos, J., and B. Sciences, 1997, "Mirror Encodes a Novel PBX-Class Homeoprotein That Functions in the Definition of the Dorsal-Ventral Border in the Drosophila Eye", *Genes & Development*, No. 11, pp. 1073–1082.

Vaccari, T., T. E. Rusten, L. Menut, I. P. Nezis, A. Brech, H. Stenmark, and D. Bilder, 2009, "Comparative Analysis of ESCRT-I, ESCRT-II and ESCRT-III Function in Drosophila by Efficient Isolation of ESCRT Mutants.", *Journal of Cell Science*, Vol. 122, No. 14, pp. 2413–2423.

Van Meer, G., and Q. Lisman, 2002, "Sphingolipid Transport: Rafts and Translocators.", *The Journal of Biological Chemistry*, Vol. 277, No. 29, pp. 25855–25858.

Walkley, S. U., 2004, "Secondary Accumulation of Gangliosides in Lysosomal Storage Disorders.", *Seminars in Cell & Developmental Biology*, Vol. 15, No. 4, pp. 433–444.

Walkley, S. U., M. Zervas, and S. Wiseman, 2000, "Gangliosides as Modulators of Dendritogenesis in Normal and Storage Disease-Affected Pyramidal Neurons" *Cerebral Cortex*, No.10, pp. 1028–1037.

Wang, D., C.-C. Chan, S. Cherry, and P. R. Hiesinger, 2013, "Membrane Trafficking in Neuronal Maintenance and Degeneration.", *Cellular and Molecular Life Sciences: CMLS*, Vol. 70, No. 16, pp. 2919–2934.

Ward, E. J., I. Thaipisuttikul, M. Terayama, R. L. French, S. M. Jackson, K. A. Cosand, K. J. Tobler, J. B. Dorman, and C. a Berg, 2002, "GAL4 Enhancer Trap Patterns during Drosophila Development.", *Genesis*, Vol. 34, No. 1-2, pp. 46–50.

Weasner, B., C. Salzer, and J. P. Kumar, 2007, "Sine Oculis, a Member of the SIX Family of Transcription Factors, Directs Eye Formation.", *Developmental Biology*, Vol. 303, No. 2, pp. 756–771.

Werth, N., C. G. Schuette, G. Wilkening, T. Lemm, and K. Sandhoff, 2001, "Degradation of Membrane-Bound Ganglioside GM2 by Beta -Hexosaminidase A. Stimulation by GM2 Activator Protein and Lysosomal Lipids.", *The Journal of Biological Chemistry*, Vol. 276, No. 16, pp. 12685–12690.

Wiedenheft, B., S. H. Sternberg, and J. a Doudna, 2012, "RNA-Guided Genetic Silencing Systems in Bacteria and Archaea.", *Nature*, Vol. 482, No. 7385, pp. 331–338.

Wiersdorff, V., T. Lecuit, S. M. Cohen, and M. Mlodzik, 1996, "Mad Acts Downstream of Dpp Receptors , Revealing a Differential Requirement for Dpp Signaling in Initiation and Propagation of Morphogenesis in the Drosophila Eye", *Development*, No. 122, pp. 2153–2162.

Yamashita, T., A. Hashiramoto, M. Haluzik, H. Mizukami, S. Beck, A. Norton, M. Kono, S. Tsuji, J. L. Daniotti, R. L. Proia, 2003, "Enhanced Insulin Sensitivity in Mice Lacking Ganglioside GM3.", *Proceedings of the National Academy of Sciences of the United States of America*, Vol. 100, No. 6, pp. 3445–3449.

Yao, J.-G., B. M. Weasner, L.-H. Wang, C.-C. Jang, B. Weasner, C.-Y. Tang, C. L. Salzer, C.-H. Chen, B. Hay, J. P. Kumar, 2008, "Differential Requirements for the Pax6(5a) Genes Eyegone and Twin of Eyegone during Eye Development in Drosophila.", *Developmental Biology*, Vol. 315, No. 2, pp. 535–551.

Yu, R.K., T. Ariga, M. Yanagisawa, G. Zeng, 2008, "Gangliosides in the nervous system: Biosynthesis and degradation.", *Glycoscience*, No.9, pp. 1671-1695.

Yu, R. K., Y.-T. Tsai, T. Ariga, and M. Yanagisawa, 2011, "Structures, Biosynthesis, and Functions of Gangliosides", *Journal of Oleo Science*, Vol. 60, No. 10, pp. 537–544.

Yuva-Aydemir, Y., A.-C. Bauke, and C. Klämbt, 2011, "Spinster Controls Dpp Signaling during Glial Migration in the Drosophila Eye.", *The Journal of Neuroscience : The Official Journal of the Society for Neuroscience*, Vol. 31, No. 19, pp. 7005–7015.